LBNL-40929
UC-000

ERNEST ORLANDO LAWRENCE BERKELEY NATIONAL LABORATORY

Liquid Phase Epitaxial Growth of GaAs

Dawnelle Ivy Wynne

Engineering Division

October 1997

M.S. Thesis

REFERENCE COPY
Does Not
Circulate

Bldg. 50 Library - Ref.
Lawrence Berkeley National Laboratory

LBNL-40929
Copy 1

DISCLAIMER

This document was prepared as an account of work sponsored by the United States Government. While this document is believed to contain correct information, neither the United States Government nor any agency thereof, nor the Regents of the University of California, nor any of their employees, makes any warranty, express or implied, or assumes any legal responsibility for the accuracy, completeness, or usefulness of any information, apparatus, product, or process disclosed, or represents that its use would not infringe privately owned rights. Reference herein to any specific commercial product, process, or service by its trade name, trademark, manufacturer, or otherwise, does not necessarily constitute or imply its endorsement, recommendation, or favoring by the United States Government or any agency thereof, or the Regents of the University of California. The views and opinions of authors expressed herein do not necessarily state or reflect those of the United States Government or any agency thereof or the Regents of the University of California.

LBNL-40929
UC-000

Liquid Phase Epitaxial Growth of GaAs

Dawnelle Ivy Wynne

Materials Science and Mineral Engineering
University of California, Berkeley

and

Engineering Division
Ernest Orlando Lawrence Berkeley National Laboratory
University of California
Berkeley, California 94720

M.S. Thesis

October 1997

This work was supported in part by NASA through the Graduate Student Researchers Program, Grant No. NGT-51303 and in part by NASA Ames Research Center, Order # A51232D through the U.S. Department of Energy under Contract No. DE-AC03-76SF00098.

Liquid Phase Epitaxial Growth of GaAs

by

Dawnelle Ivy Wynne

B.S. (University of California, Los Angeles) 1984

A thesis submitted in partial satisfaction of the

requirements for the degree of

Master of Science

in

Engineering -- Materials Science and Mineral Engineering

in the

GRADUATE DIVISION

of the

UNIVERSITY OF CALIFORNIA at BERKELEY

Committee in charge:

Professor Eugene E. Haller
Professor Timothy Sands
Doctor Carolyn Rossington

1997

TABLE OF CONTENTS

ACKNOWLEDGMENTS vi

1.0 INTRODUCTION 1

1.1 GaAs X-ray Detectors 2

1.1.1 Room Temperature X-ray Detectors 2

1.1.1.1 GaAs Room Temperature X-ray Detector Applications 4

1.1.2 Material Property Requirements 6

1.2 GaAs Extrinsic Photoconductors for the Detection of Far-Infrared Radiation 8

1.2.1 Material Property Requirements 10

1.3 Objectives of Research 11

2.0 III-V COMPOUND SEMICONDUCTOR EPITAXY 12

2.1 Survey 12

2.2 Major GaAs Epitaxial Growth Techniques 13

2.2.1 Vapor Phase Epitaxy (VPE) 16

2.2.1.1 Chloride transport 16

2.2.1.2 Metal-organic chemical vapor deposition (MOCVD) 18

2.2.2 Molecular Beam Epitaxy (MBE) 19

2.2.3 Liquid Phase Epitaxy (LPE) 21

2.3 Liquid Phase Epitaxy (LPE) of III-V Compounds 22

2.3.1 Principles of LPE of III-V Compounds 23

2.3.2 Methods of Depositing LPE Layers 30

2.3.3 Segregation Coefficients 31

2.3.4 Epilayer Growth Rate and Thickness Calculations 34

2.3.5 Microscopic Growth Mechanisms 37

2.3.6 Influence of Impurity Concentration on Epilayer Surface Morphology 43

2.3.7 Influence of Constitutional Supercooling on Epilayer Surface Morphology 46

2.3.8 LPE Growth Apparatus for III-V Compound Epilayers 49

2.4 LPE of Pure Epilayers of GaAs by the Tipping Boat Method 51

2.4.1 Apparatus 51

2.4.2 Preparation of Process Chamber and Graphite Components 56

2.4.3 Choice and Preparation of the Substrate and Solution Materials 57

2.4.3.1 GaAs Substrates 57

2.4.3.2 GaAs Used For the Growth Solution 58

2.4.3.3 Gallium Used For the Growth Solution 59

2.4.4 Epilayer Growth Procedure 59

3.0 EPILAYER CHARACTERIZATION

3.1 Electrical Characterization 63

3.1.1 Common Residual Impurities in High-Purity GaAs LPE Layers 63

3.1.2 Hall Effect Measurements 63

3.1.3 Identification and Elimination of Chemical Impurities in the Epilayers 65

3.2 Structural Characterization 70

3.2.1 Visual Observations of Epilayer Structures 70

3.2.2 X-ray Rocking Curve Measurements 72

4.0 CONCLUSIONS AND FUTURE WORK 73

APPENDIX I: Methods of Depositing LPE Layers 74

APPENDIX II: Derivation of the Segregation Coefficient 78

APPENDIX III: Diffusion-Limited Growth Theory 86

APPENDIX IV: Apparatus Used For LPE Growth Of III-V Semiconductor Compounds 100

APPENDIX V: Choice of System and Growth Materials For High-Purity LPE Growth 110

APPENDIX VI: Determination of Convection Conditions in the Solution 117

APPENDIX VII: Most Common Impurities in GaAs LPE Layers 120

APPENDIX VIII: Hall Effect Measurements 127

APPENDIX IX: Secondary Ion Mass Spectroscopy (SIMS) 137

APPENDIX X: Photothermal Ionization Spectroscopy (PTIS) 139

APPENDIX XI: Photoluminescence (PL) Measurements 148

APPENDIX XII: X-Ray Rocking Curve Analysis 155

REFERENCES 160

ACKNOWLEDGMENTS

I would like to thank Professor Eugene Haller for providing me with the opportunity to pursue my graduate studies at UC Berkeley. In addition to providing support and guidance, he was also patient during my struggle to write this thesis, for which I'm very grateful. I would also like to thank Dr. Carolyn Rossington-Tull for her support, guidance, and the encouragement she's given me throughout my graduate studies.

Jeff Beeman, Bill Hansen, Dick Davis, Dr. Wladek Walukiewicz, and Dr. Edith Bourret at LNBL have given me excellent advice and assistance regarding the work documented in this thesis. I would also like to thank Mark West, Kevin Tedder and Brad Krieger for their help with building the Liquid Phase Epitaxy system. And thanks to David Hom, whose sense of humor kept things from being boring.

The graduate students and postdocs who I have worked with while at UC Berkeley have been a great support group, and have given me an enormous amount of help and advice. It would have been much more difficult (and less fun!) to complete my studies and research without them.

I would like to acknowledge my family and Brian Ferguson, who encouraged me to pursue my studies beyond obtaining the Master's degree.

I would also like to gratefully acknowledge NASA for supporting a portion of my graduate studies and research through the Graduate Student Researchers Program, Grant No. NGT-51303. This work was also supported in part by NASA Ames Research Center, Order # A51232D through the U.S. Department of Energy under Contract No. DE-AC03-76SF00098.

1.0 INTRODUCTION

Research into new semiconductor materials for measurement of electromagnetic radiation over a wide range of energies has been an active field for several decades. There is a strong desire to identify and develop new materials which can lead to improved detectors. Such devices are expected to solve problems that cannot be solved using the semiconductor materials and device structures which have been traditionally used for radiation detection.

In order for a detector which is subjected to some type of irradiation to respond, the radiation must undergo an interaction with the detector. The net result of the radiation interaction in a broad category of detectors is the generation of mobile electric charge carriers (electrons and/or holes) within the detector active volume. This charge is collected at the detector contacts and it forms the basic electrical signal. Typically, the collection of the charge is accomplished through the imposition of an electric field within the detector which causes the positive and/or negative charges created by the radiation to flow in opposite directions to the contacts. For the material to serve as a good radiation detector, a large fraction (preferably 100%) of all carriers created by the interacting incident radiation must be collected. Charge trapping by deep level impurities and structural defects can seriously degrade detector performance. The focus of this thesis is on far infrared and X-ray detection.

In X-ray detector applications of p-i-n diodes, the object is to measure accurately the energy distribution of the incident radiation quanta. One important property of such detectors is their ability to measure the energy of individual incident photons with high energy resolution (Haller and Goulding, 1993).

In far infrared detector applications of extrinsic photoconductors, the environment is often the low photon background of outer space. The radiation from a

weak infrared source, i.e., the signal radiation, must be detected above the background radiation. Semiconductors that are used for far IR detection have a long wavelength cutoff which is given by the ionization energies of the shallow dopants (Haller, 1994).

The traditional semiconductor materials used for the applications described above have one limitation or another, whether it is low sensitivity to the radiation energy of interest, trapping of charges generated by the incident radiation, or the need for cryogenic cooling to reduce leakage currents. GaAs, if it can be grown with sufficiently low dopant and defect concentrations, shows promise for use in two types of radiation detectors. One is an extrinsic photoconductor for detection of far infrared radiation to wavelengths of approximately 210 μm, and the other is as a Schottky barrier or p-i-n diode for detection of X-rays for energies of a few keV to 60 keV and higher.

1.1 GaAs X-ray Detectors

1.1.1 Room Temperature X-Ray Detectors

An X-ray detector operated at room temperature must exhibit a low enough reverse bias leakage current for adequate signal detection. The larger the bandgap of the semiconductor used for the detector, the smaller the thermally-generated current will be, and therefore the smaller the reverse bias leakage current (assuming that there are few mid-gap states contributing to leakage current). A major advantage of GaAs over Si for room temperature X-ray detector applications is the larger bandgap of 1.42 eV vs. 1.1 eV. This represents a 10^7 decrease in the number of thermally generated carriers at 300 K.

Another important X-ray detector parameter is the energy resolution. It is influenced by a number of factors, including the number of electron-hole pairs produced, the fluctuation in this number, charge collection efficiency, detector capacitance and leakage current, and electronic noise in the first amplifier stages.

Charge collection efficiency (CCE) is defined as the ratio of the charge generated by the particle or photon incident on the detector to the charge collected at the contacts (Bauser, 1994). While charge collection efficiency can be close to 100% in Si and Ge detectors, it is typically much less than 100% in all compound semiconductor detectors. Since X-rays can interact anywhere in the detector volume and depending on the interaction point the resulting electrons and holes will travel different distances to the contacts, any significant carrier trapping will seriously degrade the energy resolution. All deep donors and deep acceptors act as carrier traps (Haller and Goulding, 1993) and compound semiconductors typically have more deep donors and acceptors than Si or Ge, thus trap more. In order to measure the energies of incident photons as accurately as possible one strives for the highest energy resolution possible.

Work by Eberhardt *et al.* (1970) and Gibbons and Howes (1972) using epitaxial GaAs layers as X-ray detector material, demonstrated an energy resolution high enough to generate interest in the X-ray detector community. However, not much progress was made beyond these early studies, presumably because of the success of Si X-ray detectors and difficulties in growing GaAs epilayers of sufficient quality. More recently Grant *et al.* (1993), using thick (100 μm or more) high purity GaAs epilayers grown by liquid phase epitaxy (LPE), have also produced devices with good energy resolution. J. Lauter *et al.* (1995) has claimed approximately 100% charge collection efficiency for 60 keV X-rays detected by such GaAs devices.

Since GaAs epilayers are generally too thin to absorb X-rays of energies above approximately 60 keV (see Figure 1 for absorption efficiency of GaAs and Si at selected thicknesses), attempts have been made to produce detectors from bulk GaAs. However, devices fabricated using single-crystal bulk GaAs grown by various techniques, including Liquid Encapsulated Czochralski (LEC), Horizontal and Vertical Bridgman growth (HB & VB), and Vertical Gradient Freeze (VGF), have shown poor

performance characteristics (D.S. McGregor *et al.*, 1994; T.J. Sumner *et al.*, 1992, Moore *et al.*, 1996). The poor performance is due to incomplete charge collection and can be attributed to high impurity and high defect concentrations in the GaAs. It should be kept in mind that deep levels are introduced deliberately at high concentrations in some bulk GaAs single crystals in order to make it semi-insulating. As expected, the charge collection efficiency (CCE) has been found to increase with decreasing thickness of bulk GaAs wafers. For example, S.E. King *et al.* (1996) measured a CCE of 76% for a 100 μm thick device, and a CCE of 38% for a 635 μm thick device, for ^{241}Am α particles entering from the Schottky barrier side of the detector. At this point in time there is apparently no advantage to be gained from using bulk GaAs to make thick X-ray detectors unless the deep level concentrations can be significantly reduced. Bulk GaAs devices used for timing purposes in high energy physics experiments may produce good enough signals for this application.

1.1.1.1 GaAs Room Temperature X-ray Detector Applications

There are several promising applications for GaAs room temperature X-ray detectors such as in medical imaging and protein crystallography which makes use of X-rays with energies from approximately 10 to 60 keV. Phosphor imaging technology and film have traditionally been used for both of these applications. Detector arrays fabricated from GaAs offer the potential for real-time digital imaging and reduced radiation dose to the patient, compared with phosphor plates and film (C. Rossington, 1997).

Another application of GaAs is in detectors for X-ray imaging telescopes. For X-ray imaging telescopes up to 30 keV there is a need for detectors with a stopping power greater than the current generation of silicon CCDs (charge coupled device) can offer. To provide good imaging at the focal point of such an X-ray telescope, a thin

detector is preferable, in order to avoid problems with depth of focus (Sumner *et al.* 1994). Detectors fabricated from GaAs could offer improvements compared with Si CCDs in that they could be operated at room temperature (Si CCDs require cooling to -120 °C to reduce leakage current), and would exhibit a greater X-ray absorption efficiency.

Semiconductor detectors based on silicon or germanium have been the traditional materials used for detection of X-rays in the energy range of interest. A disadvantage of Ge detectors (both high-purity and lithium-drifted) is that they must be cooled to liquid nitrogen temperatures to reduce the thermally-induced free carrier generation that contributes to the reverse-bias leakage current. Lithium-drifted Ge detectors must also be cooled so that the lithium doesn't redistribute within the crystal. Another disadvantage of lithium-drifted Si detectors is that after drifting, processing temperatures are limited to below about 120 °C so that the lithium doesn't diffuse out of the crystal. These detectors therefore cannot be reliably segmented into arrays and integrated with on-chip read out electronics (Rossington, 1997). High-purity Si p-i-n diodes can be used for detecting X-rays with energies up to approximately 30 keV, limited by the thickness of the device. Cooled Si p-i-n detectors have outstanding energy resolution which has not been matched by any other semiconductor.

The thickness of the detection layer is limited by the depletion depth which can be attained before avalanche breakdown occurs. Detection layers of 500 μm to 3 mm are commonly used, with maximum layer thicknesses of up to 7 mm (Pehl *et al.*, 1986). At X-ray energies below 30 keV, Si absorption efficiency and attainable detector thicknesses are adequate for many applications. Figure 1 shows the absorption efficiency of 3 mm thick Si vs. 100 μm and 400 μm thick GaAs. At an X-ray energy of 30 keV, 62% of the radiation is absorbed by a 3 mm thick Si detector. In comparison, a 400 μm thick GaAs diode fabricated with an epilayer absorbs 94.5% of 30 keV X-

rays. The GaAs maximum thickness of 400 μm was chosen because it is approximately the thickest high purity GaAs layer that can be grown by modern epitaxial methods. Increasing the X-ray energy to 60 keV reduces the absorption in a 400 μm thick GaAs epilayer to 34.0%. The strong dependence of the photon absorption on atomic number Z is one of the driving forces for the search for high Z semiconductors with good charge collection properties.

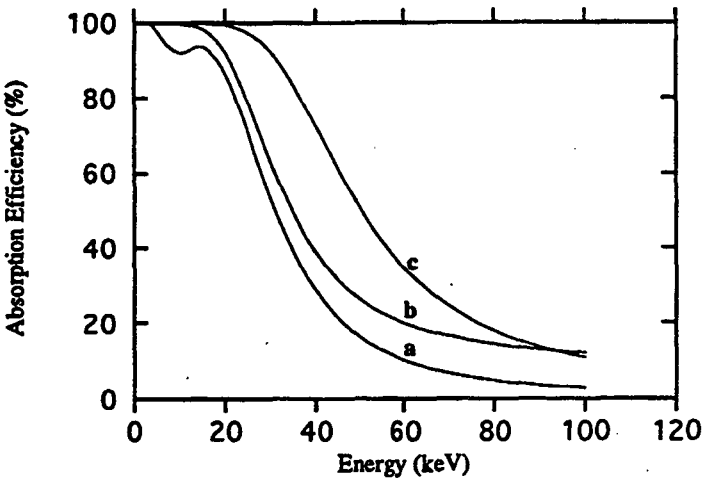

Figure 1. Photon absorption efficiency for selected thicknesses of Si and GaAs
a) GaAs, 100 μm thick; b) Si, 3 mm thick; c) GaAs, 400 μm thick

1.1.2 Material Property Requirements

A large **bandgap** is desired to minimize the reverse bias current, as discussed previously. The current from thermally generated carriers in the depletion layer of a GaAs p-i-n diode is expected to be small enough ($\leq$ nA) to allow low-noise room temperature operation (Bradshaw, 1980).

An advantage of GaAs over Si is that the probability of a photoelectric effect event which converts the full X-ray energy into the kinetic energy of electrons depends on the nuclear charge as Z^5 (Haller and Goulding, 1981). GaAs with $Z_{avg} = 32$ has

larger linear absorption coefficients for incident X-ray photons than Si with Z = 14. Therefore the higher the **atomic number** of the detector material, the more efficiently the X-ray photons are absorbed.

Other high atomic number (and wider bandgap) semiconductors which have been used for room temperature X-ray detection are HgI_2, CdTe and CdZnTe. Although research has been conducted for some time on detectors made with these materials, there are still severe problems with poor carrier transport properties due to imperfect material, and it is still only possible to grow relatively small crystals. Furthermore, none of these materials can be purified appropriately for p-i-n diode operation, thus resistive detectors are typically used.

For a GaAs p-i-n detector, the **effective thickness**, i.e., the depletion layer width, should be 100 μm or more to provide adequate detection efficiency (see Figure 1). The width of the depletion layer is related to the net-impurity concentration $|(N_D - N_A)|$ and the applied voltage by the equation

$$d = \sqrt{\frac{2V\varepsilon_{GaAs}\varepsilon_0}{q|(N_D - N_A)|}} \text{ (cm).} \tag{1}$$

The maximum voltage that can be applied to the device is limited to that at which breakdown occurs due to avalanche processes. Typically, the lower the net-impurity concentration, the larger the depletion layer thickness that can be obtained before breakdown occurs.

Low dopant compensation ($N_{minority}/N_{majority}$) is advantageous in moderately to heavily doped semiconductors because at low temperatures the carrier mobility is affected less by neutral impurities than by ionized impurities.

A low concentration of deep levels is important for a long mean free path of the charge carriers, leading to excellent charge collection efficiency, which is an important requirement for good energy resolution.

In order to fulfill all of these materials requirements appropriate crystal growth and device processing technologies must exist for the potential detector material. The growth technology of electronic device-quality GaAs are well-developed for both bulk crystals and epilayers. Other advantages of GaAs are well-developed device fabrication technologies including n- and p-type doping, Schottky barrier formation, surface passivation, etc. It may even be possible to integrate electronic devices onto the detector (such as field-effect transistors (FETs)). A further advantage of devices fabricated from GaAs is the potentially fast response time due to high electron mobility, compared with Si and Ge.

The attractiveness of using LPE GaAs in X-ray detector applications is due to the high material purity which can be attained compared with bulk crystal growth methods (Silier *et al.*, 1992; Amano *et al.*, 1993) and the capability of growing thick epilayers much more efficiently than with other epitaxial growth methods (Silier *et al.*, 1992; Alexiev and Butcher, 1992). In short, high purity and hundreds of μm thick epilayers are the primary requirements for the manufacture of high resolution, room temperature GaAs X-ray detectors.

1.2 GaAs Extrinsic Photoconductors for the Detection of Far Infrared Radiation

There exists a strong interest in far infrared (far IR) detectors by the astronomy and astrophysics communities. Semiconductor photoconductive detectors with cut-off limits near 250 μm are being used with high altitude or space-based telescopes at low backgrounds to image galaxies and to study star formation in the far IR. Important

spectral features in this region include, for example, the carbon and nitrogen ionization features at 158 and 202 μm, respectively.

Ge photoconductors, doped with shallow donors or acceptors are currently used as far IR detectors but have cut-off limits of approximately 130 μm (caused by the ionization energies of shallow-level impurities). The cut-off limits of Si photoconductors are considerably less, because the binding energies of dopants in Si are typically four times larger than in Ge which translates directly into a shorter wavelength limit. For far IR radiation studies beyond 130 μm two kinds of detectors are used at this time. They are stressed Ge:Ga photoconductors with a cut-off limit between 200 and 250 μm depending on the maximum stress which can be applied, and cryogenic bolometers. Neither the massive mechanical stressing rigs required for stressed Ge photoconductors, nor the severe cooling requirements for high performance bolometers (< 300 mK), are convenient for future applications, especially not for large detector arrays. A photoconductor with a long cut off wavelength, which does not require extreme operating conditions, is highly desirable.

Lightly doped n-type GaAs may be such a photoconductor material due to the very low electron binding energies of shallow donor impurities, which are approximately 5.9 meV (or 210 μm in wavelength) for the dopants silicon, selenium, sulfur, germanium and tin (Sze, 1981). Ionization via bound excited states pushes the cut off limit to approximately 300 μm (Wolfe *et al.*, 1977). (P-type GaAs is less attractive as a photoconductive material because the shallowest acceptor energy in GaAs is 23 meV, more than twice as much as the shallow dopants in Ge!) GaAs would not require mechanical stressing as Ge:Ga does, nor the mK cooling of bolometers.

1.2.1 Material Property Requirements

In order to obtain high resistivity, sensitive semiconductor IR photoconductors, the free carrier concentration has to be "frozen out" by cooling. Furthermore hopping conduction has to be reduced by lowering the doping concentration and the compensation. For these reasons very pure single crystal epilayers of GaAs are required for far IR photoconductor fabrication. The reason that bulk-grown n-type GaAs cannot be used is because significant impurity banding effects (overlap of the large donor orbitals, $r_{Bohr} \approx 100$ Å) occur in this material which has impurity concentrations near 10^{15} cm^{-3}. Impurity banding leads to dramatic dark current increases. Figure 2 shows detector responsivity as a function of frequency for different donor concentrations in GaAs (Wolfe *et al.*, 1977). Typical residual impurity concentrations obtained for bulk-grown GaAs for device applications (LEC method) are in the 10^{15} cm^{-3} range (M/A COM, Sumitomo, 1995), and high 10^{14} cm^{-3} for VGF-grown material (AXT, 1996). This is clearly not pure enough for the fabrication of sensitive photoconductive detectors.

The effective detector thickness should be 100 μm or more, to provide adequate detection efficiency. A 100 μm thick layer of 10^{13} cm^{-3} n-type GaAs leads to 21.5% absorption of 6 meV (or 48.4 cm^{-1}) IR photons, and a 400 μm thick layer leads to 61.9% absorption (Stillman *et al.*, 1977).

The best epilayers grown using the LPE technique exhibit net-impurity concentrations on the order of 10^{12} cm^{-3}, and epilayers with thicknesses of up to approximately 400 μm have been grown (Silier *et al.*, 1992; Amano, *et al.*, 1993), which leads to the conclusion that LPE GaAs could be an excellent material for far IR detectors.

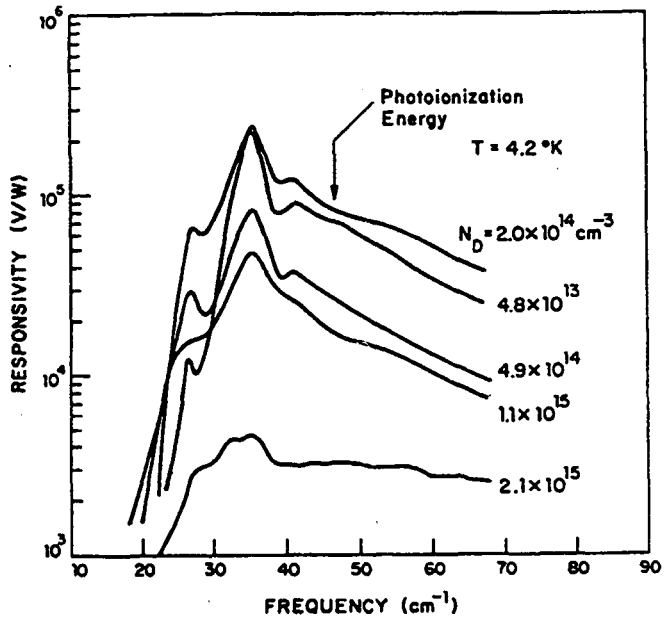

Figure 2. Responsivity spectra at 4.2 K for five GaAs photodetectors with the donor concentrations shown (courtesy of Wolfe *et al.* 1977)

1.3 Objectives of Research

The objectives of this research are the LPE growth and characterization of ultra-pure epilayers of GaAs onto single crystal GaAs substrates. These epilayers will be used for developing two types of radiation detectors, far infrared photoconductive detectors with a long wavelength cut-off limit of up to approximately 210 μm, and room temperature X-ray detectors for a few keV to above 60 keV detection. The scope of this thesis is development and characterization of the GaAs epilayers only, not the fabrication of devices. The epilayer characteristics required for device fabrication are a thickness of 100 μm or greater, net donor concentration of approximately 10^{12} cm^{-3} and an electron mobility of greater than 200,000 cm^2 / V.s at 77 K. Such high mobilities are reached only in low compensation material.

2.0 III-V COMPOUND SEMICONDUCTOR EPITAXY

2.1 Survey

The word "epitaxy" is derived from the Greek words *epi* , meaning "on", and *taxis*, meaning "arrangement" (Sze, 1981). The term epitaxy implies the alignment of one crystal lattice (e.g., a thin film) on another crystal lattice (e.g., a substrate). Epitaxy is commonly used to describe the procedure for growing a single crystal layer (epilayer) on a single crystal substrate.

The concept of epitaxy was first described by by Royer (1928). From the above definition of epitaxy, it follows that the crystal structure of the epilayer and substrate must be of the same crystallographic space group (Astles, 1990) and that the unit cell dimensions (or lattice parameter) of the epilayer and substrate must be closely matched. However, with the non-equilibrium growth methods now available, such as metal-organic chemical vapor deposition (MOCVD) and molecular beam epitaxy (MBE), epilayers can be grown with a higher lattice mismatch than Royer originally envisioned as possible for epitaxy.

When the epilayer and substrate have the same chemical composition (except for impurity type and concentration) the process is known as **homoepitaxy**. When the epilayer and substrate have different chemical composition, the process is known as **heteroepitaxy** . This thesis will address the subject of homoepitaxy only.

Epitaxy is an important process because it allows the growth of defect-free single crystal layers with controllable thickness, composition, and doping. This is useful for a wide variety of electronic devices, because they are generally fabricated within a few micrometers of the surface of a single crystal slice of semiconductor. Thin epilayers on supporting substrates are adequate for many device applications, for example in the huge market area of light emitting diodes.

The reasons why the epitaxial growth methods are capable of producing III-V compound semiconductor epilayers of higher purity than bulk-grown crystals are related to the crystal growth temperature. The temperatures at which epitaxial growth can be performed are generally much lower than the melting temperature of the bulk crystal, required for bulk-grown material. For example, epitaxial growth of GaAs is performed between 500 and 900 °C, while the melting temperature of GaAs is 1238 °C, required for bulk-grown GaAs. The reduced growth temperature leads to the following advantages. First, native defects always exists in all semiconductor crystals in thermodynamic equilibrium. They are formed by antisite defects, i.e., group III atoms on lattice sites of group V atoms or vice versa, by atoms in an interstitial position, and by vacancies. The formation of all these defects is thermally activated and increases with temperature. A fraction of these defects will be frozen in during cooling of the crystal from a higher temperature. For these reasons crystal or epilayer growth at reduced temperatures generally leads to lower native defect concentrations (Jacob and Müller, 1984).

Second, at reduced temperatures there is potentially less impurity contamination of the epilayer from all the materials used in the growth process. This includes the crucible in which growth occurs (Deitch, 1975), either by dissolution of the crucible or by diffusion of impurities from the crucible.

The impurities and the native defects described above can act as shallow or deep donors, or shallow or deep acceptors (Hurle, 1979), all of which can degrade device performance.

2.2 Major GaAs Epitaxial Growth Techniques

As there are specialized methods for the epitaxial growth of each III-V compound, the specifics of epitaxial growth will be given for GaAs only.

Each epitaxial growth method has one or more advantages for achieving certain epilayer and/or device characteristics. As was described in Section 1, very pure, hundreds of μms thick GaAs epilayers are required for the development of the targeted X-ray and far IR devices so the different growth methods were evaluated for their ability to meet these requirements. The main techniques used to grow epilayers of GaAs are chloride transport vapor phase epitaxy (VPE), metal-organic chemical vapor deposition (MOCVD), molecular beam epitaxy (MBE), and liquid phase epitaxy (LPE).

Note that all of these epitaxial growth processes are conducted in a vacuum tight process chamber to prevent oxidation and contamination of the growth materials, and/or to contain toxic materials and waste products. Selected characteristics of these epitaxial growth techniques are compared in Table 1, followed by a brief description of each epitaxial growth method.) Descriptions of each method are given to show why GaAs epilayers grown by LPE can be of higher purity than epilayers grown by the other methods.

TABLE 1:

Comparison of Epitaxial Growth Techniques for GaAs

	LPE	Trichloride VPE	MOCVD	MBE
Range of growth rates (μm/min)	.01~10[D]	.03~0.5 [W]	.01~.5[W]	.01~.1[W]
Typical growth rate (μm/min.)	1[W]	.1[S]	.05[CC]	.01[S]
Doping range (cm^{-3})	10^{12} [S, Am] ~10^{19} [A]	10^{13}~10^{19}[Do]	10^{14}~10^{20}[A]	10^{13}[S]~10^{19}[A]
Best 77 K electron mobility (cm^2/V.s)	>250,000[S,A m]	200,000[Do]	120,000[W]	150,000[A]
Run-run variation of layer thickness	± 10%[A]	± 5%[HP]	± 3%[E]	± 3%[E]
Layer thickness uniformity (over 2 cm)	± 10%[A]	± 5%[HP]	± 0.5%[E]	± 0.5%[E]
Abruptness of interface, Å (typ.)	500[A]	100[W]	monolayer[E]	monolayer[E]

References:

A: Astles, 1990

Am: Amano *et al.*, 1993

S: Silier *et al.*, 1992

CC: Chang-Hasnain, 1996

E: Epitaxial Products International, 1997

HP: Hewlett-Packard Optoelectronics Division, 1997

D: Deitch, 1975

Do: Dorrity *et al.*, 1985

W: Weyrich and Plihal, 1984

S: Shur, 1987

2.2.1 Vapor Phase Epitaxy (VPE)

The two techniques commonly used for the VPE growth of GaAs are chloride transport and metal-organic chemical vapor deposition (MOCVD). The chloride transport VPE process (specifically, the trichloride process) is capable of producing epitaxial layers of higher purity than MOCVD (Dorrity *et al.*, 1985, Hasegawa, 1990), but MOCVD is preferred for high volume epilayer production because more wafers can be processed in each growth run.

2.2.1.1 Chloride transport

The trichloride and hydride processes are both variations of the chloride transport process in which Ga is transported in the form of GaCl and reacted with arsenic. Growth is carried out in a hot-wall silica process chamber in a flowing H_2 ambient in both methods but the reactive species are generated in different ways. These processes are illustrated schematically in Figure 3.

In the **trichloride** process, $AsCl_3$ is passed over a heated Ga or GaAs source at approximately 850 °C. The substrate temperature is held at about 750 °C. Upon heating $AsCl_3$ decomposes to form As_4 (and As_2) and HCl:

$$4AsCl_3 + 6H_2 \rightarrow As_4 + 12HCl \qquad (2)$$

If the Ga source is used, the As_4 is initially taken in by the Ga until the Ga becomes saturated, at which point a thin crust of GaAs forms on the surface.The HCl from reaction (2) combines with the GaAs to form GaCl:

$$2GaAs\ (g) + 2HCl \rightarrow 2GaCl + H_2 + As_2 \qquad (3)$$

The GaCl and As (as As_2 and As_4) pass downstream and over the substrate where the epilayer deposition occurs according to the reactions

$$6GaCl + As_4 \rightarrow 4GaAs + 2GaCl_3 \quad (4)$$

$$2GaCl + As_2 + H_2 \rightarrow 2GaAs + 2HCl \quad (5)$$

The GaAs epilayers are purer if a liquid Ga source is used instead of a solid GaAs source, in part because Ga is available commercially with higher purity than GaAs, and because Ga is a liquid metal which getters many impurities. Purity of the epilayers is also strongly dependent on the molar fraction of $AsCl_3$ flowing into the reactor. At low molar fractions (10^{-3}) the unintentional doping level can be as high as 10^{16} cm^{-3}. At larger molar fractions (up to 10^{-2}) this number can drop to 10^{13} cm^{-3} or below in a good system (Shur, 1987). This effect is due to the reduction of the HCl reaction with the SiO_2 reactor tube.

In the **hydride** process (Olsen and Zamerowski, 1979), GaCl is generated directly by passing HCl over the gallium source and As_4 is generated from the pyrolysis of arsine (AsH_3). Free HCl is also injected directly into the deposition zone to reduce the gas phase supersaturation.

The addition of HCl must be done carefully in both of the chloride transport processes because an excess of HCl will cause etching of the substrate, for example due to the reversal of equation (5) for the trichloride process. Often free HCl is injected into the reactor to etch the substrate surface and therefore clean it before the epilayer growth process begins.

Of the two chloride transport processes, the trichloride process produces the purest epilayers; the purity of epilayers grown by the hydride process is limited by the purity of commercially-available HCl.

The disadvantages of using the chloride transport growth methods are that the reactants and waste products are toxic, and the growth rates are low.

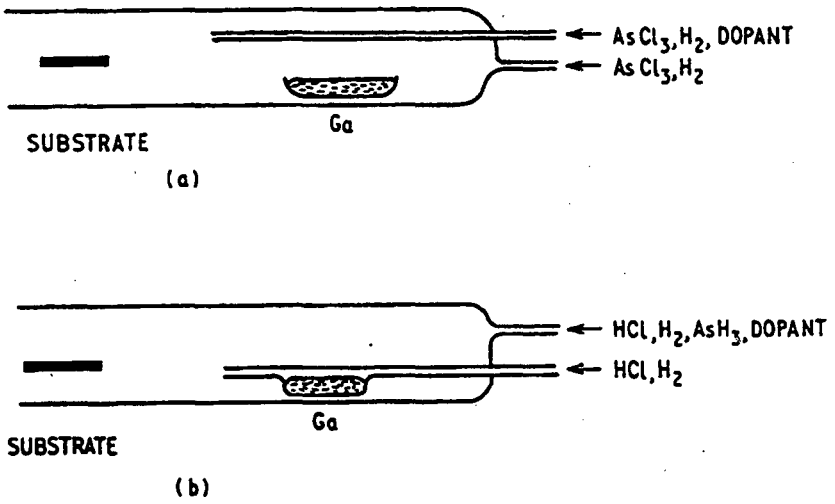

Figure 3. Schematic diagram of main features of GaAs VPE chloride transport reactors: a) trichloride process, b) hydride process. (Dorrity *et al.*, 1985)

2.2.1.2 Metal-organic chemical vapor deposition (MOCVD)

MOCVD growth of GaAs involves the pyrolysis of a vapor phase mixture of arsine (AsH_3) and most commonly, trimethyl gallium (TMG) or triethyl gallium (TEG). Free Ga atoms and As_4 molecules are formed and these species recombine on the hot substrate surface in a reaction to form GaAs:

$$R_3Ga\ (g) + AsH_3\ (g) \rightarrow GaAs\ (s) + 3RH\ (g) \qquad (6)$$

$$R = CH_3 \text{ or } C_2H_5$$

(Dorrity *et al.*, 1985).

This process was first successfully demonstrated by Manasevit and Simpson (1969). Growth is carried out in a cold-wall silica process chamber in flowing H_2 at atmospheric or low pressure. The substrate is heated to temperatures of 650-750 °C (Shur, 1987), either by inductively or radiatively heating a graphite susceptor. The metal-organics are transported to the growth zone by bubbling H_2 through liquid sources which are held in temperature-controlled bubblers. Figure 4 shows a simple schematic of an MOCVD system.

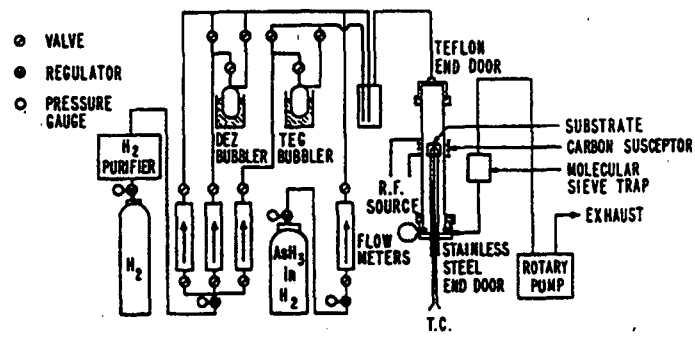

Figure 4. Schematic drawing of an MOCVD system (Chang *et al.*, 1981)

Disadvantages of this method are that the reactants and waste products are toxic and pyrophoric, and the growth rates are low.

2.2.2 Molecular Beam Epitaxy (MBE)

MBE is the growth of epilayers by the reaction of thermally evaporated and directed atomic or molecular beams on a crystalline surface under ultra-high-vacuum (UHV) conditions. The basics of the system are illustrated schematically in Figure 5. MBE systems generally consist of multiple chambers including a load-lock (used to preserve the vacuum in the growth chamber), a preparation chamber (not shown in Figure 5), and a growth chamber. The various chambers are constructed of stainless

steel and base pressures of 10^{-11}-10^{-10} torr are obtained with an elaborate system of pumps. The use of UHV conditions for MBE enables the incorporation of high-vacuum based surface analytical and diagnostic techniques (some equipment is included in the growth chamber and some is installed in the preparation chamber to minimize contamination problems). There are shutters in front of the heated evaporation (Knudsen) cells, so that the thermal effusion of material from any cell can be started or stopped abruptly. This allows for the growth of very sharp layer interfaces. These heated evaporation cells are surrounded by liquid nitrogen-cooled shrouds to lessen impurity outgassing. The substrate heater is rotated during growth to improve the thickness and doping uniformity. The advantages of this system are that an epilayer can be grown a monolayer at a time, and that in-situ analysis of the layer as it grows is possible. The disadvantages are the high costs of the UHV system, the low layer growth rates and the low throughput (only one wafer can be processed at a time). The growth of GaAs by MBE is typically carried out at temperatures from 500 - 650 °C (Shur, 1987).

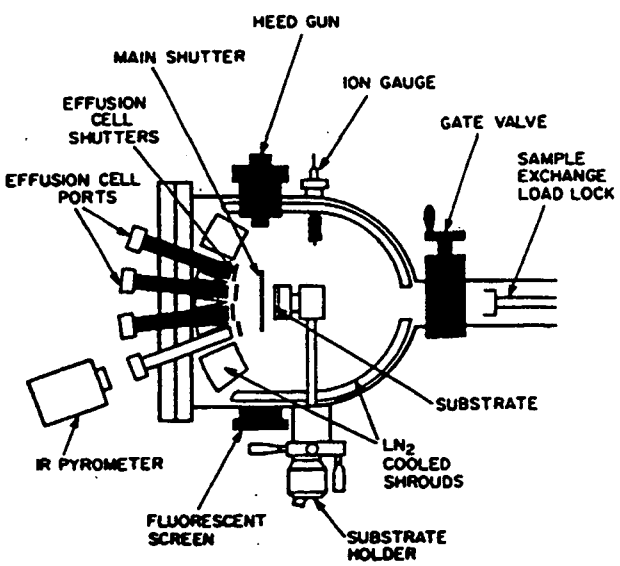

Figure 5. Schematic diagram of an MBE growth chamber (Drummond *et al.*, 1981)

2.2.3 Liquid Phase Epitaxy (LPE)

LPE is a technique used to deposit an epitaxial layer onto a single crystal substrate from a solution (liquid phase) saturated with atoms of the material to be deposited.

In the case of semiconductor epilayers (especially of III-V compounds), growth from a liquid phase involves precipitation of a single crystal layer from a molten solution made up of a low melting point metal solvent and a very dilute solute (the epilayer component(s)).

There are several advantages of using the LPE technique, one of which is that LPE is a simpler process than the other epitaxial growth methods discussed previously. The only growth parameters which can be varied are substrate orientation, solution composition, temperature, cooling rate, and growth time (Hsieh*et al.* 1976a). The equipment required for the LPE process is much simpler (thus cheaper and also potentially purer) than the other methods, which is important when controlling contamination. It is important to note that of the epitaxial growth methods mentioned previously, only LPE has demonstrated the capability of producing epilayers of the thickness required for radiation detector applications. Epilayers of the highest purity have also been produced by LPE. Epilayers with net donor impurity concentrations in the 10^{12} cm^{-3} range have been produced, with electron mobilities of greater than 250,000 cm^2 / V.s at 77 K (Silier *et al.*, 1992; Amano *et al.*, 1993). Also, LPE is inherently safer than VPE and MOCVD because the raw materials and waste products are less toxic and are not pyrophoric (as in the case of MOCVD).

Limitations of the LPE technique include difficulty in obtaining uniformity of impurity doping in the growth direction due to the segregation coefficient of components in the growth solution (not a concern for the research conducted for this thesis), and a

rougher surface morphology of epilayers grown by LPE (relative to other epitaxial growth methods). This can be a concern for device fabrication.

Temperatures at which LPE GaAs layers are grown range generally from about 600 to 900 °C. The temperature of the growth chamber must be above 600 °C in order for the H_2 gas, generally used in the growth chamber, to reduce the oxides on the surface of the substrate and solution. The high temperature limit is due to a higher risk of contamination of the solution by the growth boat or crucible (usually graphite), and to increased degradation of the substrate and solution by the preferential loss of As.

2.3 Liquid Phase Epitaxy (LPE) of III-V Compounds

LPE apparently originated in the nineteenth century (Moon, 1980), when sodium nitrate was epitaxially grown on freshly cleaved calcite by Frankenheim (1836). Alloyed Ge and Si diodes and transistors were first made by dissolving the Ge or Si in the molten impurity desired and then regrowing the Ge or Si onto part of the original crystal (For example see R.N. Hall, 1952). Growth of epitaxial layers from molten metal solutions was not put into widespread practice until 1963 when Nelson described LPE and demonstrated its usefulness by fabricating Ge tunnel diodes and GaAs lasers (Nelson, 1963). Since then, Nelson's approach has been modified to grow many materials. LPE has become a method used mainly, but not exclusively, for the growth of III-V alloys and magnetic garnet materials. Most aspects of LPE have been studied in some detail since 1963 and this has led to an great number of articles. Many review articles have appeared during this time (Dawson, 1972; Deitch, 1975; Hsieh, 1980; Moon, 1980; Astles, 1990).

LPE of semiconductors, particularly III-V compounds, is typically performed with molten metal solutions. For LPE of high purity epilayers of III-V compounds, dilute solutions are used which contain a group III element, such as Ga, as the solvent,

which is also a component of the epilayer. Group V elements are not used as solvents due to their high vapor pressure.

So far, LPE has not been used for the growth of high purity elemental semiconductor layers, such as Si, because the solution is made up of atoms of Si as the solute, plus a solvent of another material such as Ga or In (Linnebach and Bauser, 1982; Konuma *et al.*, 1993) which is then incorporated to some extent in the growing epilayer resulting in moderate to heavily doped material (e.g., Si grown from an In solution is doped with approximately 10^{16} In cm^{-3}).

Since the temperatures of substrate and solution are essentially equal during the entire growth period, an LPE layer is grown under near-equilibrium conditions (Deitch, 1975). Also, the thermal stress at the interface is small (Astles, 1990), and LPE usually produces epilayers with lower dislocation densities than the substrate on which they are grown (Weinstein *et al.*, 1966; Nohavica, 1970; Saul, 1971; Kumer and Takagi, 1977). The epilayers are often very pure because many unwanted impurities are fortuitously segregated preferentially into the metal solution. Segregation coefficients will be discussed in Section 2.3.3 and in Appendix II.

2.3.1 Principles of LPE of III-V Compounds

The thermodynamic basis of the LPE technique can best be described with the phase diagram which provides information on the composition of the solution and the solid crystal (or epilayer) in equilibrium as a function of temperature. Methods to calculate the phase diagram using simplified solution models and experimental data have been determined for binary compounds (see, for example, Thurmond, 1965; Stringfellow, 1971; Kaufman, 1983). A review of phase diagrams and their use in both crystal growth and the study of the properties of semiconductors can be found in a series of books (Alper, 1970). A more detailed description of the phase diagram is

presented in other texts (Zernike, 1955; Reisman, 1970). These phase relationships are only briefly discussed here with the emphasis being placed on their use specifically for LPE growth of III-V compounds. When discussing the principles of LPE, only molten metal solutions will be considered.

Figure 6 shows the phase diagram for a simple binary or pseudo-binary system for an idealized system. T_A is the melting temperature of the metal solvent, *A*, and T_B is the melting temperature of the dilute solute (the component(s) of the crystal or epilayer to be grown), *B*. Component *A* in Figure 6 may be a single element or a eutectic alloy, component *B* may be a single element or a compound (Deitch, 1975).

The "liquidus line" labeled in Figure 6 defines the temperature - composition states from pure *A* to pure *B* where the solid solute and the solute components of the liquid are in equilibrium (Astles, 1990; Deitch, 1975). A solution of composition X at temperature T_X is represented by position 1 in the completely liquid part of the diagram (represents the unsaturated solution). If the temperature is reduced to T_C on the diagram, the solution is now saturated with *B* (at position 2). Further cooling to T_D (position 3 on the diagram) will cause a supersaturation of *B* in the solution, because the completely liquid solution is now in the two-phase solid-liquid region (which represents the saturated solution and crystallized solute) and it can be seen that the solubility of *B* in *A* decreases as the temperature is reduced. There is a driving force for precipitation of solid *B*, to bring the system back to solid-liquid equilibrium (position 4 on the liquidus line). In reality, the solution can be "supercooled" below T_C by a certain amount before solid material is homogeneously nucleated in the solution.

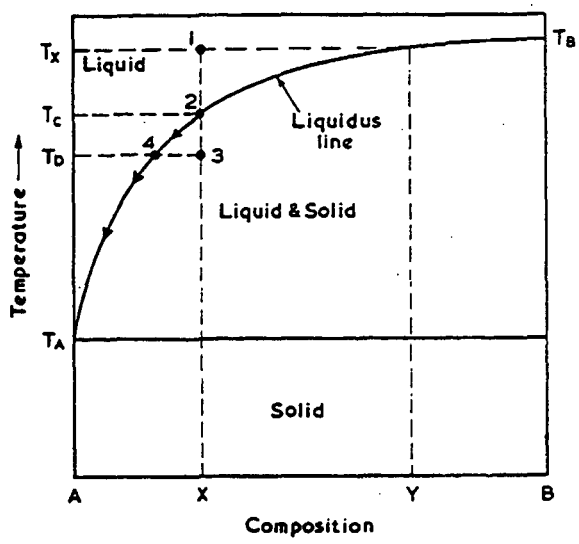

Figure 6. Generalized temperature-composition equilibrium phase diagram for the system A - B (Deitch, 1975). Analogy to the liquid phase epitaxy process: the liquid region is unsaturated solution, the liquid + solid region is solution + recrystallized solute.

For the LPE growth of III-V compounds, another common way of producing supersaturation is the introduction of a temperature gradient in the solution perpendicular to the growth interface. At the hotter end of the solution (for example at position 1 on Figure 6) is a source of solute, and at the cooler end (for example at position 3 on Figure 6) is a substrate on which growth will occur. The temperature gradient induces solute transport from the source to the substrate. This type of growth is called "steady state" growth.

For a binary system, if the solution of composition X at temperature T_C is brought into contact with a single crystal substrate of composition *B* also at temperature T_C, the system is still in equilibrium. This is so since point 2 lies on the liquidus and the solution is already saturated with *B* (Dawson, 1972). This cannot be said about ternary alloys (Hsieh, 1980), but this situation will not be discussed as it is outside the scope of this thesis.

The substrate provides energetically favorable sites for nucleation and crystal growth. This is the case because the critical supercooling of the solution below the equilibrium temperature needed to produce precipitation on the substrate is found to be approximately 0.1 °C (Crossley and Small, 1972; Rode, 1973), while the critical supercooling needed for homogeneous nucleation in a Ga-As homogeneous solution has been reported to be 10 °C (Panish, 1970; Crossley and Small, 1971; Hsieh, 1974) and 6 °C (Doi *et al.*, 1976).

Since the average composition of the entire solid-liquid system must remain constant during this process, the solution becomes richer in *A* as *B* precipitates from it (Deitch, 1975). The amount of solid *B* which is formed at a given temperature is given by applying the *lever rule* to Figure 6. For example, drawing a "tie line" on Figure 6 from T_D through point 3 to the *B* vertical line on the right side of the diagram, the amount of *B* that will precipitate out of the solution = $(C_X - C_4)/(1 - C_4)$ where the C's are the concentrations of *B*. The composition of remaining liquid follows the liquidus line towards T_A as indicated by the arrows.

The Gibbs phase rule states that the number of degrees of freedom in a system, f, is given by $f = c - p + 2$, where c is the number of components, p is the number of phases, and the "2" refers to the variables temperature and pressure.
For the normal conditions of LPE growth, the pressure in the process chamber is approximately constant at close to 1 atmosphere, and the partial pressures of the solution components are << 1 atmosphere. Therefore, the pressure variable is neglected, and $f = c - p + 1$. For a binary or pseudo-binary system, for example *A* and *B* whose compositions are fixed, $c = 2$ and $p = 2$ (solid, liquid) and so $f = 1$ (one degree of freedom, being the temperature). Consequently, the equilibrium temperature at the solid-liquid interface and the composition of the liquid at the interface are determined by thermodynamics.

For comparison with the simple binary equilibrium phase diagram, Figure 7 shows the Ga-As equilibrium phase diagram. The vertical line at 50% As corresponds to the GaAs solid phase composition. From the left side of the phase diagram (0% As) to this vertical line, the diagram looks very similar to Figure 6 with *A* being Ga, *B* being GaAs. The high-purity GaAs LPE process is conducted on this Ga-rich side of the diagram. Although the GaAs solid phase composition in Figure 7 is represented by a thin vertical line at 50% As, the existence region actually has a finite width as shown in Figure 8, showing that GaAs may exist with deviations from exact stoichiometry on both the Ga-rich and the As-rich sides. It can be seen that at the low temperatures at which LPE occurs (approximately 500 - 900 °C), the deviations from stoichiometry are small, whereas at the melting point (1238 °C) at which melt-grown crystals are produced, the deviations are much larger (Astles, 1990).

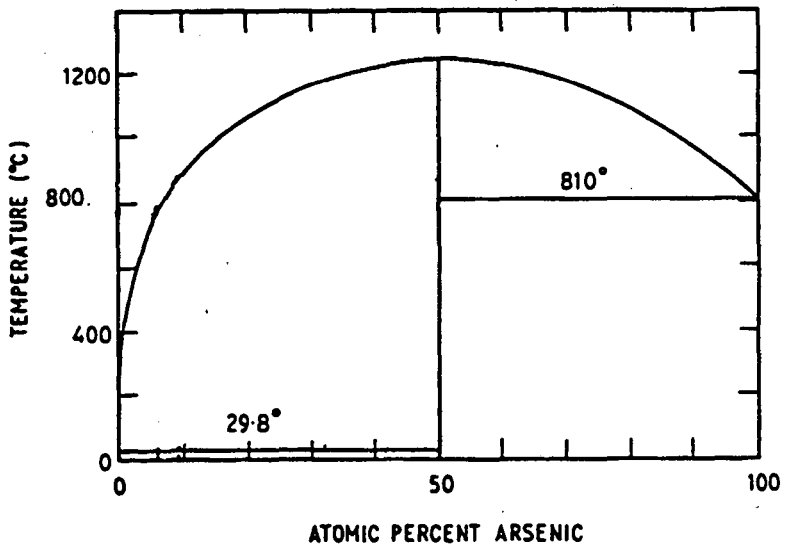

Figure 7. Schematic of Ga - As phase diagram (Dorrity, 1985)

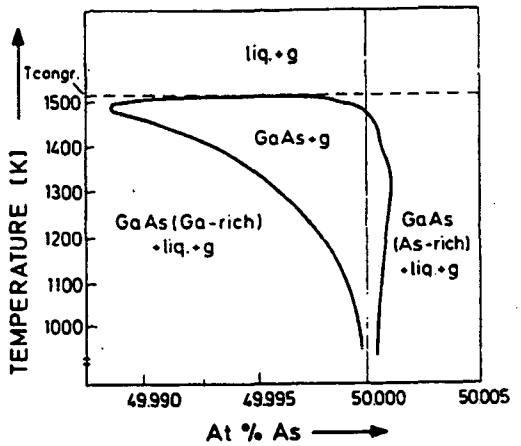

Figure 8. Existence region for GaAs, calculated by Logan and Hurle (Benz and Bauser, 1980)

An important advantage of the LPE growth of GaAs over melt growth is the reduction in vapor pressure of the volatile Group V component due to its small concentration in the growth solution. The total pressure of the As species at the melting point of GaAs is about 1 atmosphere (Rosenberger, 1979). Special precautions must be taken when growing GaAs bulk crystals from a stoichiometric melt to avoid the loss of As, such as floating liquid B_2O_3 on top of the melt (Liquid Encapsulated Czochralski Method). Figure 9 shows the partial pressures of the Ga and As species that are in equilibrium with the liquidus curve on the Ga-rich side of the Ga-As system. Referring to Figure 9, for LPE growth at approximately 808 ^oC from the Ga-rich side of the phase diagram, the dominant vapor species is As_2, with a vapor pressure of about 10^{-7} atm., a level which leads to a negligible loss of As from the solution during growth.

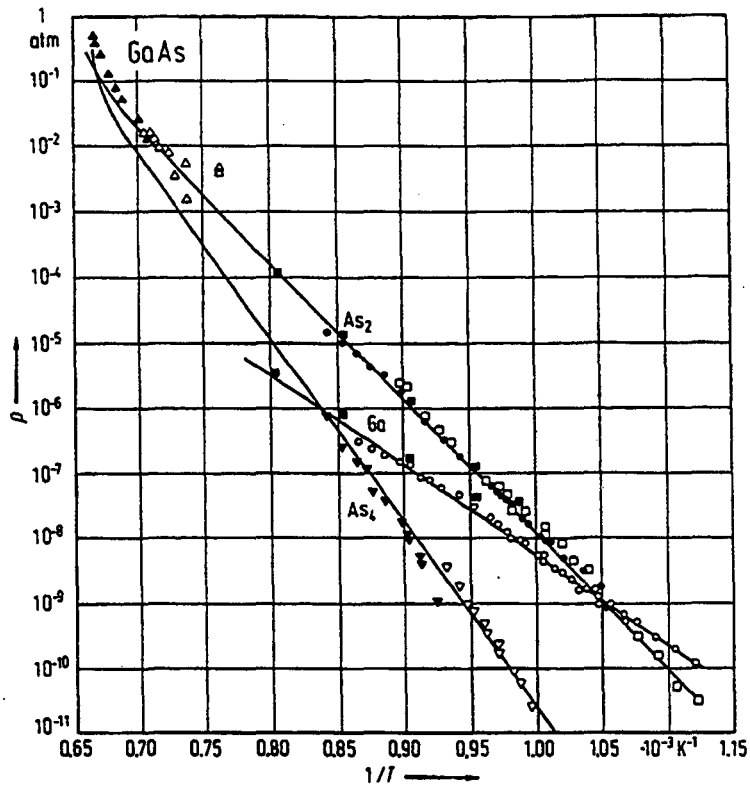

Figure 9. Equilibrium pressure p of As_2, As_4, and Ga over GaAs along the Ga-rich portion of the Ga - As liquidus vs. reciprocal absolute temperature 1/T. Continuous lines are calculated curves (Arthur *et al.*, 1967; Pupp *et al.*, 1974)

For the usual range of compositions and temperatures over which III-V compound LPE growth occurs, Hsieh (1974b) has represented the liquidus curve by an expression of the form $x = A\exp(-T'/T_L)$, where x is the atom fraction of the group V nonmetal in the saturated solution, T_L is the absolute liquidus temperature, A is a dimensionless parameter, and T' is a is a temperature parameter. A straight line is therefore obtained when x is plotted on a logarithmic scale as a function of $1/T_L$. Figure 10 is a plot of this type showing the experimental data for the Ga-rich liquidus of the Ga-As system between 650 and 950 °C. Hsieh observed experimentally that an excellent fit to the data is given by the straight line corresponding to the equation $x_{As} = 2352.8 \exp(-12404/T_L)$.

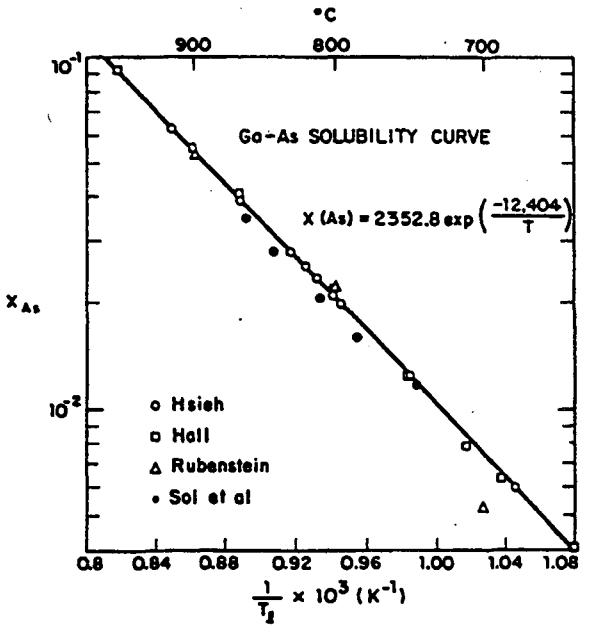

Figure 10. Liquidus data for Ga-rich solutions in the Ga - As system. The atom fraction of As in the saturated solution, X_{As}, is plotted vs. reciprocal absolute liquidus temperature, $1/T_l$ (Hsieh, 1974b).

2.3.2 Methods of Depositing LPE Layers

Researchers have developed various ways of creating the supersaturation in a solution to produce LPE growth. The two major methods or systems used are **transient systems** involving the controlled cooling of a solution in which the desired epilayer components have been dissolved, and **steady-state systems** in which the epilayer components are transported by the use of a thermal gradient in the solution (Dawson, 1972).

Some of the more common methods of LPE deposition are briefly discussed in Appendix I.

The LPE growth method chosen depends on the material parameters required for the particular application, such as epilayer thickness and surface topography.

The supercooled growth technique was chosen for the research conducted for this thesis, for the following reasons. First, epilayers of 100 μm and thicker have been

grown reproducibly by several groups (Silier *et al.*, 1992; Alexiev and Butcher, 1992). Second, as explained in Appendix I, epilayers with the smoothest surface topographies are produced by the supercooled method. Third, epilayers of the required purity have been reproducibly grown (Silier *et al.*, 1992; Amano *et al.*, 1993), and fourth, the equipment required for the supercooled growth method is simpler than that required for the steady state growth method.

2.3.3 Segregation Coefficients

As mentioned previously, the LPE method can be a purification process as well as a method of crystal growth or epilayer growth. Many impurities are left behind in the liquid (or segregated into the liquid) as the solid grows.

The equilibrium segregation coefficient was first defined by Pfann (1952) for melt growth of bulk crystals, with the aid of a phase diagram of a binary system with a solute (a soluble impurity) and a solvent (components of the crystal) as components (Shah, 1975). Figures 11a and b schematically represent portions of such diagrams near the melting points of solvents. The equilibrium segregation coefficient k_0 is defined as the ratio of the concentration of the solute in the solid C_S to that in the C_L when the solid and liquid phases are in equilibrium, i.e.,

$$k_0 = \frac{C_S}{C_L}. \tag{7}$$

From Figure 11 it can be seen that C_S and C_L are the values of solute concentration given by the intersection of a tie line (at a temperature T) with the solidus and the liquidus. It can also be seen that for a solute which incorporates less in the solid than in the liquid, $k_0 < 1$ and the solidification temperature of the system is lowered (Figure

11a). For a solute which is preferentially incorporated in the solid, $k_0 > 1$ and the solidification temperature of the system is raised (Figure 11b).

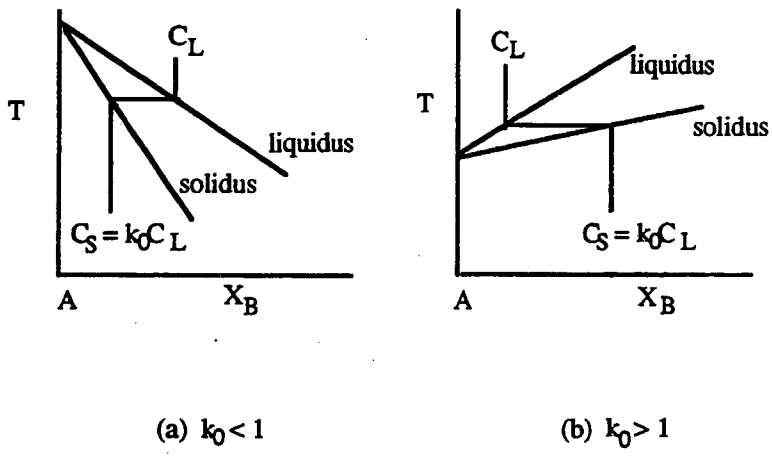

Figure 11. Portions of phase diagrams in which the solidification temperature is a) lowered, b) raised by the solute, and corresponding segregation coefficients k_0 (Rosenberger, 1979)

Rosenberger has described the **effective segregation coefficient, k**, of a component between bulk phases:

$$k = \frac{C_0^S}{C_\infty^L} \frac{\rho^L(\infty)}{\rho^S(0)} \tag{8}$$

where the subscript ∞ designates "far away from the (solid-liquid) interface", the subscript 0 means "at the interface", C_0^S is the concentration of the solute in the solid (at the interface), C_∞^L is the bulk liquid concentration, ρ^L is the liquid density, and ρ^S is the solid density.

Most work with segregation coefficients has dealt with impurity-in-melt systems where $\rho^L/\rho^S \sim 1$. But for LPE growth where the solid (crystal or epilayer) and liquid (mostly solvent) have different compositions, the density ratio must be included.

If the solid and liquid are in mass transfer equilibrium at the interface, then k becomes equal to the **equilibrium segregation coefficient** $\mathbf{k_0}$ which depends only on the thermodynamic properties of the system rather than the mass transfer kinetics at the interface (Rosenberger, 1979). This case of fast interface kinetics can often be assumed in LPE growth of III-V compounds.

Equilibrium segregation coefficients are not constant because they generally depend on the temperature, pressure, and concentration of the component of interest, as well as on the presence of other components. (See Appendix II for discussion of the derivation of the segregation coefficient by several researchers who have considered thermodynamics, and the electrical properties of the solid crystal.)

Calculation of segregation coefficient from measured carrier concentrations.

The segregation coefficient k_0 can also be calculated from the majority impurity carrier concentration in the epilayer as measured by the Hall effect (See Appendix VIII for discussion of the Hall effect).

Calculating the segregation coefficients using atom fractions, Astles (1990) used the equation

$$k_0 = \frac{(N_D - N_A)}{2N} \frac{MW_S}{\rho_S X_2^L} \tag{9}$$

Where (N_D-N_A) or (N_A-N_D) is the net donor or acceptor concentration, N is Avogadro's number, MW_S is the molecular weight of the solid, ρ_S is the density of the solid and X_2^L is the atom fraction of the impurity "2" in the growth solution. The impurity atom must be electrically active as a donor or acceptor to be measured by the Hall effect, and the net carrier concentration as measured by the Hall effect is assumed to be equal to the impurity concentration (i.e., negligible compensation). The other assumptions that are made in this analysis are that the Hall factor (r) is one, all of the impurity atoms of interest are fully ionized at room temperature, the impurity atoms can only exist in neutral or singly ionized states, there is negligible compensation and there are no precipitates of the impurity of interest.

This method of calculation of the segregation coefficient is valid if the impurity concentration in the solid is a linear function of the concentration in the liquid, which is not always the case for high impurity concentration.

It should be noted that for LPE growth that covers a wide temperature range, such as cooling from the growth temperature all the way to room temperature, a depth dependent impurity concentration can result because of the temperature dependence of the segregation coefficient.

2.3.4 Epilayer Growth Rate and Thickness Calculations

For bulk semiconductor crystal growth from a melt, the growth rate is usually determined by the rate at which the heat of fusion is removed from the solid-liquid interface. It reaches from 1-10 cm/hr (Dawson, 1972; Haller, 1997). In comparison, most cases of LPE growth occur from such dilute solutions that the growth rate is determined mainly by the transport of the solute to the solid-liquid interface, either by diffusion, convection, or stirring. For the LPE growth conducted for this thesis (and also for many cases of LPE growth), the effects of convection are eliminated and the

solution is not stirred. With these conditions, the growth rate is determined solely by the diffusion of the solute to the solid-liquid interface. This type of growth is known as diffusion-limited growth.

As a crystal or epilayer grows from solution, the concentration of solute component(s) (such as As for GaAs growth) in the solution at the solid-liquid interface is reduced and a concentration profile similar to that shown in Figure 12 results. This figure shows a one-dimensional representation of the concentration profile C(x,t). Diffusion of solute components through the solution to the growth (solid-liquid) interface supplies the additional material needed in order for the crystal or epilayer to continue growing. Originally, the solution is homogenized and the solute concentration is C_0. As the temperature is reduced, the equilibrium concentration of solute in the solution, C_e, will vary from C_0. For GaAs, C_e will be reduced (solute (As) solubility decreases with decreasing temperature). It is usually assumed for III-V growth that interface kinetics are fast, which means that at all times for a given temperature the solute concentration at the solid-liquid interface C_i is equal to the equilibrium concentration C_e (Astles, 1990), and the growth rate is controlled by solute diffusion in the solution. The situation in Figure 12 corresponds to a supersaturated solution with $C_0 > C_e$.

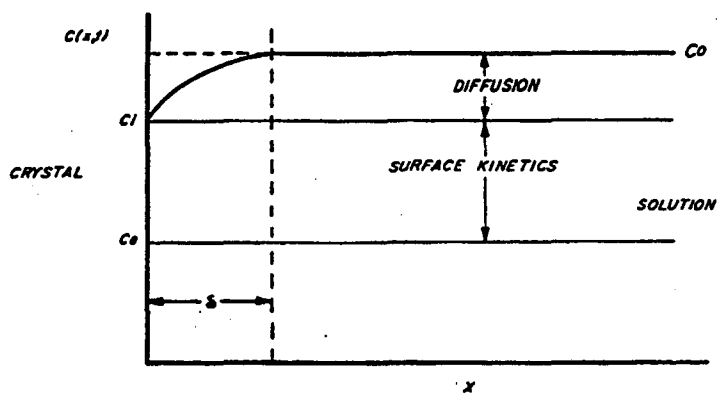

Figure 12. Solution concentration gradients showing the driving forces of diffusion and interfacial kinetics (White and Wood, 1972)

Diffusion-limited growth theory

The simple diffusion-controlled model of LPE growth has been used for the calculation of epilayer growth rate and thickness for a wide range of growth temperatures and growth methods (see for example Oe and Sugiyama, 1978; Tiller and Kang, 1968; Small and Barnes, 1969; Minden, 1970; Rode, 1973).

There are a number of papers that contain a discussion of the calculations and theory in detail including publications by Hsieh (1980); Deitch (1975); Ghez and Giess (1975); Moon (1980); Astles (1990). Only the details of these theories that pertain to LPE growth of GaAs by the supercooling method (combination of step-cooling and ramp-cooling methods) will be reviewed here, since this is the growth method that was used for the research conducted for this thesis. See Appendix III for details of the diffusion-limited growth theory.

The results of the theory will be briefly discussed here. The simplest equation for calculating the epilayer thickness H(t) is derived for short growth times ($Dt/L^2 < 1$, where D is the diffusion coefficient, t is the time, and L is the solution thickness) using a number of assumptions detailed in Appendix III:

$$H(t) = \frac{2}{C_S m}\sqrt{\frac{D}{\pi}}\left(\Delta T t^{1/2} + \frac{2}{3}\alpha t^{3/2}\right) \tag{10}$$

where C_S = concentration of the solute (As) in the solid, m = slope of the liquidus curve, α = cooling rate, ΔT = difference between the temperature at which the solution is saturated with the solute and the temperature at which growth actually begins (supercooling).

When $Dt/L^2 > 1$, C(x,t) becomes fixed and therefore advances at the rate with which the boundary condition changes, i.e., at αt. After long growth times H(t) is

proportional to [αtL - constant] (Moon, 1974). This expression however still requires correction (Malinin and Nevsky, 1978; Malinin *et al.*, 1978).

Hsieh (1980) observed that the experimentally measured thickness of epilayers grown by the ramp-cooled method fell below the calculated thickness after approximately 65 minutes of growth. He pointed out a possible cause based on the observation of precipitates of GaAs on the surface of the growth solution beginning to form at about 30 minutes after the solution and substrate were brought into contact. He found that precipitates were always formed in sufficiently long ramp-cooling experiments, and postulated that this situation occurred because the continuous reduction of the temperature without a significant change in solute concentration at the solution surface eventually caused a degree of supercooling there which exceeded the critical temperature for spontaneous nucleation.

2.3.5 Microscopic Growth Mechanisms

It is important to understand the microscopic mechanisms of LPE growth, in part because these mechanisms are applicable to crystal growth in general (Bauser, 1985).

LPE layers grow by a lateral stepwise growth (LSG) process (Strickland-Constable, 1968; Bennema and Gilmer, 1973; Chernov, 1983; Abe, 1974). In this growth process adatoms or admolecules are attached to the epilayer surface at the edges of steps (Bauser and Rozgonyi, 1980) (Figure 13). As a result, as growth proceeds, the steps move in a "lateral" direction approximately parallel to the epilayer surface. The macroscopic growth of the epilayer, which proceeds in the direction perpendicular to the epilayer surface, arises from a superposition of all lateral step motions (Bauser, 1985).

There are a number of possible growth mechanisms that result in this general LSG process. The dominant growth mechanism will depend on the geometrical

configuration of the steps initially present on the substrate surface (Benz and Bauser, 1980).

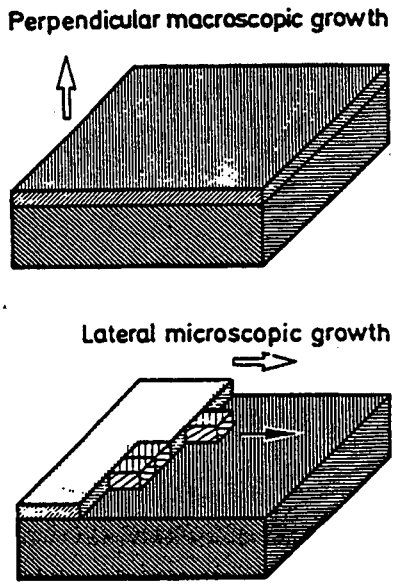

Figure 13. Lateral stepwise growth process (Bauser, 1985)

Therefore, an important parameter of LPE growth is the initial orientation of the substrate surface that exists when epitaxial growth begins. To study the influence of surface misorientation from a low-index plane on layer surface morphology without introducing any other processing variation, E. Bauser evaluated the effect of different misorientations on the same substrate by growing epilayers on GaAs substrates that were oriented parallel to the (100) plane, then spherically-shaped by polishing so that there were a range of misorientations from (100) from 0.05° to 5° present on each substrate. Different surface morphologies on differently-oriented parts of the substrate indicated different growth mechanisms. Figure 14 (Bauser, 1985) gives a schematic cross-section of an LPE layer grown on a spherically-shaped substrate.

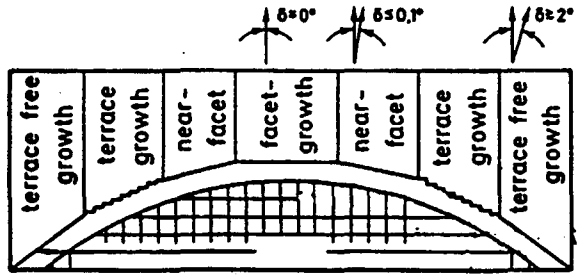

Figure 14. Schematic cross section of spherical GaAs substrate with LPE layer. The misorientation angle δ is exaggerated in this schematic. (Bauser, 1985)

When the substrate misorientation is below about 1' from a low index plane (such as the (100) plane), misorientation steps are absent, and the steps for growth are provided by dislocations which terminate at the substrate surface (Frank, 1949; Burton *et al.*, 1951). Steps originating from dislocations arrange themselves around the dislocations' emergence points in either spirals or closed loops (Bauser, 1985). The steps are usually of minimum possible height, corresponding to a monolayer of the compound (Greene, 1986) and equidistant, and the interstep distances are large compared to the step heights. Surfaces appear extremely flat and mirror-like, and are called "growth facets" by Bauser. Figure 15 shows this type of growth. This process of "**dislocation-controlled facet growth**" is extremely uniform (Bauser and Loechsner, 1981). Impurities are incorporated homogeneously at these types of interfaces because the step height at the interface does not change and the lateral velocity of the steps is always the same (Bauser, 1985).

Growth facet →

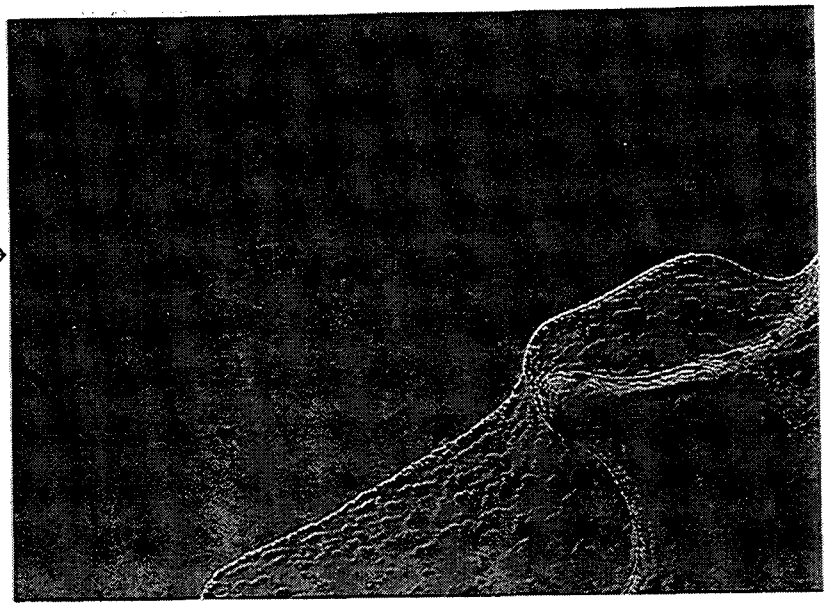

Figure 15. Growth facet, LPE layer 35 (magnification 250X). The photo is of a layer grown for this thesis. The right lower corner of the photo shows a terraced structure for comparison.

If there are no dislocations terminating at the substrate surface, facet growth requires two-dimensional nucleation at high supersaturation (Nishinaga *et al.*, 1983; Mühlbauer and Sirtl, 1974). Nucleation is random, which leads to the formation of steps which may be several monolayers high. Because of this, dopant inhomogeneities may develop and have been reported for silicon melt growth by Witt and Gatos (1966).

The surface morphology of **near-facet** growth is nearly as smooth as surfaces formed during facet growth. Near-facet growth occurs when the substrate misorientation from a low-index plane is between 1' and 6', and occurs in an area between facet growth and terrace growth. Near-facet growth differs from dislocation-controlled facet growth in that the growth steps are "misorientation steps" and therefore are not as regularly distributed as the growth steps originating from dislocation sources.

These "misorientation steps" are at most a few monolayers high. Surface terraces do not develop, even on thick epitaxial layers.

Near-facet growth exhibits far better interface flatness and morphological stability than terrace-free growth, described later (Bauser, 1985).

A **terraced** area will be formed on the epilayer surface if the substrate is misoriented in a range of angles from approximately 0.1 to 2°. Many "misorientation steps" are present on the surface before growth starts. Their density depends on the angle of misorientation. These misorientation steps extend along the intersection lines of the substrate surface and the low index crystal plane [such as (100)] (Bauser *et al.*, 1974). The heights and mutual distances of misorientation steps are randomly distributed. With this starting condition, a step-bunching process may occur during formation of the layer (Bennema and Gilmer, 1973). This is schematically shown in Figure 16, and occurs because as growth units attach to the step ledges, the steps with smaller height will grow faster than the steps with larger height. This difference in growth rates will cause a "bunching" up of the steps, which causes an increase in the average height and distance of steps at the epilayer interface. Due to this increase in height and distance, the steps become easily visible on the surface of thick LPE layers and are usually referred to as surface terraces or rippled structures (Benz and Bauser, 1980). Figure 17 shows the typical terraced structure observed on the surface of LPE layers.

A surface terrace consists of a flat tread and a steep riser (Figure 18). Surface terraces are one of the most common defects in LPE growth and they may lead to severe dopant inhomogeneities (Bauser and Rozgonyi, 1980).

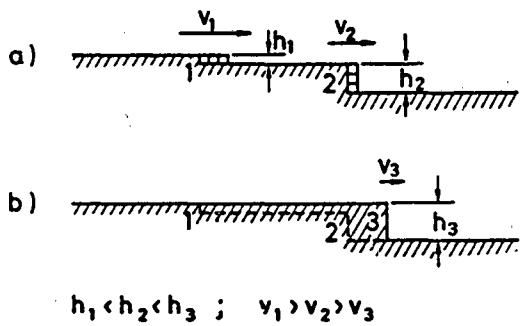

Figure 16. Process of step bunching (simplified). (a) Steps 1 and 2 move laterally by attachment of new molecules at their edges. Lateral velocity $v \sim h^{-1}$. (b) Step 1 catches up with step 2 and advances to position 3. Note that $v_3 < v_2 < v_1$. (Bauser, 1985)

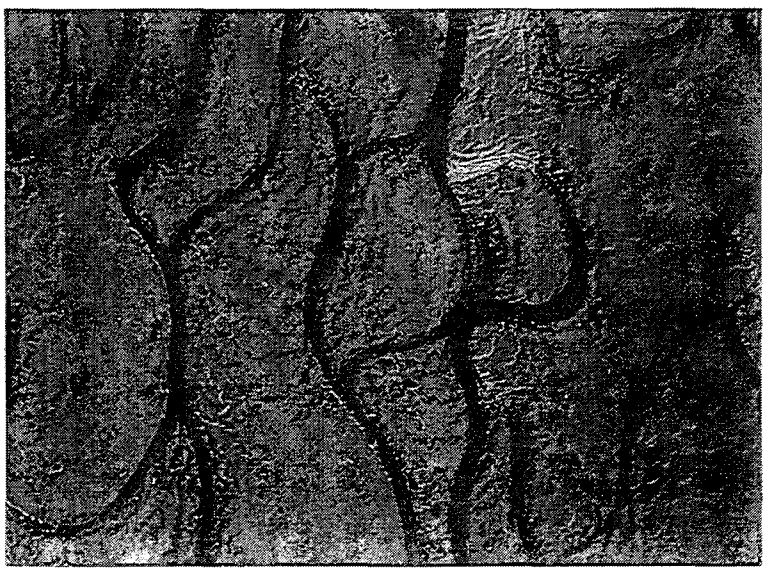

Figure 17. Terraced structure, LPE layer 35 (magnification 250X).

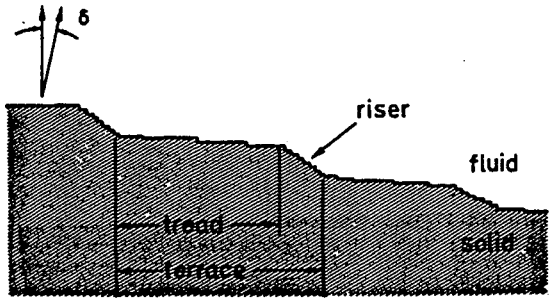

Figure 18. Profile of a terraced growth interface. The angle δ denotes the average misorientation of the growth interface and the initial substrate misorientation in epitaxial growth. (Bauser, 1985)

The terraces will disappear when the substrate misorientation exceeds a "critical" value of more than about 2°. Bauser calls the corresponding mechanism **terrace-free growth.** According to a theory by Rode (1975), a critical orientation of the substrate exists which prevents the formation of terraces during epitaxial growth. Angles for the critical misorientation are expected to cover the range of up to several degrees and they should increase with greater layer thickness (Benz and Bauser, 1980). According to Rode's theory, the surfaces of thick layers grown on critically oriented substrates exhibit a long wavelength sinusoidal structure.

2.3.6 Influence of Impurity Concentration on Epilayer Surface Morphology

After growing epilayers with varying impurity concentrations, I have observed that the epilayer surface is smoother for layers with higher impurity concentrations and becomes rougher as the impurity concentration decreases.

A reduction of terracing on III-V LPE layer surfaces with increased impurity concentration has been observed by other researchers also [for example E. Bauser *et al.*, 1978 (GaAs); Y.Z. Liu, 1978 (InP); Kajimura *et al.*, 1977 (GaP)]. Impurity

concentration has a strong effect on surface terracing, greater than that due to temperature gradients or supersaturation (Benz and Bauser, 1980).

The models for the smoothing effect due to the presence of impurity atoms are still under discussion. Kajimura *et al.* (1977), Fischer *et al.* (1978), and Bauser *et al.* (1978), show that for GaP and GaAs impurities tend to segregate preferentially at the risers (see Figure 19), which may support a model described by Chernov (1974). According to Chernov, small steps are usually generated at the bases of macrosteps (terraces), and it is probable that the presence of impurities enhances the generation of these small steps. The average terrace height may therefore be continuously reduced when high impurity concentrations are present. Bauser used spatially resolved photoluminescence spectra to show that impurities are preferentially incorporated at the risers of high terraces (Benz and Bauser, 1980).

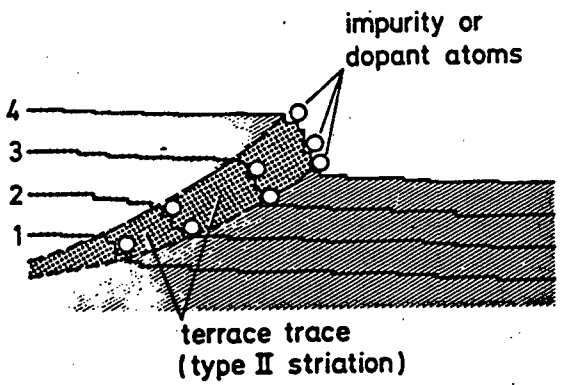

Figure 19. Development of a growth terrace. The positions of the liquid-solid interface at four time intervals 1 - 4 are noted on the figure. The lateral velocity of the terrace decreases as its height increases. The probability of impurity and dopant atoms being incorporated into the crystal is higher at the steeply stepped riser portion of the terrace than on the smooth terrace tread. Terrace risers therefore cause traces of increased impurity concentration, denoted as type II striations, in the material. (Bauser, 1985)

However, Liu (1978) suspected that the preferential segregation of impurities with respect to terraces is not related to the smoothing effect caused by impurities. Liu speculated that the impurity atoms incorporated into the solid more or less uniformly in

the presence of terraces. Liu's model for the smoothing effect due to the dopant atoms is as follows. The wavelength of the terrace (tread plus riser lengths) is governed by the density of nucleation centers. Because the impurity atoms have different bond configurations from that of the host atom, they act as nucleation centers which promote lateral growth from the impurity site. In the initial phase of the growth from a doped melt, since there are more nucleation centers on the substrate, the terraces will be closely spaced and and their height reduced, which accounts for the smoothing effect due to doping. Liu observed that even after a heavily terraced growth interface is established, such as on an undoped layer, the growth of the doped layer on top of it will smooth out the terraced growth interface.

The micrographs of Figure 20 show the surface morphologies of two GaAs epilayers with different impurity concentrations grown for this thesis. The terraces of the epilayer with the higher impurity concentration (Figure 20b) are both smoother and narrower than the terraces of the epilayer with the lower impurity concentration (Figure 20a). This change in surface morphology supports Liu's model that impurity atoms form nucleation centers on the treads of the terraces as well as at the risers.

Appendix II also discusses how the electrical properties of the epilayer (such as the Fermi level) affect the incorporation of impurity atoms into the growing epilayer.

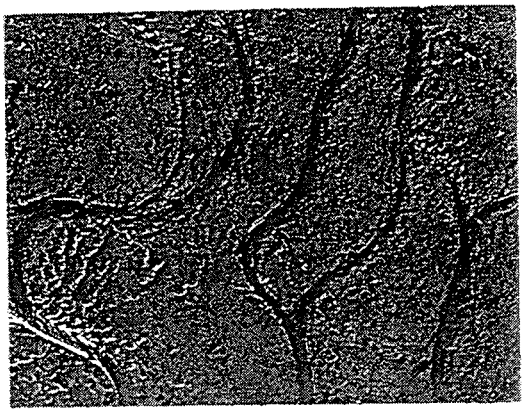

a) Layer 35, n = 7×10^{14} cm^{-3}

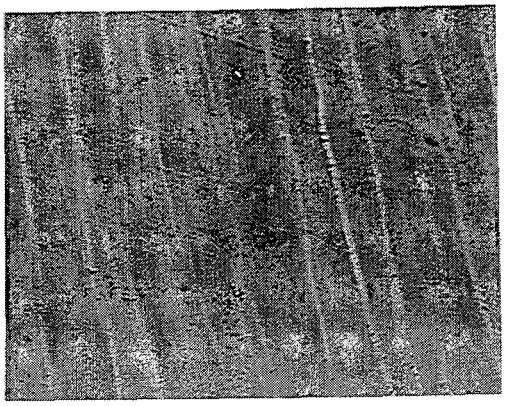

b) Layer 38, n = 1×10^{16} cm^{-3}

Figure 20. Surface morphologies of LPE layers with different impurity concentrations (both micrographs, magnification 250X)

2.3.7 Influence of Constitutional Supercooling on Layer Surface Morphology

In the past, several researchers have attributed the often rough surface morphology of LPE epilayers to the effect of constitutional supercooling, which can also be observed in melt-grown crystals (Astles, 1990). For any impurity with segregation coefficient $k \neq 1$, a concentration gradient will develop between the solid-liquid interface and the bulk solution as the crystal or epilayer grows. This concentration gradient produces a change in the solution melting temperature near the solid-liquid interface. For example, for a solution of As in Ga the As is depleted near the interface and the melting temperature is lowered (see Figure 21).

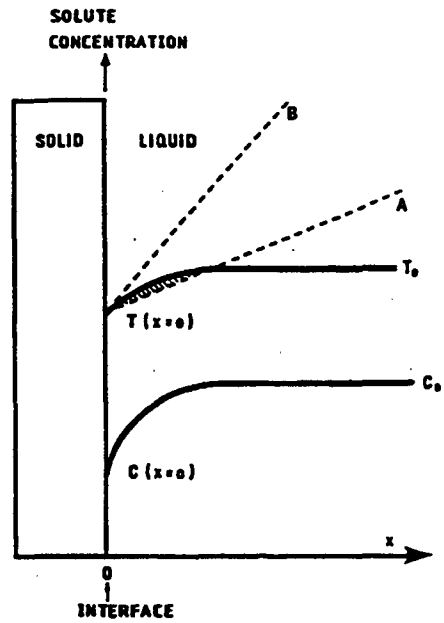

Figure 21. Solute concentration C, as a function of distance x from the solid-liquid interface, and the corresponding profile of liquidus temperature. Lines A and B represent low and high interface temperature gradient respectively, with a region of constitutionally supercooled liquid. (Astles, 1990)

If there is a small or zero temperature gradient in the solution (temperature increasing into the solution from the interface), there will be a region of the solution in front of the interface which becomes supersaturated with As -- this region is "constitutionally supercooled" (see for example, the shaded region in Figure 21 between line A and T_0). Imposing a steep enough temperature gradient (such as line B in Figure 21) will remove this region of constitutional supercooling. Crossley and Small (1973) have suggested that the effects of constitutional supercooling should not be seen in the nucleation stage of the epilayer, when the concentration gradient at the growth interface is small. The LPE substrate-epilayer interface generally appears very smooth which suggests that even if constitutional supercooling has occurred, it has no detrimental effect on epilayer deposition at the beginning of growth (Hsieh, 1980).

As stated previously, for long growth times GaAs crystallizes at the solution surface as well as at the growth interface. Minden (1970) states that measurements of epilayer thicknesses show that far more GaAs crystallizes homogeneously in the bulk of the solution than epitaxially on the substrate. This homogeneous crystallization tends to deplete the melt of arsenic and prevents constitutional supercooling until an appreciable layer thickness is grown.

However, as the furnace cools during an LPE growth run (for example for ramp-cooled growth), the temperature gradient in the furnace eventually tends to zero while the temperature gradient required to prevent constitutional supercooling increases. The effects of constitutional supercooling will eventually become significant and the solid-liquid interface will become spatially unstable (Tiller, 1968). It is this condition that causes the uneven surface quality of solution-grown epilayers. The epilayers often also have Ga inclusions near the surface (Minden, 1970). The criterion Minden used for interface stability is

$$\frac{\partial T}{\partial x} \geq \frac{\partial C}{\partial x}\frac{dT}{dC}, \tag{11}$$

where dT/dC = m is the slope of the liquidus line.

This effect of constitutional supercooling is observed on the surfaces of GaAs epilayers grown for this thesis. For example, in Figure 22 solvent inclusions are exhibited on the surface of a representative LPE layer.

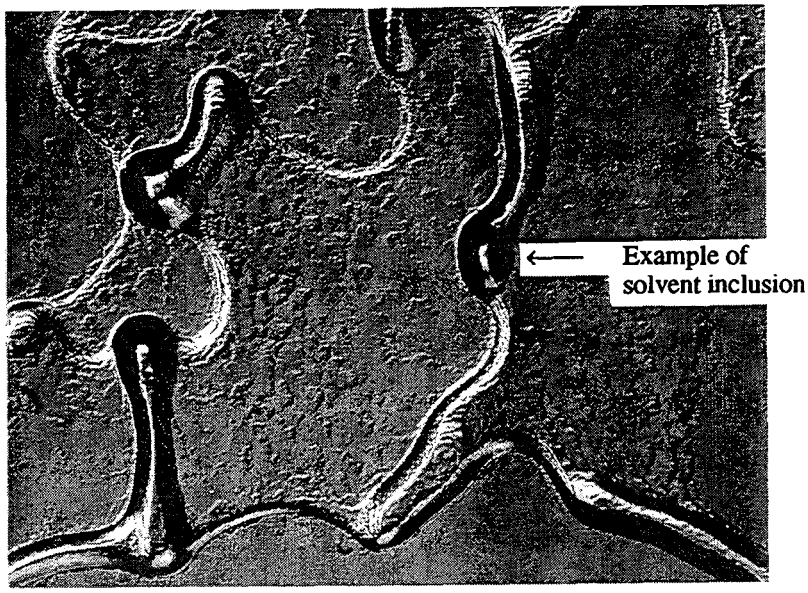

Figure 22. Solvent inclusions on the surface of LPE layer 35 (magnification 250X).

2.3.8 LPE Growth Apparatus for III-V Compound Epilayers.

A wide variety of methods have been developed to implement the LPE process for the growth of III-V epilayers, including variations in both the process method and equipment design (Moon, 1980). The growth systems which are used for LPE are generally of either horizontal or vertical type with each having certain advantages. Both techniques are used for the growth of III-V epilayers.

The process of LPE can be considered to consist of four stages (Greene, 1986). The first stage is the production of a solution composed of a solvent saturated at a growth temperature T_g with an amount of solute determined by the corresponding equilibrium temperature on the liquidus of the binary (solvent-solute) phase diagram of interest. The solution is generally heated to a T_{sat} of between 1 and 20 °C above T_g to ensure that the solute completely dissolves in the solvent. The second stage is the production of a supersaturation of solute in the solvent, as discussed previously. The

third stage is bringing the solution and substrate into contact, and either cooling the saturated solution in a controlled manner for the time needed to grow the epilayer thickness required (transient growth methods), or by keeping the substrate and solute in contact with the solution for the time needed for the epilayer thickness required (constant-temperature-gradient growth). The fourth stage is ending the growth by separating the solution from the epilayer. The main components of an LPE system are a well-controlled furnace, a growth chamber that can provide the necessary ambient for epilayer growth [and can keep the substrate and solution (contained in a boat or crucible) at a particular position within the furnace], a gas-handling system with purifier, and a pumping system for evacuating the growth chamber.

Tipping, dipping, and sliding are the three main techniques that have been used to establish/terminate contact between the solution and substrate (Hsieh, 1980). The first growth systems used were the tipping device (Nelson, 1963) and the dipping device (Rupprecht *et al.*, 1967). Both systems have been found appropriate for growing single, reasonably homogeneous epilayers of many III-V compounds (Bauser and Benz, 1980). The original tipping and dipping systems have since been modified to permit multi-substrate or multilayer growth (see for example Saul and Roccasecca, 1973; Verleur and Moest, 1973; Scheel, 1977). See Appendix IV for a description of the different LPE system configurations.

Modifications of the LPE equipment and process have been made by many researchers to solve one or more of the above problems. A variation of the original tilting furnace method has been described by Mitsuhata (1970), André and Le Duc (1972), (Deitch, 1975) and Bauser (1985) . In this variation, the growth boat is rotated about a horizontal axis to bring the solution and substrate into contact (so the furnace is not tilted). This arrangement leads to more stable thermal conditions. This type of

system is used for the LPE growth performed for this thesis, and will be discussed in detail in Section 2.4.

2.3.9 Choice of System and Growth Materials For LPE Growth.

There are a number of important aspects of a LPE growth system which must be considered, for both the LPE process itself and for high purity epilayer growth. Appendix V gives the criteria for selection of the various growth materials and LPE system components including the solution materials, growth boat, process chamber, growth atmosphere, gas delivery system, and furnace design.

2.4 LPE of Pure Epilayers of GaAs By the Tipping Boat Method

2.4.1 Apparatus.

The tipping boat LPE system used for the work conducted for this thesis is shown in the drawing of Figure 23 and in the photograph of Figure 24. The main components of the system as it currently exists are as follows:

The process chamber is a 6.0 cm inner diameter (I.D.) X 6.4 cm outer diameter (O.D.) silica tube, approx. 1.4 m long[1]. The process tube is necked down to a 2.5 cm-long, 0.34 cm I.D. X 0.64 cm O.D. tube at one end. This 0.34 X 0.64 cm silica tube is connected to a 1/4-inch O.D. type 304 stainless steel gas line, using a type 316 stainless steel glass-to-metal seal[2] which includes DuPont Kalrez sulfur-free O-rings[3]. A specially-designed seal connects the other end of the process chamber to the pump tee (see Fig 23) which leads to the pumping system. This seal consists basically of two viton[4] O-rings with a space between them which is pumped out separately from the

---

[1]Semiconductor-grade G.E. 214 silica tubes and G.E. 124 silica rods, from G.M. Associates, Hayward, CA
[2]Cajon "UltraTorr" glass-to-metal seal from Oakland Valve and Fitting, Oakland, CA
[3]DuPont Kalrez sulfur-free O-rings from Bay Seal Co., Hayward, CA
[4]From Bay Seal Co., Hayward, CA

main chamber (i.e a differentially-pumped seal), to minimize the possibility of a hydrogen leak from the process chamber to the room.

A 1.0 cm I.D. X 1.6 cm O.D. silica cantilevered tube[1] extends inside through the middle of the process chamber, and the end of the tube inside the process chamber is sealed. This tube is attached to the pump tee which leads to the pumping system (see Figure 23) with a differentially-pumped seal, similar in construction to the seal described above.

The ultrapure graphite boat in which epilayer growth occurs[5] has an indentation which allows it to fit onto the end of the silica cantilevered tube inside the process chamber.

The process chamber is heated by a three-zone tubular resistance furnace[6] incorporating Kanthal A-1 resistance wire and type R thermocouples.

Type 304 1/4-inch O.D. stainless steel tubing and type 321 stainless steel flexible hose is exclusively used to deliver gases to the process chamber from the hydrogen purifier and argon cylinder and from the process chamber to the exhaust. The stainless steel tubing received a hot solvent clean inside and out (as did all the stainless steel connections and components), after which it was kept wrapped in oil-free aluminum foil until assembly with glove-protected hands. After assembly, the stainless steel tubing was heated with a hand-held hot air gun while the process gas was flowing.

Type 316 stainess steel high-vacuum fittings[7] connect the stainless steel tubing from the gas sources to the process chamber and from the process chamber to the exhaust. Type 316 stainless steel metering valves[8] are used to control the flow of process gases into the process chamber.

---

[5]Ultrapure graphite boat and other graphite boat components supplied from Carbone of America, Ultracarbon Division, Bay City, Michigan
[6]Marshall three-zone resistance furnace by Thermcraft, Winston-Salem, NC, model 1046-32
[7]Cajon VCR fittings from Oakland Valve and Fitting, Oakland, CA
[8]Nupro micrometer needle valve, from Oakland Valve and Fitting, Oakland, CA, part # SS4BMRG, VCR

The process chamber is evacuated via a turbomolecular pump[9], backed by a roughing pump[10]. The pumping system controller (Balzers/Pfeiffer model TCP 380) controls the simultaneous roughing pump on/ turbomolecular pump windup to minimize backstreaming of hydrocarbon vapors from the roughing pump. An isolation valve[11] (which isolates and vents the roughing pump in the event of a power out condition) and a molecular sieve oil vapor trap[12] further reduce the possibility of oil vapor contamination of the LPE system during pump-down.

The differentially-pumped seals are evacuated via a roughing pump[13] which is separate from the process chamber roughing pump. A low flow of dry nitrogen is fed into both roughing pumps to minimize oil vapor backstreaming.

The hydrogen process gas is purified by diffusing it through the Pd-Ag cell of a hydrogen purifier[14] prior to entering the gas line to the process chamber. As described in Appendix V, hydrogen is used as the process gas because it reduces oxides on the substrate and solution surfaces, providing intimate substrate-solution contact during epilayer growth. The argon gas (used as a purge gas) is research grade[15] (5-9's pure). The process gas flow is monitored by a flowmeter[16] on the vent side of the process chamber.

---

[9]Balzers/Pfeiffer turbomolecular pump, Hudson, NH, model TPH 170
[10]Alcatel direct drive pump, refurbished, from Pumps International, Morgan Hill, CA, model # 2008A
[11]Auto Isolation valve (Vacuum Sentry), HPS Div. of MKS Instruments, Boulder, CO, part # 145- 0025K-120 V/60 Hz
[12]MDC Vacuum Products Corp., Hayward, CA, model KMST-100-2
[13]Duo Seal vacuum pump, W. M. Welch Mfg. Co., Chicago, IL, Ser. # 37095-0
[14]Engelhard Industries Gas Equipment Div., Newark, NJ, model 20-150D
[15]From Air Products, Allentown, NJ, purity of 5-9's +
[16]Porter Instrument Co., Hatfield, PA

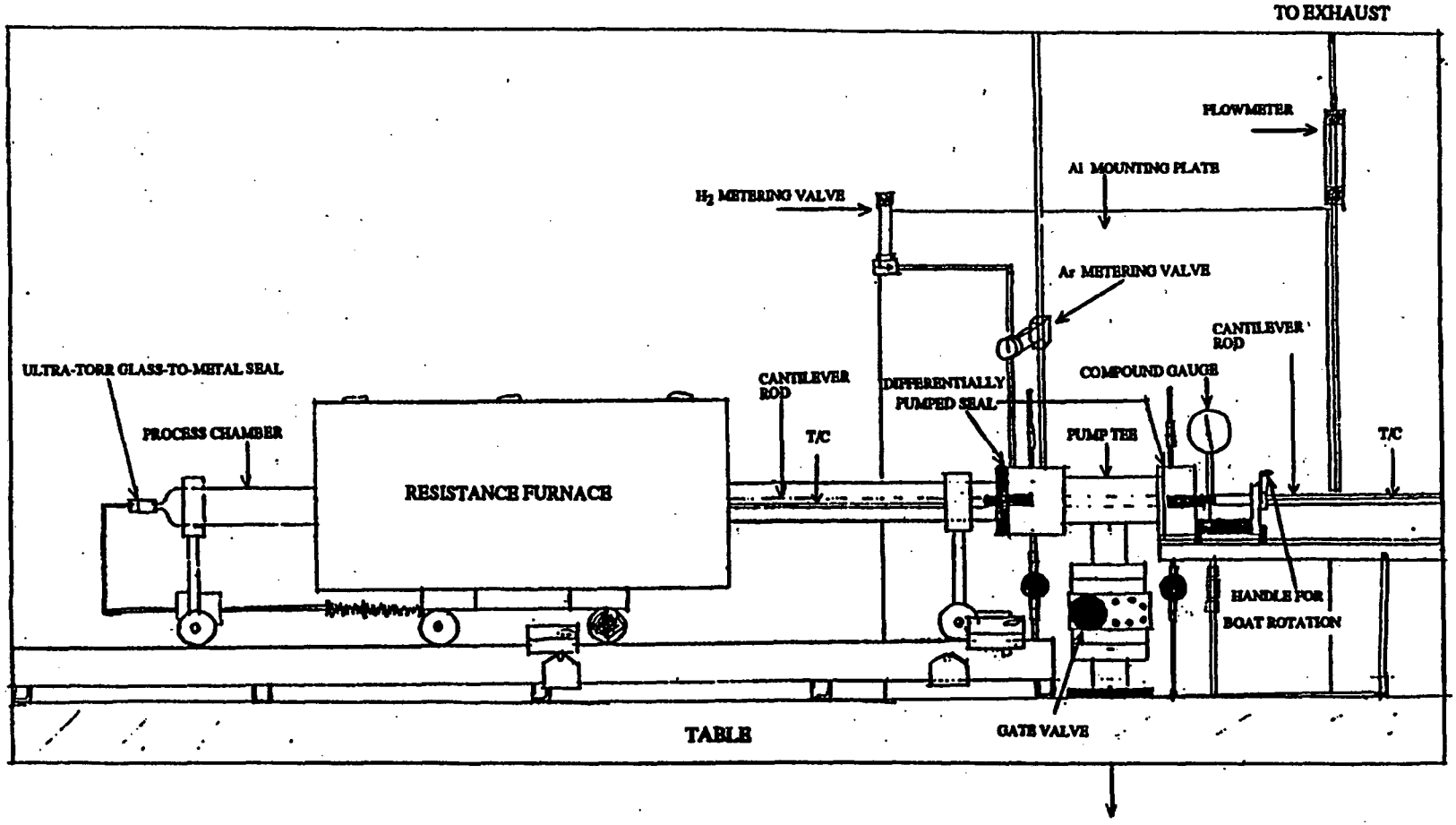

Figure 23. Schematic of LPE Growth System

PUMPING SYSTEM:
TURBOMOLECULAR PUMP, BACKED BY
ALCATEL DIRECT-DRIVE ROUGHING PUMP

Side view →

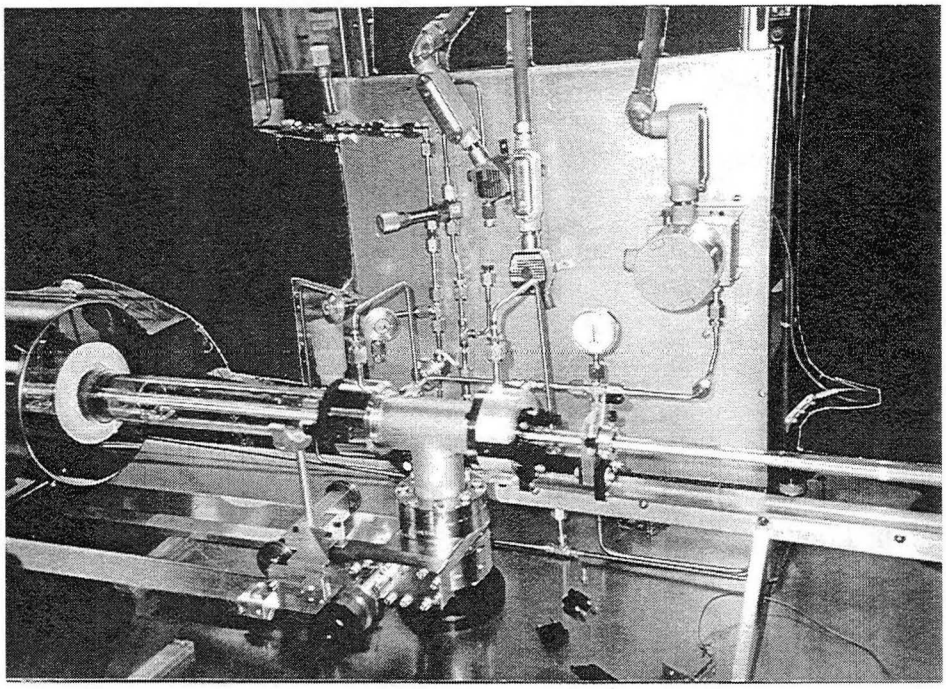

Top view →

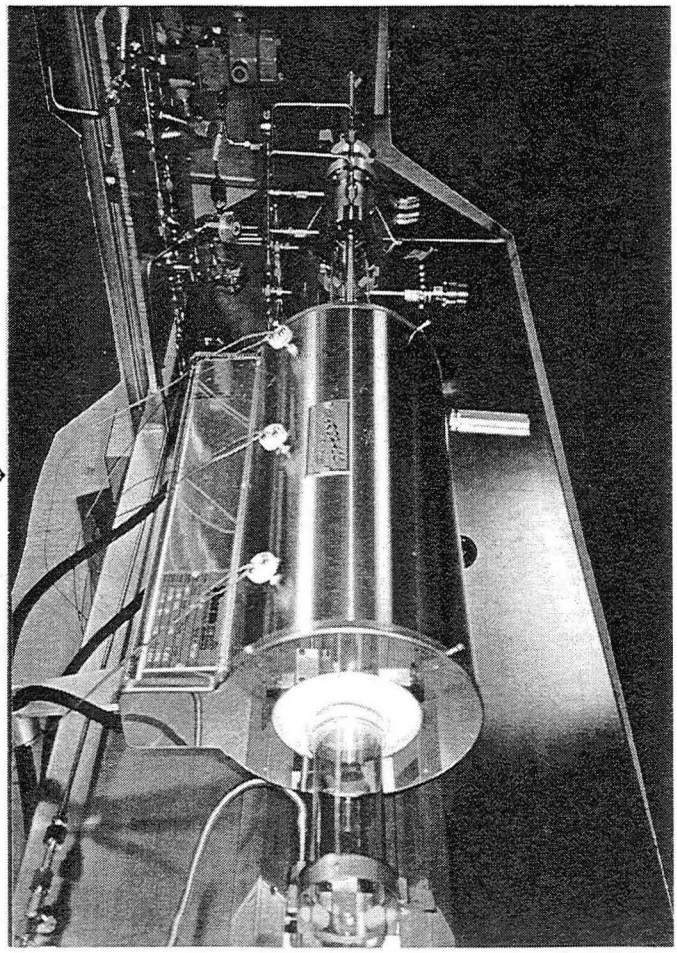

Figure 24. Photographs of LPE system: side view, top view

2.4.2. Preparation of Process Chamber and Graphite Components

Note that protective gloves[17] are always worn when handling any part of the LPE system or growth materials. Such gloves protect the human operator from corrosive and toxic chemicals but also isolate the crystal growth system from impurities.

The silica components of the process system are etched in (3:1) HF : HNO_3[18] to remove organic contaminants, rinsed with D.D.I. (distilled and de-ionized) water, etched with HCl[19] to remove metal contaminants, rinsed with D.D.I. water, rinsed with distilled methanol[20], blow-dried with dried nitrogen, vacuum-baked in-situ at 950 °C, and baked at approximately 850 °C with flowing hydrogen prior to epilayer growth.

The ultrapure graphite boat (along with any other graphite components to be used in the epilayer growth process), is received from the supplier purified to a residual impurity level of 5 ppm (procedure described in Appendix V), and then baked in the LPE system at 950 °C at a pressure of 10^{-6} torr or below for extended periods of time (discussed further in Section 3.1.3). Ga is then placed in the boat, and it is baked in flowing hydrogen in the process chamber at approximately 850 °C for approximately 5 hours before use for layer growth.

---

[17]CLV-100 washed vinyl gloves, Oak Technical Co., Stow, Ohio; or Hypoclean 100 latex gloves from Safeskin, San Diego, CA

[18]HF is Mallinkrodt Transistar Grade, HNO_3 is J T Baker VLSI Low Particulate Grade

[19]HCl is J T Baker Electronic Grade

[20]Methanol is J T Baker Low Sodium CMOS Grade, distilled in-house

2.4.3 Choice and Preparation of the Substrate and Solution Materials

2.4.3.1 GaAs substrates

All chemical operations are performed in Teflon PTFE (polytetrafluoroethylene) evaporating dishes[21], with Teflon PFA (perfluoroalkoxyl) tweezers[22], and a Teflon PFA graduated cylinder[21]. When these items were purchased they were dedicated exclusively to GaAs LPE processing. All chemical operations are carried out in a laminar flow hood.

The orientation of GaAs substrates used for the layer growth is (100), which allowed square samples of approximately 1 cm^2 to be easily cleaved along (110) planes (using a scriber with a tungsten carbide tip[23]) from purchased semi-insulating or conducting wafers. The substrate wafers were received optically polished from the supplier. Specifications of the substrates are listed in Table 2. Substrate suppliers utilized are Sumitomo[24] (semi-insulating wafers), and American Xtal Technology (AXT)[25] (semi-insulating and conductive wafers). The conductive wafers were n-type, Si-doped, with carrier concentrations in the 10^{16} and 10^{17} cm^{-3} ranges. Wafers were purchased from these suppliers because they could meet the substrate orientation specification required for this project ((100) +/- 0.05°) to ensure terrace-free growth conditions. The substrate was prepared for layer growth by etching in hot HCl for approximately 1/2 hour to remove surface oxides, rinsing in D.D.I. water, immersing in hot distilled methanol, and air drying just before loading into the graphite boat.

---

[21]Cole-Parmer Instrument Company, Vernon Hills, Illinois
[22]Fluoroware, Inc., Chaska, MN
[23]VWR Scientific, San Francisco, CA
[24]Sumitomo wafers supplied by Semia, Inc., San Francisco, CA
[25]American Xtal Technology, Fremont, CA

TABLE 2: Selected characteristics of semi-insulating and doped GaAs wafers used for LPE

Wafer type	Dopant	Carrier Concentr. (cm^{-3})	Resistivity (Room T.) (Ω-cm)	Mobility (Room T.) ($cm^2/V.s$)	Etch Pit Density (cm^{-2})	Orientation
Undoped (source)	None (C-contr.)	---	> $1x10^7$	~ 7000	~ $(1\text{-}5)x10^4$ (LEC)*	(100)+/- 0.05°
Doped (sub.)	Si	$(3\text{-}5)x10^{17}$	$(4\text{-}6)x10^{-3}$	2500-2700	< 1000 (VGF)*	(100)+/- 0.05°
Doped (sub.)	Si	$2x10^{16}$	$(7\text{-}9)x10^{-2}$	5000-5100	< 2500 (VGF)*	(100)+/- 0.05°

* Crystal growth methods: LEC = Liquid Encapsulated Czochralski
VGF = Vertical Gradient Freeze

2.4.3.2 GaAs used for the growth solution

The following preparation steps were followed for dissolving the GaAs material into the gallium to created the solution ("source GaAs"):

- Weigh out of sufficient GaAs to saturate the gallium solution with arsenic at the chosen growth temperature
- Etching in hot HCl for 1/2 hour;
- Rinsing in D.D.I. water
- Etching in (3:1) H_2SO_4 : H_2O_2[26] at 50 °C, for 2-5 minutes each side
- Rinsing with D.D.I. water
- Immersing in hot distilled methanol
- Air drying

Enough GaAs for several epilayer growth runs is generally prepared at one time, and stored in a laminar-flow hood in a PTFE evaporating dish covered with a cleaned and etched pyrex lid. This prepared GaAs is etched in hot HCl, rinsed with D.D.I.

[26] H_2SO_4 is J T Baker VLSI Low Particulate Grade, H_2O_2 is General Chemical Particulo Grade

water, immersed in hot distilled methanol, and air dried just before loading into the graphite boat for epilayer growth.

To determine the effect of the starting materials on epilayer purity, undoped GaAs source material were evaluated from Laser Diode[27], M/A COM[28], Freiberg[29], and from AXT[25]. All of these sources of GaAs produced epilayers with similar purity.

2.4.3.3 Gallium used for the growth solution

Rhône-Poulenc[30] supplies the purest Ga (in ingot form) commercially available, 8-9's pure, and so is the supplier of choice for high-purity epilayer growth. Several methods of processing the Ga were evaluated to determine if any further improvement in epilayer purity could be realized, including: no processing of the gallium -- straight from the packaging to the graphite boat; rinsing the gallium ingot in distilled methanol, blow-dry with dry nitrogen before loading into the boat; etching the gallium with HCl before loading into the graphite boat (this was tried with a sample of 7-9's pure Ga[31]). None of these gallium treatments resulted in a superior epilayer purity, so the gallium is not processed before loading into the graphite boat.

2.4.4 Epilayer Growth Procedure:

The epitaxial layers were grown under a variety of conditions:

- Beginning growth temperatures varied from 500 - 850 °C
- Cooling rates ranged from 0.45 - 3 °C per minute

---

[27]Laser Diode, Inc., Metuchen, NJ
[28]M/A COM, Lowell, MA
[29]Supplied from Dr. E. Bauser's laboratory at the Max-Planck-Institute
[30]Rhone-Poulenc, Shelton, CT
[31]Johnson-Matthey /Alfa, Ward Hill, MA

- One-day growth of the layers vs. two-day (one day for solution preparation and the next day for layer growth)
- Bake time of the solution materials and substrate in the graphite boat from 3 to 29 hours

The initial epilayer growth conditions were adapted from Dr. E. Bauser's LPE growth conditions at the Max-Planck-Institute in Stuttgart, Germany. Layer growth is accomplished by clamping the GaAs substrate on one side of the graphite boat, placing the Ga and GaAs for the solution into the other side of the boat (see Figure 25). The graphite boat is then attached to the end of the cantilevered rod, and rotated slightly via a handle to keep the solution materials away from the substrate. The boat/rod assembly is then pushed into the process tube. Any components that go into the hot zone of the process chamber are handled with Texwipe TX1010 cleanroom wipers[32] in addition to wearing gloves. All seals are tightened, and the process chamber is pumped to the low 10^{-6} torr range. The process chamber is filled with hydrogen and pumped out to the low 10^{-6} torr range again. This double pump-out is performed to ensure that all air has been removed from the chamber. The temperature inside the process chamber is ramped up to at least 300 ^{o}C while the system is pumped out to ensure all water vapor adsorbed when the system is open to the atmosphere is removed. The chamber is then filled with hydrogen to approximately 1/3 psi above atmospheric pressure. The maximum pressure in the process chamber is controlled by a check valve[33] which opens at 1/3 psi above atmospheric pressure. Keeping the hydrogen pressure in the process chamber above atmospheric pressure prevents air from getting into the chamber in the event of an air leak, which could produce an explosive situation when mixed with the hydrogen. Any air leak would also introduce impurities into the growing epilayer.

---

[32]The Texwipe company, Upper Saddle River, NJ
[33]Nupro "C" series poppet check valve, supplied by Oakland Valve and Fitting, Oakland, CA

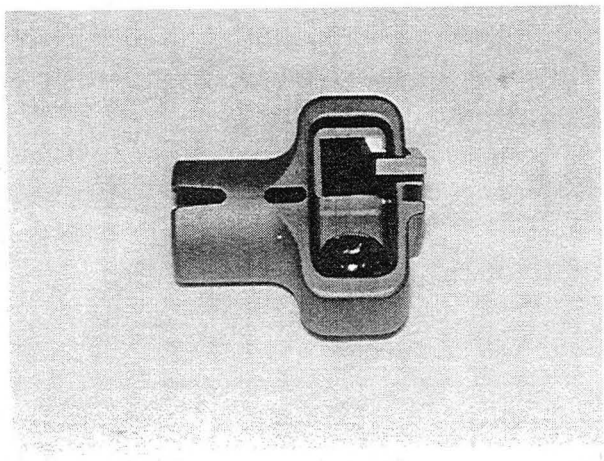

Figure 25. Graphite boat containing substrate and solution.

The furnace temperature is then ramped up to the growth temperature. The standard time the furnace is maintained at the growth temperature is four hours. This time is needed to dissolve and homogenize the solid GaAs in the gallium, and to remove volatile impurities from the solution. At the end of the bake-out time, a controlled-rate cooling program is started. When the solution has cooled for approximately 2 ^{o}C the cantilevered rod is then rotated via a handle so that the boat also rotates and the solution is poured over the substrate. The system continues on the controlled cooling program until growth is terminated, generally at 100 ^{o}C or below. Figure 26 illustrates the generalized heating schedule and corresponding graphite boat/growth material positions.

When the growth is to be terminated, the flow of hydrogen is stopped and the flow of argon purge gas is started. Argon is flowed at approximately one liter/min. for approximately one hour through the process chamber before the LPE system is opened.

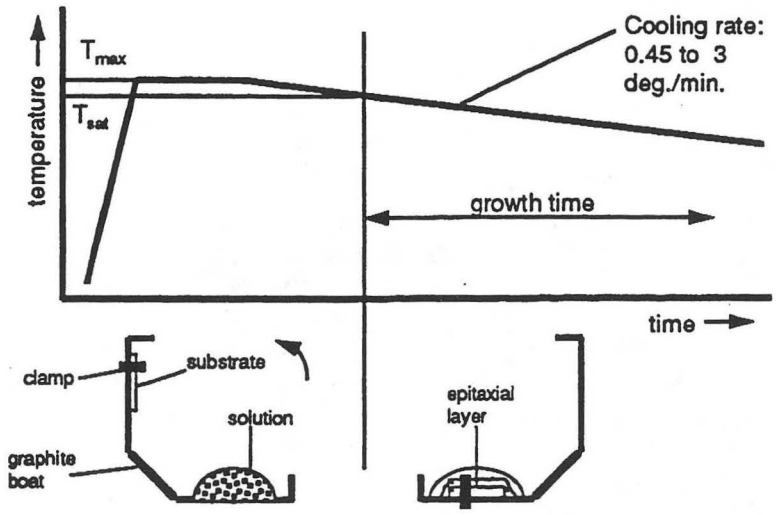

Figure 26. Schematic of the temperature profile and graphite boat positions during one growth cycle.

When the system is opened and the growth materials are removed, the solution must be manually removed from the substrate, because during the course of cooling a crust of GaAs forms on the solution surface. The remaining solution is wiped off the layer with a Q-tip while the solution/epilayer/substrate is immersed in hot distilled methanol. The epilayer is then etched in hot HCl to remove any remaining Ga.

The effect of the beginning growth temperature on the final epilayer thickness was investigated. It was found that for growth temperatures below 600 °C, epilayer growth on the substrate was "spotty", indicating that not all of the oxide had been removed from the substrate and/or solution surface before the solution was flowed over the substrate and epilayer growth began. At 600 °C and above, the epilayer thickness increased with growth temperature: approximately 5 μm at 600 °C, 30 μm at 750 °C, 50-60 μm at 800 °C.

3.0 EPILAYER CHARACTERIZATION

3.1 Electrical Characterization

3.1.1 Common Residual Impurities in High Purity GaAs LPE Layers

The four major sources of impurities in the case of LPE originate from the solution materials (Ga and GaAs), emanate from the graphite boat, reside in the H_2 process gas, and are the result of reactions between gases and materials in the growth system at the temperatures at which LPE growth takes place (Astles 1990).

In the case of GaAs epilayers grown from Ga solutions, the most common impurities are generally C (shallow acceptor), O (deep donor), Si (shallow donor or acceptor) (for example see Soloman, 1968; Hicks and Greene, 1970; Otsubo *et al.*, 1973; Skromme *et al.*, 1982; Shealy and Woodall, 1982), and S (shallow donor) (Greene, 1986).

Appendix VII lists the most common impurities detected in high purity LPE GaAs and which materials in the growth system are sources of these impurities.

3.1.2 Hall Effect Measurements

The characterization technique generally used to determine the carrier concentration and mobility of the epilayers is combined measurement of the Hall effect and the resistivity.

The Hall coefficient measurement made with the van der Pauw method (van der Pauw, 1958) is one of the most frequently used electrical measurements to determine the average concentrations of electrically active impurities in LPE layers (Hsieh, 1980). In order to perform this measurement on an epilayer on a substrate, the epilayer must be electrically isolated from the substrate. This can be achieved by either growing the

epilayer on a substrate of the opposite conductivity type so that a p-n junction is formed at the interface (junction isolation), or by using a high resistivity substrate. In the work conducted for this thesis, epilayers were grown on semi-insulating GaAs substrates.

As described in more detail in Appendix VIII, the sign of the Hall coefficient indicates whether the epilayer is n- or p-type, and the magnitude gives the net carrier concentration, which is equal to the difference between the concentration of the donors and acceptors.

Ohmic contacts (as small as possible) are made on the epilayer surface at the four corners of a square sample. These same contacts are used for resistivity measurements, making it possible to determine the mobility of the carriers as well as their concentration. An analysis to identify the particular impurities can be made by complementary analysis techniques, which will be discussed in Section 3.1.3.

A Hall set up with a van der Pauw sample geometry and a 100G magnetic induction was used for the measurements. Room temperature and 77 K Hall voltage and resistivity measurements were performed to determine the carrier concentration (net impurity concentration) and mobility of each epilayer. The measurements at 77 K were made for comparison, because these measurements should be less affected by phonon scattering and therefore be more sensitive to compensation (ionized impurity scattering).

The LPE reactor was used to grow a series of GaAs epilayers. It should be noted that all epilayers grown using this LPE reactor are n-type. Hall Effect analysis showed that the first series of epilayers contained a net donor concentration in the range of 10^{16} cm^{-3}. Since the desired impurity concentration is approximately $5x10^{12}$ cm^{-3}, the source of the donor contamination in the LPE system had to be determined, so that it could be eliminated from the growth system. Since many of the shallow donors in GaAs have very similar electron binding energies (differing on the order of 0.1 meV), variable-temperature Hall effect measurements do not allow us to distinguish between

the shallow donor binding energies. Therefore, additional characterization methods were required to determine the identity of the donor impurities.

3.1.3 Identification and Elimination of Chemical Impurities in the Epilayers

Secondary Ion Mass Spectroscopy (SIMS) was performed on a representative epilayer with 10^{16} cm^{-3} net donor concentration and revealed that sulfur was a major contaminant. These results were confirmed with Photothermal Ionization Spectroscopy (PTIS). Figure 27 shows that sulfur and silicon were identified as the major donor impurities, using PTIS. See Appendix IX for a brief description of SIMS analysis, and Appendix X for a discussion of PTIS.

After these initial results, the growth system was modified to remove any possible sources of sulfur. The viton O-rings on the gas inlet side of the LPE system (in the Ultra-Torr glass-to-metal-seal fitting) were replaced with Kalrez sulfur-free O-rings[3]. The graphite boat was more highly purified (using the high-temperature halide process described in Appendix V). After these changes, Hall effect measurements revealed a much reduced net donor concentration of between $5x10^{13}$ cm^{-3} and $1x10^{15}$ cm^{-3}.

Table 3 shows the results of these measurements. Epilayers that showed a significant change in the net donor concentration are reported, along with growth conditions and/or changes that contributed to the change in net donor concentration.

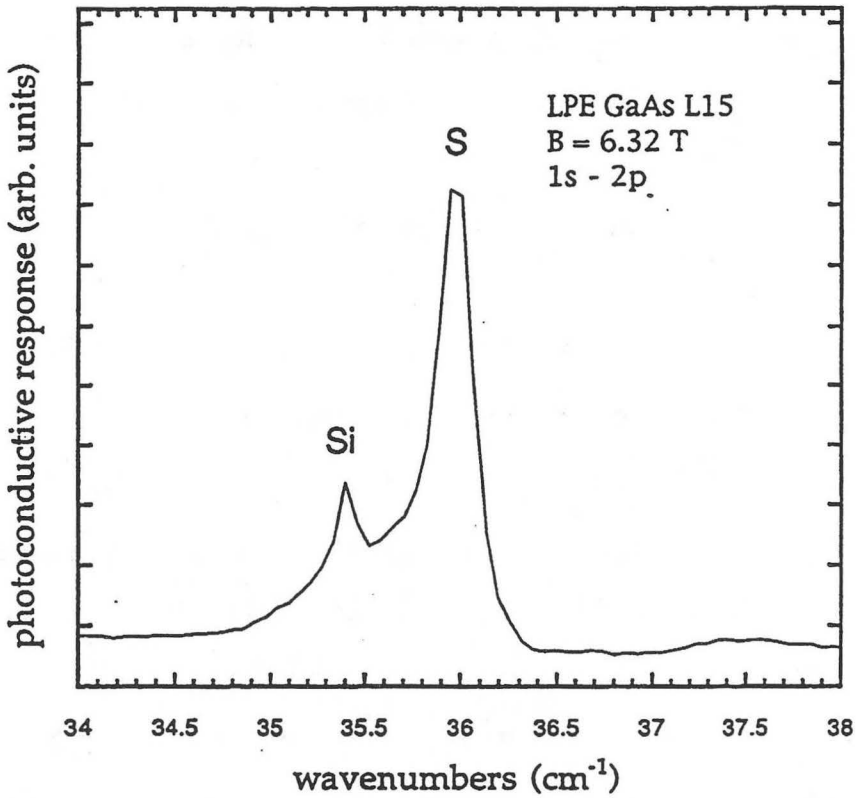

Figure 27. Photothermal ionization spectrum of epilayer 15. Measurement performed by Leon Hsu, University of California at Berkeley and Lawrence Berkeley National Laboratory, 1994.

TABLE 3: Purity of LPE Layers

Layer #	n (cm^{-3}), 77 K	μ_e ($cm^2V^{-1}s^{-1}$), 77 K
41	1.4×10^{15}	43,800
42	2.3×10^{15}	40,850
43	1.6×10^{15}	32,700
44	(used as source material for L45)	
45	9.4×10^{14}	48,820
VACUUM BAKE, 880 ^oC		
46	1.4×10^{14}	75,100
47	1.5×10^{14}	70,230
48	3.4×10^{14}	78,500
VACUUM BAKE, 900 ^oC, 1 hour		
50	6.7×10^{13}	74,400
VACUUM BAKE, 840 ^oC, 1.5 hours		
51	5.0×10^{13}	94,270
52	6.0×10^{13}	120,000
VACUUM BAKE, 930 ^oC, 1 hour		
VACUUM BAKE: 850 ^oC, 3 hours; 950 ^oC, 3 hours		
66	2.3×10^{13}	114,000
VACUUM BAKE: 900 ^oC, 5 hours; 950 ^oC, 39.5 hours		
70	1.4×10^{13}	148,000

When the net donor concentration in the epilayers fell below 10^{16} cm^{-3}, SIMS was no longer sensitive enough to reveal the nature of the residual impurities. PTIS is effective at revealing the majority donor impurities in n-type samples but not the compensating acceptor impurities. Photoluminescence (PL) measurements were therefore performed to identify the acceptor impurities. See Appendix XI for a description of PL measurements. Silicon and carbon have been identified as the major acceptor impurities, as shown in Figure 28. Relatively smaller amounts of germanium and copper were also identified. It should be noted that although Si is found as an acceptor and donor in the epilayers, it is incorporated mainly as an acceptor at standard LPE growth temperatures (lower than about 850 ^{o}C). Silicon as an acceptor reduces the mobility in the epilayers due to compensation of the donor impurities.

To help solve the impurity challenges a collaboration has been performed with the scientists at the Max-Planck-Institute in Stuttgart, Germany, who are experienced with the growth of high purity GaAs epilayers using the LPE method. This collaboration included a visit to the laboratory at the Max-Planck-Institute to study their process, and an exchange program of Ga and GaAs source materials used for the solution from which the epilayers are grown. Hall Effect measurements were performed on epilayers grown (in this lab) using Ga and GaAs from the Max-Planck-Institute, but no improvement in epilayer purity was detected. This result demonstrated that a source in the LPE system used for the work in this thesis was contributing impurities to the epilayers.

While investigating process modifications to increase the epilayer purity, it was found that the most dramatic improvement in epilayer purity was gained by high-temperature vacuum bakes of the LPE system -- specifically the silica process chamber and the graphite growth boat. A series of vacuum bakes were conducted. After approximately 24 hours of vacuum baking at 950 ^{o}C, Hall effect measurement results

revealed a new net donor impurity concentration of approximately $5x10^{13}$ cm^{-3}. After approximately 45 hours

of vacuum baking at 950 °C, Hall effect results showed a net donor impurity concentration of $2x10^{13}$ cm^{-3}.

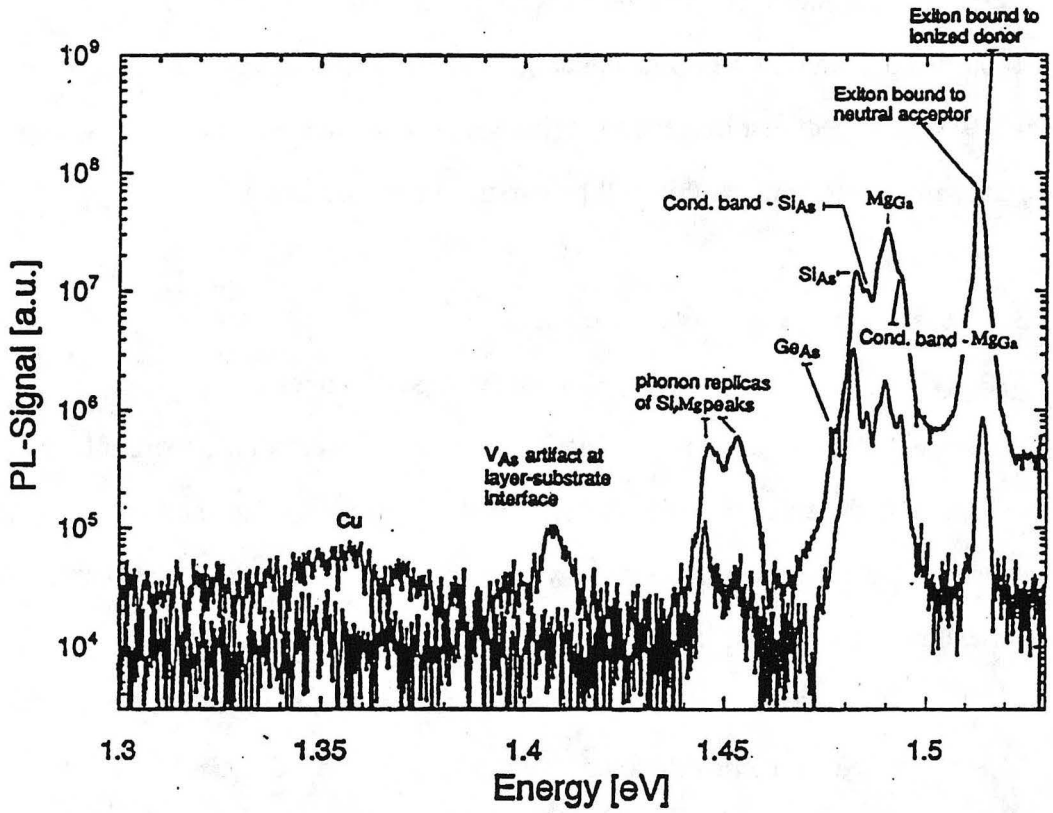

Figure 28. Photoluminescence measurements of epilayer 50 ($n = 7x10^{13}$ cm^{-3}) grown for this thesis (upper labeled peaks), and of a high purity GaAs LPE layer grown at the Max-Planck-Institute for comparison (lower peaks). Measurements were performed at a temperature of 4.5 K. Magnesium and silicon are observed to be the major acceptor impurities in both samples. The PL measurements were performed by Joachim Krueger, Lawrence Berkeley National Laboratory, 1995.

A 77K electron mobility of 200,000 cm^2/V.s or higher is a sign of very low compensation and high purity. The best films grown for this thesis work to date

demonstrate an electron mobility of approximately 148,000 $cm^2/V.s$ which, taken in conjunction with the donor concentration results, indicated that further work is needed to reduce the impurity concentration in the LPE system.

The nichrome furnace element that was installed by the manufacturer failed during the first set of vacuum bake experiments, and a higher temperature furnace element was installed (Kanthal A-1), with a maximum use temperature of approximately 1200 ^oC compared to the original nichrome element with a maximum use temperature of 1000 ^oC. I expect that longer and higher temperature bake-outs will lead to further purity improvement, and this will be pursued in further work.

3.2 Structural Characterization

3.2.1 Visual Observations of Epilayer Structures

Figures 15 and 17 in Section 2.3.5 show the microscopic morphologies observed on the epilayer surface after growth. The effect on the surface morphology of substrate surface deviation from a low-index plane as well as epilayer impurity concentration were discussed in Sections 2.3.5 and 2.3.6.

Figure 22 shows solvent inclusions observed in the epilayer surface which are believed to be due to constitutional supercooling, described in Section 2.3.7.

In addition to observation of surface morphologies, samples were cleaved and features of the cleaved surface were delineated with the light-sensitive etch H_2O:HF:H_2O_2 (10:1:1). Figure 29 shows the interface morphology with and without substrate meltback. It can be seen from the figure that the interface morphology with substrate meltback is smoother -- any damage or contamination on the substrate surface has been dissolved into the solution, and a smoother growth surface is obtained.

A calibrated scale on one eyepiece of the microscope allowed approximate determination of the epilayer thickness. To determine the accuracy of the scale, the

thickness of a representative epilayer was measured using first the scale and then a profilometer. The microscope and profilometer measurements differed by approximately 10%, so the microscope scale was used as an approximate measure of epilayer thickness.

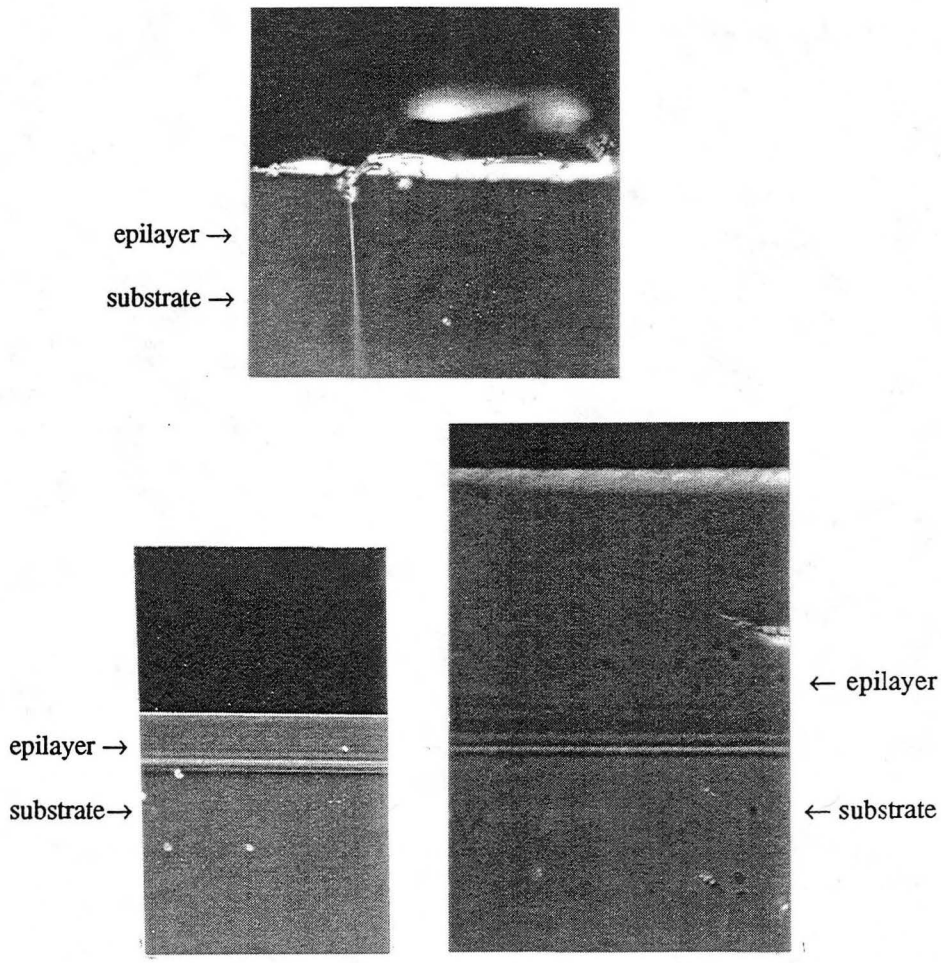

Figure 29. (a) Layer 35 (625X magnification), grown with substrate meltback. Note that it is barely possible to resolve the substrate-layer interface, even after using an etch to delineate the interface. (b) Layer 36 (250X and 1250X magnification), grown without substrate meltback.

3.2.2 X-ray Rocking Curve Measurements

In addition to visual observations of the epilayer structures, X-ray rocking curve measurements were performed on a representative epilayer. See Appendix XII for a brief description of X-ray rocking curve analysis. Both the epilayer and substrate yielded rocking curve peaks with full widths at half maximum of approximately 17 arcsec. This demonstrates that the epilayers are of the same high crystalline quality as the substrate.

4.0 CONCLUSIONS AND FUTURE WORK

As stated previously, the best epilayers grown to date for this work demonstrate a net donor concentration of $2x10^{13}$ cm^{-3}, and a 77 K mobility of 148,000 $cm^2/V.s$. Walukiewicz *et al.* (1982) have estimated that these epilayers have a compensation ratio of between 60% and 70%, which means that the total shallow impurity concentration in these epilayers is as high as $3.4x10^{13}$ cm^{-3}. The net donor concentration is low enough and the 77 K mobility is high enough for the successful fabrication of p-i-n X-ray detectors and far IR photoconductors, but these epilayer characteristics can still be improved upon. There are several approaches that can be taken to accomplish this:

- Additional LPE system vacuum baking at 950 ^oC or higher.
- Vacuum baking of the graphite growth boat at approximately 1500 ^oC. A high temperature vacuum-bake system is being constructed for this purpose.
- Introduction of a few ppm of water vapor or oxygen to the hydrogen gas stream. As detailed in Appendix VII, this will oxidize the Si in the growth solution and reduce the amount of Si incorporated into the solution. The water vapor can be introduced via a bubbler which has been obtained for this purpose, or more controllably, via an oxygen leak source.

Any deep-level impurities will be determined using an analysis method called Deep Level Transient Spectroscopy. This method requires a p-n junction diode and will be discussed in my Ph.D. dissertation.

APPENDIX I: METHODS OF DEPOSITING LPE LAYERS

The research for this master's thesis was based on the transient system of thin film crystal growth, therefore this system will be discussed in more detail than the steady state system of growth. The method of Peltier growth will also be briefly discussed.

The most often used transient methods are ramp-cooling, step-cooling, supercooling (a combination of ramp- and step-cooling), and two-phase solution cooling techniques. To describe the procedures followed in the transient techniques, refer to Figure 30, a schematic plot showing the temperature during LPE growth runs as a function of time (it is assumed that the substrate and growth solution do not differ in temperature).

At the beginning of each process run (for all of the transient methods), with the substrate and solution separated, the growth system is heated to a temperature higher than that of the beginning growth temperature (at which the solution is saturated with the solute) for an extended period of time. The system is then cooled at a controlled rate. For each transient method an arrow indicates the temperature and time at which the substrate and solution are brought into contact.

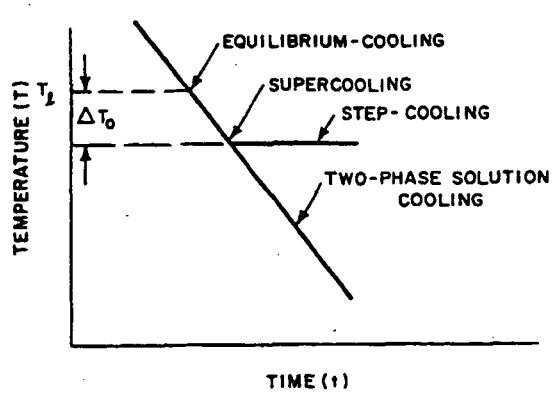

Figure 30. Solution cooling procedure for four different LPE growth techniques. The arrows indicate the times at which the growth solution is initially placed in contact with the substrate (Hsieh, 1980).

Transient growth techniques

Ramp (or equilibrium)-cooling

The ramp cooling technique uses a constant controlled cooling rate throughout the growth run. The cooling rate is very slow, from approximately 0.1 to 5 ^{o}C/minute (Moon, 1980), so the epilayer growth proceeds under near equilibrium conditions. The solution is originally saturated with a certain solute at a given growth temperature either by adding the amount of solute needed for saturation, or by keeping the solution in contact with a source of the solute at the growth temperature so that the solution dissolves enough solute to become saturated. After the solution is equilibrated at the growth temperature, the solution and substrate are brought into contact (any source of solute is removed) and cooling is begun. The cooling causes the solute solubility in the solution to decrease below the value that existed at the starting temperature. The solute therefore becomes supersaturated in the solution. The substrate is usually placed in contact with the solution near the beginning of the cooling program before any homogeneous nucleation in the solution occurs. The layer thickness increases as $t^{3/2}$ (see Appendix III), as long as the substrate and solution are in contact. Therefore, this growth method is useful when thick layers (10-100 microns) are required.

Two-phase solution growth

This method is a variation of ramp-cooled growth where the solid solute is present in the solution throughout the growth run, due either to the addition of excess solute material or to having cooled the solution far enough below the liquidus temperature that spontaneous nucleation has occurred. The advantage of this method is that it is not necessary to accurately weigh the small amounts of the solute required for

the solution saturation. The disadvantage is that the growth rates can be variable because there are now competing nucleation sites in the solution (Astles, 1993).

Step-cooled growth

The step-cooling technique can be used if growth solutions that are not in contact with a crystal or the epilayer can be cooled below the liquidus temperature (supercooled) appreciably without the occurrence of spontaneous nucleation (Hsieh, 1980).

Step-cooled growth uses a method of cooling where the temperature of the solution is lowered from an initial value to a new value and held at this new value. If the solution is saturated initially, the reduction in temperature produces a supersaturation condition. The supersaturation produced by this method enhances the nucleation driving force. Placing a substrate into a supercooled solution causes the growth of an epilayer which thickens as $t^{1/2}$ (see Appendix III). The epilayer growth is initially rapid and then slows down. This process is self-limiting due to the fixed temperature change, and is good for producing thin epilayers (Moon, 1980).

Supercooled growth

A combination of step-cooling and ramp-cooling is often used for epilayer growth. As in the step-cooling technique, the substrate and solution are cooled at a constant rate to a temperature below the liquidus temperature without spontaneous nucleation, then brought into contact. Cooling is continued at the same constant rate without interruption, until the solution and substrate are separated (Crossley and Small, 1972b; Hsieh, 1974a, b). This growth method has been observed to produce epilayers with a smoother surface morphology than that produced by ramp-cooling alone, due to the enhanced nucleation driving force.

Peltier growth

An interesting variation of growth is the Peltier-induced or current-induced LPE. An electrical current driven through leads embedded in the growth boat produces electromigration, and cooling at the solid-liquid interface by the Peltier effect (thermal energy is absorbed to increase the average kinetic energy of electrons that move across the solid-liquid interface from the metal into the semiconductor (Barrett *et al.*, 1973)).

Steady-state growth techniques

Constant-temperature-gradient growth

Constant-temperature-gradient (often called steady-state) growth uses a temperature gradient induced across a solution to provide the driving force for growth. A source (of solute) and substrate are placed in the solution, with the source at a higher temperature than the substrate. Solute material is transported from the source to the substrate. This method is good for producing thick layers (> 100 μm) and for producing epilayers with uniform composition (Moon, 1980; Astles, 1990). However, large variations in epilayer thickness across a substrate are often obtained (Long *et al.*, 1974).

APPENDIX II: DERIVATION OF THE SEGREGATION COEFFICIENT

A brief introduction to the thermodynamics of interphase mass transfer.

The derivation of the general thermodynamic conditions for mass transfer between phases has been reproduced in many texts (see for example Rosenberger, 1979; Lupis, 1983). It has been demonstrated that the general condition for mass transfer or distribution equilibrium is for a two-phase system:

$$\mu_i^{(1)} = \mu_i^{(2)} , \tag{12}$$

(where μ_i is the chemical potential of component "i") i.e., "two phases cannot be in equilibrium unless the chemical potential for each component "i" is equal in both phases" (Rosenberger, 1979). This relation characterizes mass transfer equilibrium for any kind of contact between phases as long as the referenced components can pass through the phase interface freely (Haase, 1971).

For evaluation of the equilibrium condition, the Gibbs function is used:

$$dG = -SdT - XdY + \mu dn , \tag{13}$$

where S is the entropy, T the temperature, μ is the chemical potential and n is the number of moles of material. In the absence of other external fields XdY = PdV, where P is the pressure and V is the volume. The Gibbs function is minimized at equilibrium for a system with constant T, P, and n. For LPE growth the pressure is generally fixed at a value close to atmospheric and n is approximately constant, distributed over the phases present in the system. Although the condition of constant T is not strictly

applicable for LPE growth over a large temperature range, analysis of the growth can be broken up into segments of small ΔT.

If the chemical potential of a component i differs in two phases in contact, for example if $\mu_i^1 < \mu_i^2$, there will be a transfer of component i from phase 2 to phase 1, since only then will the Gibbs function of the total system decrease. The system is at equilibrium when the Gibbs function is minimized.

The chemical potential is a function of temperature, pressure, and other external effects that may be present. Therefore, it cannot be assumed that mass transfer or diffusion of a component always proceeds in the direction of decreasing concentration, unless the temperature and pressure are uniform in the system, and the influence of any external effects are negligible compared to the effects of the concentration difference. This is shown by the following examples. A solute can have a large concentration gradient across the interface of a liquid and solid phase, with no net mass transfer occurring. This is called segregation of the solute, and is used for the purification of materials and play an important role in connection with many crystal growth processes (Rosenberger, 1979). Another example of segregation is that a solute can have a concentration difference in two sections of a solution if these two sections differ in temperature.

Derivation of the segregation coefficient for an impurity

The equilibrium segregation coefficient for an impurity between two phases has been derived by Ratner (1933), Vaslow and Boyd (1952) and Rosenberger (1979) from thermodynamic parameters. For example, Rosenberger approximates the equilibrium segregation coefficient from measurable parameters for an impurity in crystal growth from a solution as

$$k_0 = \frac{\gamma'_{2L}}{\gamma^{sat}_{2L}} \frac{X^{sat}_{1L}}{X^{sat}_{2L}} \exp\left(-\frac{\Delta h^d_{2S} + T\Delta s^{vibr}_{2S}}{RT} \right) \tag{14}$$

where γ'_{2L} is the activity of the impurity in the solution, γ^{sat}_{2L} is the activity of the pure impurity in equilibrium with its saturated solution, X^{sat}_{1L} and X^{sat}_{2L} are the fractions of solvent and impurity, respectively, in a solution saturated with both (at a certain temperature T), Δh^d_{2S} is the energy required to transfer the pure molten impurity into the solid crystal, Δs^{vibr}_{2s} is the vibrational entropy change of the crystal upon transferring the impurity into it, and R is the gas constant. The numerator of the exponential term represents the "excess chemical potential" (deviation from ideality) for dissolution of the impurity in the solid crystal.

Defining the segregation coefficient of an impurity between two phases as an equilibrium parameter implies that the segregation coefficient is not dependent on either the growth rate or the crystal orientation during crystal growth. However, experimental results exist which show the dependence of the segregation coefficient on both crystal growth rate and orientation (for example Saul and Hackett, 1970; Rosztoczy, 1968; Beneking and Vits, 1968; Kang and Greene, 1968), demonstrating that the incorporation of impurities during crystal growth can be a process far from equilibrium.

Burton *et al.* (1953) have considered the change of segregation coefficient with crystal growth rate in some detail. They derived the change in segregation coefficient with growth velocity as

$$k = \frac{k_0}{\left[k_0 + (1 - k_0)\exp\left(\frac{-v\delta}{D} \right) \right]} \tag{15}$$

where k_0 is the equilibrium segregation coefficient, v is the growth velocity, D is the diffusion coefficient of the solute or impurity of interest, and δ is the boundary layer thickness. In general, when diffusion is predominant δ depends on the degree of stirring of the melt or solution (Kröger, 1973).

Hall (1953) noted that since the measured diffusion coefficients of impurities in liquid metals cover a limited range of values for any given metal, the effect of limited mixing should be comparable for different impurities in either Ge or Si. He observed however, that the change in segregation coefficient with growth rate is more pronounced for donor impurities than for acceptor impurities and the segregation coefficient also depends on the crystal orientation.

Hall modeled the observed changes in segregation coefficient with growth temperature and orientation by assuming that the number of impurity atoms picked up by the crystal is determined by the adsorption of impurities at the solid-liquid interface (see also Buckley, 1951) as well as by the accumulation of impurities in the liquid due to incomplete mixing. He defined k_s as the as the concentration of adsorbed donor atoms in the surface layer of the crystal relative to that in the melt or solution, k_s being generally larger than the equilibrium segregation coefficient k_0. After each surface layer is covered by a new one, its composition will tend to approach the equilibrium value for the solid. If new atoms are added too rapidly however, the impurity atoms do not have enough time to exchange with the surface and nonequilibrium material will grow.

The above mechanism leads to variation of the segregation coefficient with the growth rate (v)

$$k = k_0 + (k_s - k_0)\exp\left(\frac{-v_i}{v}\right) \tag{16}$$

where v_i is the growth rate for which the time interval between the deposition of successive layers on the crystal is equal to the relaxation time for the change in impurity content of a layer which has just been covered up. He demonstrated that an equation of this form can be fitted very satisfactorily the experimental data, whereas equation (15) from Burton *et al.* shows a distinctly different behaviour.

It has been demonstrated by a number of researchers that the electronic properties of the solid must be considered when deriving relations for the segregation coefficient. For example, it was shown by Reiss and Fuller (1956) that the ionization of impurities in semiconductors led to departures from the solid solubility expected solely on the basis of the equilibrium thermodynamic concepts described, for example, by Rosenberger. They demonstrated that the solubility of Li in Si was also dependent on the position of the Fermi level in the semiconductor bulk, where the Fermi level is the electron (or hole) chemical potential.

Introduction of surface band bending as a dominant feature in semiconductor crystal growth and impurity incorporation was suggested by Longini and Greene (1956) who also developed concepts for the effect of the Fermi level on the incorporation of impurities. They pointed out that the spatial variation in potential due to band bending produces a difference in equilibrium impurity concentration in the surface layer and in the bulk.

The surface band bending is due to the situation which exists at the crystal surface (at the crystal-liquid interface) where the lattice of atoms is discontinuous, and there may be numerous surface defects. These phenomena cause extra electron states in the band gap, and are called "surface states". The presence of surface states tends to control the position of the Fermi level at the surface.

Because of the high density of conduction electrons in the liquid phase, the growing solid-liquid interface is considered to behave as a metal-semiconductor

Schottky barrier (Casey and Panish, 1972). Figure 31 shows an energy-band diagram for a metal n-type semiconductor surface. The assumption is made that the barrier height ϕ_{Bn} at a fixed temperature is independent of the impurity concentration in the solid, as suggested by the lower-temperature behavior of metal-semiconductor Schottky barriers (Casey and Panish, 1971). This leads to an electron concentration at the surface which is independent of the impurity concentration. It has been observed (Sze, 1969; Nannichi and Pearson, 1969) that the position of the Fermi level at the surface remains at a fixed energy above the valence band as the temperature varies: $E_g(T) - \phi_{Bn}(T) =$ constant, where $E_g(T)$ is the temperature-dependent energy gap.

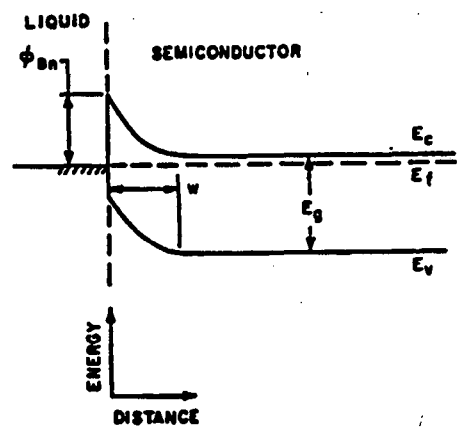

Figure 31. Energy-band diagram for a liquid n-type semiconductor interface with a surface space-charge layer width w. The barrier height ϕ_{Bn} is the position of the Fermi level (E_F) at the metal-semiconductor interface (Casey and Panish, 1972)

A simple model is presented by Zschauer and Vogel (1970) which treats the liquid phase-semiconductor interface as a metal-semiconductor Schottky barrier. Based on experimental results obtained for Si and GaP, Zschauer and Vogel extended the concept of the Schottky barrier to high temperatures and assumed a barrier height

independent of impurity concentration. This assumption enabled them to provide a simple model of the nonequilibrium incorporation of impurities.

Zschauer and Vogel used expressions for the chemical potentials of a semiconductor compound MN derived from the statistical theory of dilute solutions (Brebrick, 1962). Equating the chemical potentials for an impurity in the liquid phase with that for the solid phase (here for a donor impurity on an M site),

$$\frac{N_D}{c} = S\exp\left[\frac{\mu^0(T) - \mu_M - \mu_D^0(T) - E_F}{kT}\right] \tag{17}$$

where N_D is the concentration of the donor impurity in the solid (it is assumed that all of the impurities are ionized), c is the mole fraction of the impurity in the liquid phase, S is the concentration of lattice sites in the M sublattice, $\mu_D{}^0(T)$ is a concentration-independent term, μ_M is the chemical potential of the donor impurity on an M site, and E_F is the Fermi level. A linear relationship is only obtained between N_D and c if E_F is independent of the impurity concentration (for example, as described above, if at the interface the Fermi level is fixed independent of the impurity concentration). This case permits a growth rate dependence of the segregation coefficient in such a way that the impurity concentration at the interface is "frozen in" to a greater or lesser extent. At sufficiently high growth rates a dependence on crystal orientation is to be expected if the position of the Fermi level at the interface is orientation dependent.

At sufficiently high growth rates the impurity concentration near the interface is frozen in and a segregation coefficient can be derived from equation (17)

$$k = \exp\left[\frac{\mu^0(T) - \mu_M - \mu_D^0(T) - E_G}{kT}\right]\exp\left(\frac{\phi_B}{kT}\right) \tag{18}$$

Analysis of the existing data on diffusion coefficients shows that the main departure from equilibrium originates from the diffusion in the solid, while the liquid phase is in equilibrium in most cases (Zschauer and Vogel, 1970). Because the diffusion coefficients of metals in liquid Ga at the usual temperatures of LPE growth are greater than the growth rates, it is concluded that under typical growth conditions the liquid phase is nearly in equilibrium.

From their experiments, Casey and Panish (1972) concluded that it is the impurity diffusivity in the solid that determines whether the Fermi level of liquid phase is in equilibrium with the Fermi level of the semiconductor surface or bulk. Equilibrium between the liquid and semiconductor surface occurs for a slow impurity diffusivity in the solid (for example, for Te and Se in GaAs) and results in a linear dependence of the amount of singly ionized impurity in the solid on the amount in the liquid. Equilibrium between the liquid and the semiconductor bulk requires rapid impurity diffusivity in the solid (for example, Zn in GaAs) and results in a square-root dependence of the amount of a singly ionized impurity in the solid on the amount in the liquid (Casey and Panish, 1972).

APPENDIX III: DIFFUSION-LIMITED GROWTH THEORY

The driving potentials for diffusion:

As a crystal grows, there is selective incorporation of crystal components from the growth solution which is governed by the differences of each component's chemical potential in the two phases in contact. The chemical potentials, however, depend on the concentration of all components present and on the local temperature, pressure, etc. Both latent heat that is released during the interfacial attachment process and matter that is not incorporated into the solid must be transported away from the solid-liquid interface. Thus the mass and heat transport problems are coupled. In order to determine for example the time-dependent position and shape of an interface, equations for the conservation of mass, momentum, and energy for the system in question must be considered (Rosenberger, 1979). Fortunately, the LPE process allows for a considerable simplification of this system of equations.

For diffusive mass transfer, experiments show that the flux F of a crystal component in the absence of temperature and pressure gradients and external fields (including any forces acting between the different components of the solution) is approximately proportional to its concentration gradient, and can be described by Fick's first law (Rosenberger, 1979):

$$F = -D\nabla C, \tag{19}$$

where D is the diffusion coefficient and ∇C is the gradient of C, the concentration.

When two different types of transport processes take place at the same time, they can interact. For example, interferences between mass diffusion and heat conduction cause thermal diffusion, which is the maintenance of a concentration gradient as the result of a temperature gradient.

Evaluating all of the contributions, the diffusive mass flux is expressed in the following form:

$$J_j = J_j^C + J_j^F + J_j^P + J_j^T \tag{20}$$

which is the sum of the terms for concentration diffusion J_j^C, pressure diffusion J_j^P, forced diffusion J_j^F (all of the previous are isothermal) and the thermal diffusion J_j^T. For LPE growth, only the thermal diffusion or concentration diffusion term is significant, depending on the type of growth performed. Only concentration diffusion relates to the growth conducted for this thesis.

Diffusion-limited growth theory

The following simplified theory is often the only theory presented in the literature, but gives accurate values of epilayer thicknesses only for short growth times. This theory overestimates values of epilayer thicknesses for cases of long growth times, such as was used to conduct the epilayer growth for this thesis. The simplified calculations of LPE growth rate and thickness for short growth times will be presented first to show the basic relations between epilayer thickness and cooling rate, slope of the liquidus curve and other parameters. The deviations from this theory for long growth times are then discussed. These calculations are from equations developed by a number of authors (Tiller and Kang, 1968; Small and Barnes, 1970; Minden, 1970; Crossley and Small, 1971; Ghez ,1973; Rode, 1973; Hsieh, 1980).

Only the details of these theories that pertain to LPE growth of GaAs by the supercooling method (combination of step-cooling and ramp-cooling methods) will be reviewed here, since this is the growth method used for the research conducted for this thesis.

For the growth of a binary compound such as GaAs the following one-dimensional analysis applies in most cases (Astles, 1990):

$$\frac{\partial C}{\partial t} = D\left(\frac{\partial^2 C}{\partial x^2}\right) + V\left(\frac{\partial C}{\partial x}\right) \tag{21}$$

for solute diffusion in liquid and solid phases, and

$$\frac{\partial T}{\partial t} = K\left(\frac{\partial^2 T}{\partial x^2}\right) + V\left(\frac{\partial T}{\partial x}\right) \tag{22}$$

for heat diffusion in the liquid and solid phases. In equation (21), C is the solute concentration (As for GaAs growth), and is a function of growth time, t, and distance x from the solid-liquid interface in a direction normal to the interface. The term D is the diffusion coefficient of the solute component in the solvent (e.g. As in Ga). In equation (22), T is the temperature and K the thermal diffusivity. The term V in equations (21) and (22) represents the velocity resulting from free and forced convections and the growth rate. The above equations describe the situation in which the coordinate system is moving with the solid-liquid interface (Moon 1980).

In addition, there are continuity equations describing the mass conservation at the solid-liquid interface:

$$V\left(C_{S,x=0} - C_{L,x=0}\right) = D_L \left.\frac{\partial C_L}{\partial x}\right|_{x=0} - D_S \left.\frac{\partial C_S}{\partial C_L}\right|_{x=0} \tag{23}$$

and for the flux of heat at the interface:

$$VL\rho_S = K_S \frac{\partial T_S}{\partial x}\bigg|_{x=0} - K_L \frac{\partial T_L}{\partial x}\bigg|_{x=0} \tag{24}$$

where K_S, K_L are the thermal conductivities of solid and liquid phase, L is the latent heat diffusion, and ρ_S is the density of the solid phase. V is the same parameter as described for equations (21) and (22).

There are six assumptions that can be made for most conditions of LPE growth of a binary compound for the ramp- or step-cooled methods (Astles, 1990), which simplify equations (21-24). First one assumes that the growth solution is isothermal. This is true for most LPE situations except those where a temperature gradient is deliberately imposed (as in steady state LPE growth). This means that equations (22) and (24) may be neglected. For Ga-rich solutions, this assumption is valid (at least over the distances compared to the solution diffusion length) because of the large ratio of thermal diffusivity [0.3 cm^2/s (Long *et al.*, 1974)] to solute diffusivity [~5×10^{-5} cm^2/s at 800 °C (Rode, 1973)].

Second, the diffusion in the solid phase is negligibly slow, i.e., $D_S << D_L$. This is a good approximation for normal LPE conditions of temperature and growth rate (Astles, 1990), which means that only equation (21) for the liquid phase and equation (23) (neglecting the second term on the right-hand side) need to be solved. Figure 32 shows the change in the diffusion coefficient D of As in Ga as a function of temperature. Over the range of about 800-600 °C, D is observed to be approximately constant.

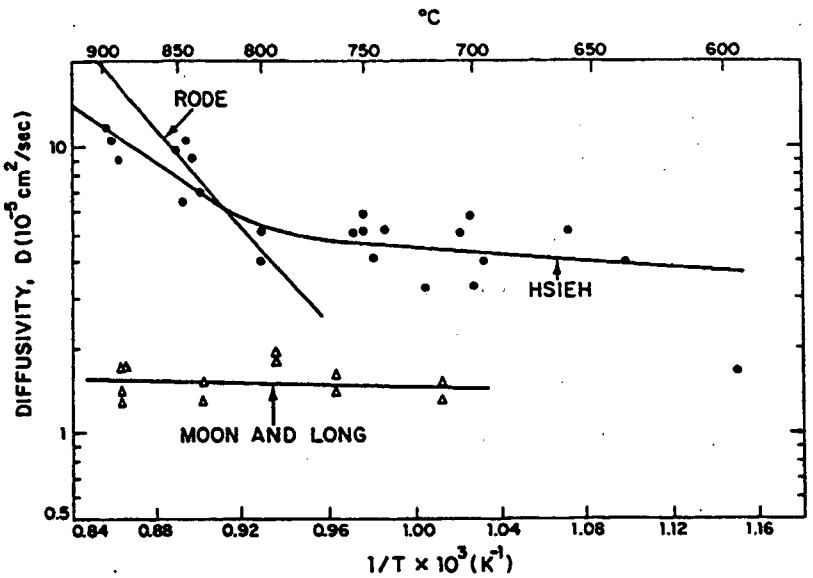

Figure 32. Temperature dependence of As diffusivity in Ga-rich solutions. The closed circles and open triangles are the data points of Hsieh (1975b) and Moon and Long (1976), respectively (Hsieh, 1980).

Third, the growth velocity V is low enough that the term $V(\partial C/\partial x)$ in equation (22) is negligible. This assumption has been shown to be an extremely good one by earlier workers (Minden, 1970; Moon, 1974), for typical LPE growth rates of 10^{-2} to 10^{-1} μm/sec. A detailed analysis dealing with induced convection arising from the epilayer growth itself shows that at low solute concentrations this convection is much smaller than that due to diffusion (Westphal and Rosenberger, 1978; Wilcox, 1972).

Fourth, the solution depth W is small enough that the effects of solutal or thermal convection may be neglected. Whether or not convection develops has been analyzed, for example by Moon (1980) and by Long *et al.* (1974) (see Appendix VI). The advantage of convective transport is the increased rate of mass transport to the solid-liquid growth interface, but the disadvantage is that, due to the cellular structure of convection currents, convection creates the conditions under which a smooth epilayer

surface becomes unstable and the growth front irregular so that solvent entrapment occurs in the epilayer (Tiller, 1968).

Fifth, equilibrium is established at the solid-liquid interface so that the solute concentration at the interface is given by the equilibrium phase diagram. This should be valid for the slow growth rates used for LPE (Hsieh, 1980).

Sixth, the solid-liquid interface remains planar and the deposition area remains constant (Moon, 1980).

Three additional assumptions were used to derive the simplified thickness-time equations, which are valid for short growth times only.

First, the growth time is much less than the diffusion time $t = W^2/D$ where W is the solution thickness and D is the diffusion coefficient. This assumption implies that the solute concentration at the free surface of the solution does not change during a growth run, and therefore that the solution is semi-infinite.

Second, it is assumed that the removal of the solute from the growth solution occurs only by deposition on the substrate, and not by precipitation within the solution or at solution boundaries (Hsieh, 1980).

Third, due to the short growth time, the temperature range over which growth is conducted is small and it can be assumed that D and m (slope of the liquidus curve) are constant.

The growth rate of LPE layers deposited from binary solutions is obtained by calculating the rate at which solute is removed from the growth solution and incorporated into the growing epilayer. The basic method of calculation is to solve the one-dimensional diffusion equation for the conditions appropriate to the experimental situation.

Solution of the diffusion equations

The analysis of the growth process with the above assumptions becomes a problem in solving the equation

$$\frac{\partial C(x,t)}{\partial t} = D\left(\frac{\partial^2 C(x,t)}{\partial x^2}\right) \tag{25}$$

subject to the relevant boundary conditions. The diffusion equation and some of its solutions can be found in the standard textbooks of Crank (1975), Carslaw and Jaeger (1959), and Luikov (1968) (Ghez and Giess, 1975).

Once the concentration profile is known, the growth rate is calculated from the equation of mass conservation at the solid-liquid interface:

$$V = \left(C_{S,x=0} - C_{L,x=0}\right)^{-1} D \left.\frac{\partial C}{\partial x}\right|_{x=0} \tag{26}$$

where C_S is the concentration of solute in the epilayer. The thickness H of the deposited film after a growth time t results by integrating the growth rate between 0 and t:

$$H(t) = \int_0^t V(t')dt' \tag{27}$$

With these equations and the expressions for the boundary conditions, a complete description for the diffusion-limited process is possible for finite (long growth time) and semi-infinite (short growth time) solutions.

For both finite (long growth time) and semi-infinite (short growth time) solutions, the **boundary conditions** are (Astles, 1990):

The **initial condition** is that at $T = T_0$, the solute concentration is initially homogeneous, i.e., $C(x,t = 0) = C_0$ for all x.

The **solute concentration** at the solid-liquid interface at any time t, $C(x = 0, t)$ has a value equal to the liquidus concentration from the equilibrium phase diagram corresponding to the solution temperature 'T' at that time, $C_e(T)$, or

$$C(x = 0, t) = C_e(T) \text{ for all } t \quad \text{(for fast interface kinetics)} \tag{28}$$

The temperature T will be a function of the growth time t which depends on the growth method being considered.

The **dimensions of the growth solution** affect the boundary condition at the free surface of the solution, opposite the solid-liquid interface. The following two conditions are usually evaluated:

Semi-infinite solution

During the growth period 't' the solute concentration at the surface of the solution remains at the original concentration C_0, and the concentration gradient does not reach the solution surface:

$$\left[\left(\frac{\partial C}{\partial x}\right)_{surface}\right] = 0 \qquad \text{for all } t > 0 \tag{29}$$

(see Figure 33). As was stated previously, this is a good approximation if the growth time $t < W^2/D$ where W is the solution depth.

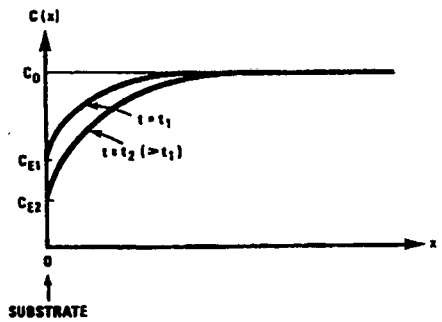

Figure 33. Solute profile for semi-infinite growth (Astles, 1990).

This case of the semi-infinite solution (with fast interface kinetics) is considered first, since it presents the simplest equations which show the basic relationships between the thickness and the cooling rate, growth time, and slope of the liquidus curve.

The easiest method of LPE growth to describe is **step-cooled growth** where the driving force for growth is caused by the supersaturation that a step lowering of the temperature produces. The amount of supersaturation in the solution that a temperature change ΔT causes is

$$\Delta C = C_0 - C_e \simeq \Delta T/m \qquad \text{(m = slope of the liquidus curve)} \qquad (30)$$

unless ΔT is larger than the supersaturation necessary to cause homogeneous nucleation. In this case the maximum value cannot be larger than the critical supersaturation value, regardless how large ΔT may be. With the boundary conditions specified above, the growth rate **R** is proportional to $t^{-1/2}$ (Moon, 1980) and the layer thickness **H(t)** is given by

$$H(t) = \frac{2\Delta T}{Csm}\sqrt{\frac{Dt}{\pi}} \tag{31}$$

H(t) is directly proportional to the temperature change producing the supersaturation and to $t^{1/2}$.

Ramp-cooling, on the other hand, continually changes the value of C_e at the solid-liquid interface by cooling the solution temperature at a controlled rate. For ramp cooling, the boundary condition in addition to those specified above is that at any time t > 0, the temperature $T = \alpha t$ where t is the growth time and α is the growth rate. Therefore $C = C_0 - \alpha t/m$ at the solid-liquid interface (x = 0).

Epilayer growth starts at the equilibrium concentration C_0 and continues as long as a situation of decreasing temperature exists, which forces a concentration change. The growth rate increases as $t^{1/2}$ so that the layer thickness grows as $t^{3/2}$ (Small and Barnes, 1969; Hsieh, 1980). The complete equation for the layer thickness **H(t)** is

$$H(t) = \frac{4}{3}\frac{\alpha}{C_S m}\sqrt{\frac{Dt^3}{\pi}}. \tag{32}$$

Note that **H(t)** is proportional to the cooling rate and that, unlike for step-cooled growth, **H(t)** can increase indefinitely as long as the solution temperature decreases. As the total temperature change increases however, the potential of a rough surface from constitutional supercooling also increases (constitutional supercooling is discussed in Section 2.3.7).

Supercooled growth: to initiate ramp-cooled growth some step-cooling is often used. The solution is supercooled by driving the furnace temperature down to a temperature below which the solution and substrate are in equilibrium. After ΔT_{sc}, the

substrate and solution are brought into contact to begin growth; growth continues while the furnace temperature program continues to cool. The total layer thickness is calculated by adding the equations for ramp-cooled and step-cooled growth:

$$H(t) = \frac{2}{C_S m}\sqrt{\frac{D}{\pi}}\left(\Delta T t^{1/2} + \frac{2}{3}\alpha t^{3/2}\right) \tag{33}$$

The equations can be added by applying the theorem that for a linear differential equation the sum of two solutions is itself a solution (Hsieh, 1980). At the beginning of growth, step-cooled growth completely dominates, with the ratio of ramp-cooled to step-cooled layer thickness equal to

$$\frac{2}{3}\frac{\alpha}{\Delta T_{sc}}t. \tag{34}$$

Experimental results of Hsieh are shown in Figure 34 for GaAs layers grown on (100) GaAs substrates. This figure shows measured thicknesses of epilayers grown by the supercooling technique, plotted with theoretical thicknesses calculated for the step- and ramp-cooled techniques. It can be seen that for very short growth times the thickness of epilayers grown by the supercooled technique closely follow the theoretical line for step-cooled growth, while for longer growth times the results move closer to the theoretical line for ramp-cooled growth. In between, the results agree well with the above equation for supercooled growth.

After a certain time, the semi-infinite model begins to overestimate **H(t)** in all cases. This difference in the estimate of **H(t)** comes about because in the finite solution case the solute supply is also finite.

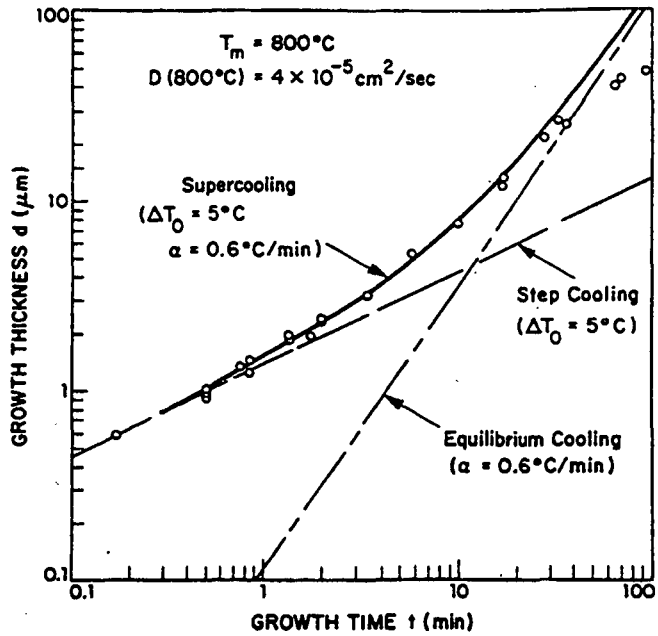

Figure 34. Growth thickness (d) as a function of growth time (t) for GaAs epilayers grown by the supercooling technique. The lines or curves for equilibrium (ramp) cooling, step cooling, and supercooling were calculated from the equations given in this Appendix (Hsieh, 1980).

Finite solution growth occurs when $t > W^2/D$. In the case of solid solute material floating on the solution surface, either in the form of excess solute (solid GaAs for GaAs LPE growth), from homogeneous nucleation (present on the solution surface after long growth times) or from an intentionally added piece of solute material, then the solute profile will be as shown in Figure 35. The boundary conditions in addition to those specified previously are:

The concentration at the solution surface is no longer constant at C_0, but now is given by the equilibrium concentration C_e:

$$C(x = W, t) = C_e(T). \tag{35}$$

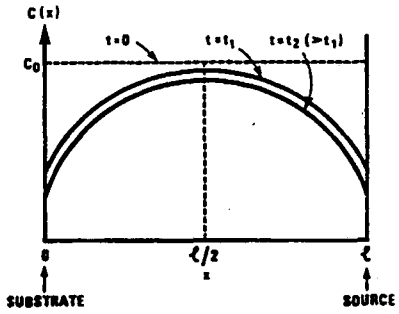

Figure 35. Solute profile for the case of solid solute material in contact with the solution (Astles, 1990).

For a finite solution with a crust of the solute on the solution surface (or if a piece of solid solute is floating on the solution surface), a mathematical description of this situation usually assumes, depending on the boundary conditions, that the growing interface is located at both +/- W/2 of a solution of thickness W or that the flux at one boundary surface is zero, by symmetry, and the growth surface is at W/2 (Moon, 1974) (see Figure 36):

$$\left[\left(\frac{\partial C}{\partial x}\right)_{x=\frac{W}{2}}\right]=0. \tag{36}$$

Moon (1980) reviews several researchers' derivations of equations for long growth times where D and m may no longer be constant. When the temperature dependence of D and m are included, the variation with temperature follows an Arrhenius expression of the form exp(-ΔH/RT), with ΔH = activation energy for diffusion (for D) or the heat of solution (for m) (Ghez, 1973; Minden, 1970; Tiller and Kang, 1968; Moon and Long, 1976).

The mathematical expression for H(t) for growth from a two-phase (finite) solution is in the form of a power series (Moon, 1980). For long growth times ($Dt/W^2 \geq 1$), $H(t) \propto \alpha Wt$ - constant (Moon, 1974). For supercooled growth, the effect due to step-cooling is only important at the beginning of growth. Therefore, only the term due to ramp-cooled growth will be affected by long growth times.

Experimental results of Hsieh are shown in Figure 34 for GaAs epilayers grown on (100) substrates. The plot shows measured thicknesses of epilayers grown by the two-phase-solution technique, compared to the theoretical epilayer thickness calculated for the equilibrium (ramp)-cooling technique.

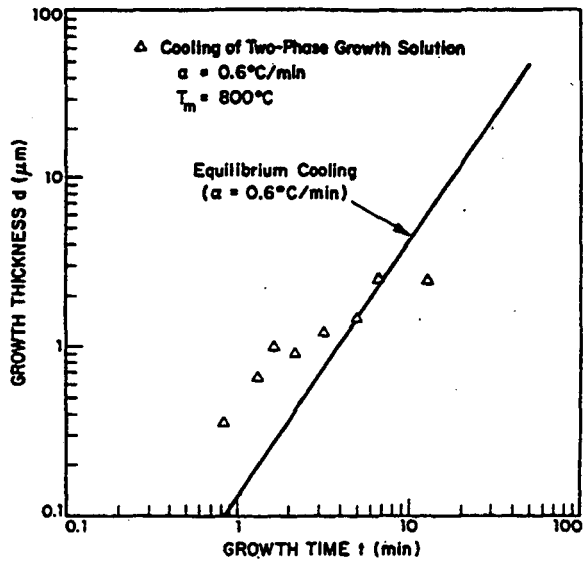

Figure 36. Growth thickness (d) as a function of growth time (t) for GaAs epilayers grown by the two-phase-solution technique. The equilibrium (ramp) cooling line was calculated using the equation given earlier in this Appendix (Hsieh, 1980).

APPENDIX IV: APPARATUS USED FOR LPE GROWTH OF III-V SEMICONDUCTOR COMPOUNDS

Horizontal LPE systems

Tipping/tilting system

In one of the first LPE experiments (Nelson 1963), doped GaAs and Ge epilayers were grown by the tipping technique. The original tipping method (see Figure 37) uses a growth boat in which the substrate is fastened at one end, and the solution (composed of a metal solvent and solid Ge or GaAs as the solute) is initially at the other end. The boat is placed inside a silica tube that allows growth to be carried out in a protective atmosphere, and the tube is placed inside a furnace that can be tipped to elevate either end of the boat. With the furnace in its initial position, the substrate end is higher than the end containing the solution. The furnace is heated until the GaAs or Ge dissolves in the solvent to form a slightly undersaturated solution. The furnace is then allowed to cool and tilted so that the solution covers the substrate. The substrate dissolves until equilibrium is reached, and on further cooling GaAs or Ge grows on it. At some suitable lower temperature the furnace is tipped back to its original position to separate the solution and substrate (Hsieh, 1980; Deitch, 1975).

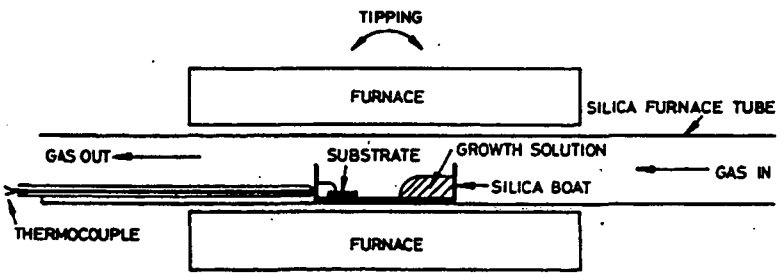

Figure 37. Tipping LPE furnace system (Astles, 1990).

As a result of the initial substrate dissolution (or "meltback") a planar growth interface is formed, and any structurally damaged surface layer (together with surface impurities) is removed prior to growth.

The drawbacks of the original tipping method are that growth is restricted to the growth of single epilayers (although it has been used for the growth of p-n junctions), and thermal conditions vary when the furnace is tilted. If growth is terminated at some elevated temperature by tipping back the furnace to remove the solution from the substrate, droplets often remain on the epilayer surface, causing additional growth under the droplets as the system is cooled to room temperature. This leads to inadequate control of layer morphology and layer thickness for some applications (Dawson, 1972). However, if the system is cooled to room temperature without removing the solution, this is not a problem.

Modifications of the original tipping system were made to improve the thermal stability of the growth system, to prevent the escape of volatile components from the system, and to grow multilayer structures, as will be discussed below.

Sliding system

Various methods have been developed for wiping the solution from the substrate after the desired amount of cooling, for better control of epilayer thickness. Wolfe and Stillman (1971) used a wiper arm in combination with the tipping of the boat. Panish *et al.* (1969) also used a sliding graphite substrate holder which moved the solution on and off the substrate when the boat was tipped. This technique, shown schematically in Figure 38, was the forerunner of the sliding boat system which is now the most common method of LPE growth (Astles, 1990).

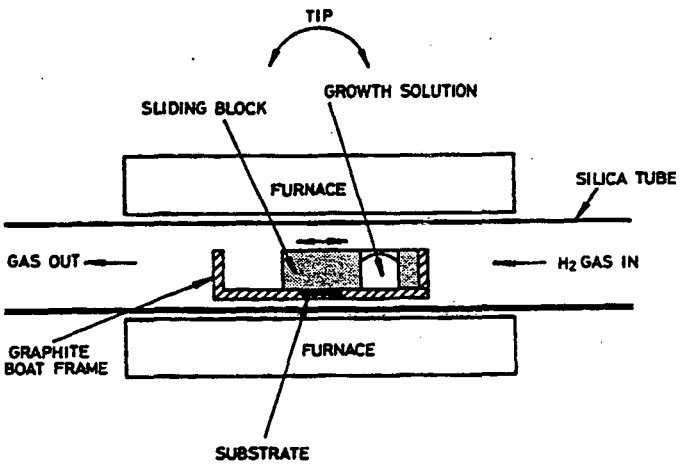

Figure 38. Tipping LPE system with sliding boat (Astles, 1990).

The most important improvement in the mechanical technology of LPE was the development of horizontal graphite boats with movable sliders. Panish *et al.* (1970) published one of the first papers on this method. The basic features of this technique are shown in Figure 39. The solutions may be positioned over the substrate as needed by moving the sliding block using an external push-rod arrangement. They also demonstrated that such a slider mechanism could be used for growth of several successive layers from a sequence of solutions.

Nelson (1971) has also described a technique which involves the sliding of a substrate under a stationary solution. This method has been widely used to grow multiple layers of $Al_xGa_{(1-x)}As$ with varying conductivity type and composition (Deitch, 1975).

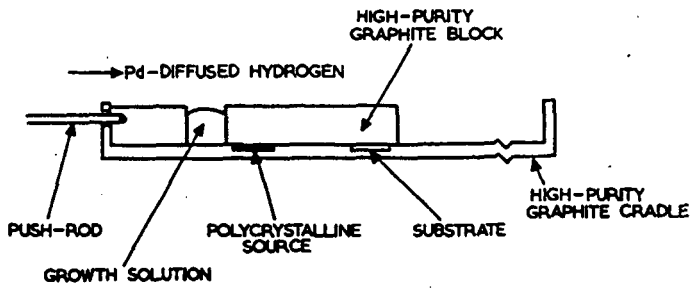

Figure 39. Basic structure of graphite horizontal sliding boat (Astles, 1990).

Many additional variations of these sliding systems have been developed, since III-V compounds for optoelectronic or microwave device applications often require the reproducible growth of thin multiple epilayers. One problem with the sliding systems is that the moving graphite parts create graphite dust that can be incorporated into the growing epilayer, creating defects. Another problem is that the epilayer surface may be scratched as the solution is wiped off.

Vertical LPE systems

Dipping system

The dipping technique using a vertical system was first described by Rupprecht (1966). A schematic of Rupprecht's system is illustrated in Figure 40.

A typical system uses a vertical process chamber made of silica and a resistance or r.f.-heated furnace. The crucible, made of graphite or silica, containing the solution is positioned at the lower end of the chamber and the substrate is fixed horizontally or vertically in a movable holder that is initially located just above the solution. The holder designs include a method of breaking through any crust on the solution surface before the substrate enters, and of providing a means of scraping off any residual solution after

withdrawing the substrate. Thus the dipping system is useful if the solution has an oxide film or other contamination on the surface.

The ambient gas in the growth chamber is usually made to flow from the top to the bottom of the chamber in order to keep the solution downstream of the substrate during heating. Usually there is a small temperature gradient through the solution with the surface of the solution hotter than the bottom. This gradient is designed to reduce convection in the solution (see Appendix VI) and to avoid constitutional supercooling (see Section 2.3.7) (Astles 1990).

The solution is heated slightly above the equilibrium (growth) temperature to ensure that the solute has completely dissolved in the solution, and then the solution is cooled at a controlled rate. The substrate is often dipped into the melt just above the equilibrium temperature to obtain a small amount of "meltback" of the substrate. After the time interval required to grow an epilayer of the desired thickness, growth is terminated by raising the holder to its original position, separating the substrate from the solution.

One of the advantages of the dipping method is that the substrate can be kept in the cooler upper part of the growth chamber before epitaxial growth, which is important if the substrate contains a volatile component which may be rapidly lost from the surface at the growth temperature. Other advantages are that it is possible to directly observe the solution by having a viewing port at the top of the growth chamber (Astles, 1990), epilayers can more easily be grown on both sides of the substrate, and on multiple substrates (Deitch, 1975).

One disadvantage of the dipping method is the relatively large volumes of solution required. When the solution is reused, there are problems with preventing contamination of or loss of components from the solution between growth runs, thus making control of doping and growth rate difficult.

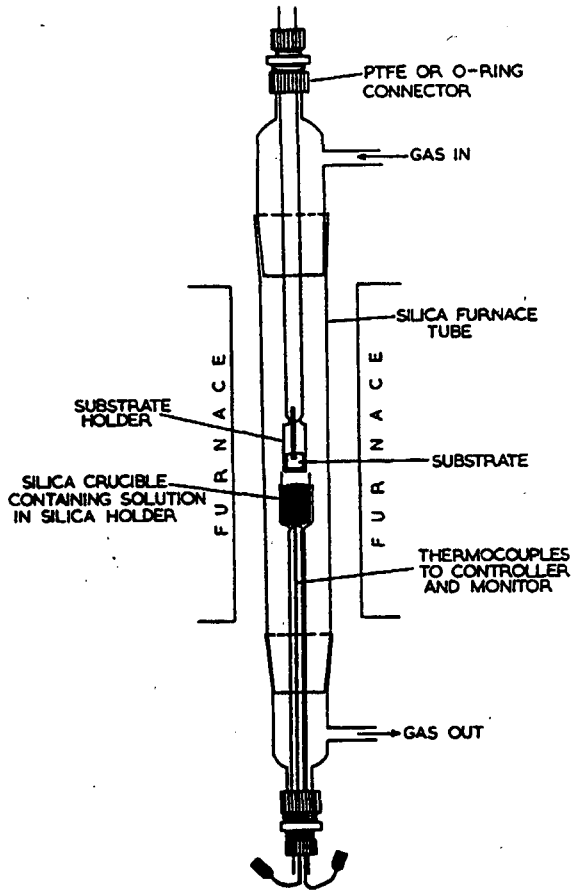

Figure 40. Dipping LPE system (Rupprecht, 1966)

Another disadvantage is that when the substrate is withdrawn from the solution at the end of the growth cycle, the solution is often not completely removed. This can lead to nonuniform epilayer thicknesses and cross-contamination of the growth solutions in multilayer growth (Hsieh, 1980). A rotating substrate method has been developed by Astles *et al.* (1976) to spin off the solution at the end of the growth period. This method was also observed to produce more uniform epilayer thicknesses.

Steady-state growth system

A horizontal constant temperature-gradient growth system has been described by Goodwin *et al.* (1969) and by Stringfellow and Greene (1971). A vertical system of this type was described by Kang and Greene (1968). Vertical LPE systems are often used for this technique because it is easier to establish a temperature gradient in the solution.

The basic technique requires a solvent that is saturated with the solute at a desired growth temperature. The solid solute (the source) and the substrate are brought into contact with the solution, with a fixed distance between the source and substrate. A temperature gradient is established by increasing the source temperature until it is slightly above that of the substrate. Since the solubility of the solute in the solvent generally increases as temperature increases, a concentration gradient is established and the solute is transported from the source to the substrate.

LPE growth using centrifugal forces

An LPE technique utilizing centrifugal forces has been described by Konuma *et al.* (1993) for the growth of Si epilayers, and by Lien and Bestel (1972) for the growth of GaP epilayers. The advantage of this method is that since there are no moving parts in the growth crucible (boat), there is no abrasion from the crucible that could create graphite dust during epilayer growth. There is also no scratching of the epilayer, which may happen with the sliding boat technique.

This technique makes use of centrifugal forces in a rotating crucible in order to transport the solutions. Rapid solution transport (adjustable by the crucible rotation speed/acceleration) produces brief contact between solution and substrates; it is therefore possible to grow extremely thin layers. The solution is completely spun away from the substrate and no residue remains (Konuma *et al.*, 1993).

The centrifugal LPE technique has been successfully applied by Konuma *et al.* to grow defect-free Si layers as well as multilayers on planar and on profiled Si substrates. Figure 41 shows a schematic longitudinal section of the LPE centrifuge. Epitaxial growth occurs in a graphite crucible that is fixed at the lower end of a rotor shaft. The rotor's upper end is part of a contactless electromagnetic suspension arrangement inside a vacuum tank. The bearing magnets and the rotor drive are outside the tank. The lower end of the rotor with the crucible extends into a silica tube. The silica tube connects the vacuum tank and a load-lock chamber. A tubular furnace outside the silica tube heats the crucible. A manipulator is used to transfer the crucible to and from the load-lock. Konuma *et al.* avoids contamination caused by the pumping system by using a cryogenic pump and a magnetically suspended turbomolecular pump backed by a completely oil-free roughing pump.

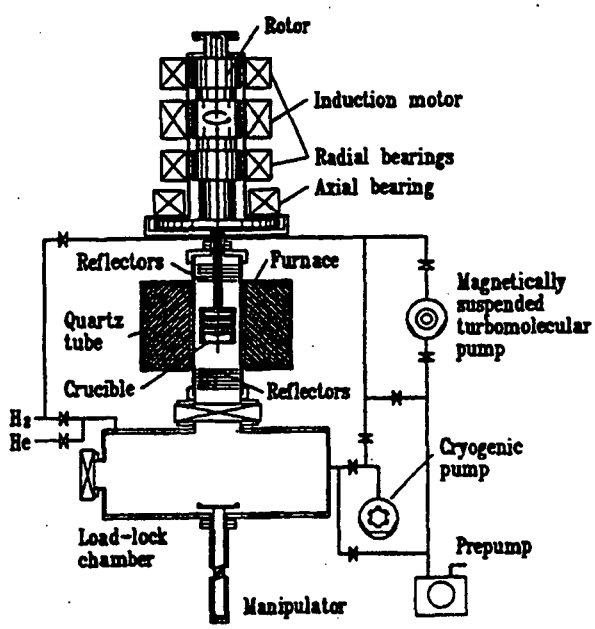

Figure 41. Schematic longitudinal section of the LPE centrifuge (Konuma *et al.*, 1993)

The crucible designed for the growth on one 100 mm diameter wafer is shown schematically in Figure 42. It consists of graphite and has four chambers. These are, shown from the top, the solution reservoir, the chamber for saturating the solutions, the growth chamber, and the chamber for the residual solution. These chambers are connected to each other by channels. The solutions in these chambers move from one chamber to the next under the effect of centrifugal forces and gravity. The shapes and slopes of the channels are designed such that at a specific rotational speed, centrifugal forces move the solutions from one position to the next. Figure 43 shows possible sequences of temperature changes and the matching rotational speeds.

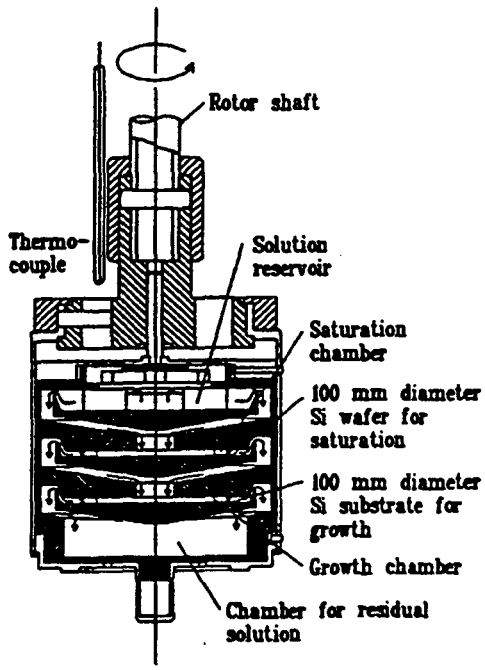

Figure 42. Crucible designed for LPE growth on one 100 mm wafer (Konuma *et al.*, 1993)

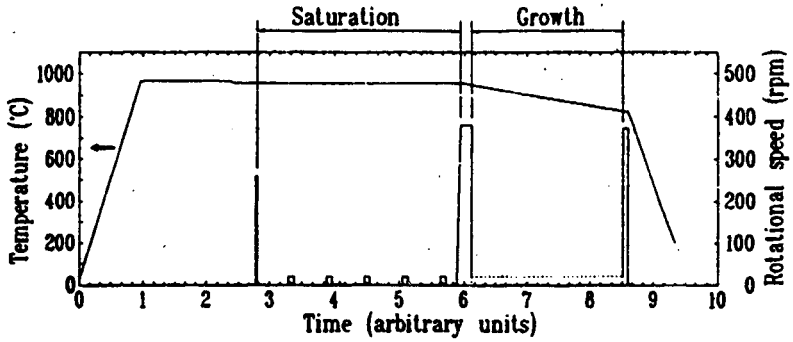

Figure 43. Possible sequences of temperature changes and the matching rotational speeds for the LPE centrifuge.

APPENDIX V: CHOICE OF SYSTEM AND GROWTH MATERIALS FOR HIGH PURITY LPE GROWTH

Solution materials -- solvent and solute

To achieve and control the desired electrical or optical properties of an epilayer, the solvent must have a very low solid solubility in the epilayer. At the least, the solvent must be an electrically inactive species in the epilayer (Dawson, 1972). Growth of high-purity layers is most successful when solvents are used which are themselves components of the epilayer -- for example, Ga is used as the solvent for high purity GaAs epilayer growth.

Other properties of an "ideal" solvent and solute are that the solvent must dissolve sufficient quantities of the solute in order to obtain layers of usable thickness (Benz and Bauser, 1980), the phase required should be the only phase formed when the solute becomes supersaturated in the solvent (Elwell, 1980), the solvent and solute in the solution should have a low vapor pressure at growth temperatures to prevent unwanted loss of solvent and to eliminate the danger of high pressures (Deitch, 1975).

The solvent and solute also should not wet or react with the crucible or boat material (Elwell, 1980), must be compatible with the ambient atmosphere of the system (Dawson, 1972), should have low toxicity (Elwell, 1980), must be available in high-purity form (low cost is also desirable), and should be easily separable from the epilayer (Deitch, 1975).

The group III metal is usually used as the solvent in the growth of III-V semiconductors, because the vapor pressure of the group V component is generally much higher than that of the group III element at a given temperature. The liquid metals Ga and In are excellent solvents for LPE, having low melting points and high boiling

points. Furthermore, these liquid metals also do not wet the graphite which is generally used to contain them.

Crucible or boat in which layer growth occurs

There are several reasons why graphite is often used as the growth boat for the growth of III-V semiconductors. Graphite can be easily machined into the necessary shapes to tight tolerances, is available in high-purity form, is self-lubricating (good for horizontal sliding boat systems), is inert to most solution components, and has a high thermal conductivity leading to evenness of the temperature distribution.

For LPE growth of III-V compounds, the graphite boat must be carefully purified. A common method used by suppliers of high-purity graphite is to bake the finished graphite boat in a halogen gas atmosphere at a temperature greater than 2000 ^{o}C. In this environment metallic impurities will convert to volatile halide compounds which can be pumped out of the cleaning system or swept out by flowing gases. To reduce the concentration of volatile impurities such as sulfur, the graphite should then be baked in vacuum at as high a temperature as possible (as high as approximately 2000 ^{o}C) at a pressure of 10^{-6} torr or lower.

A disadvantage of using graphite is that it is porous, which leads to adsorption of atmospheric O_2 and H_2O during the loading of growth materials. Vacuum baking the boat and growth materials at just above 300 ^{o}C in situ before beginning the growth procedure will remove these adsorbed contaminants.

The pure graphite boat can be coated with a thin layer of either carbon or another material such as SiC, using chemical vapor depostion (CVD). These CVD layers are denser than the graphite used for the boat and so allow less adsorption of water vapor or other impurities into the boat. The disadvantages are that the deposited coating cannot be made as pure as the purified bulk graphite and the bulk graphite cannot be purified

once the coating has been applied. Through the repeated temperature cycling of processing runs, pinholes or cracks usually develop in the coating which allow outgassing from the bulk graphite. Graphite boats coated with pyrolytic (CVD) carbon were experimented with in the research conducted for this thesis. Epilayers grown with these boats were not of higher purity than epilayers grown using boats of pure graphite with no coating.

Other materials such as silica, glassy carbon, and sapphire have been used as boat materials, and have yielded high purity LPE layers, but have not found widespread use due to the difficulty of manufacture (Astles, 1990).

Process chamber

A sealed process chamber is necessary to create and maintain a suitable environment for epilayer growth (Moon, 1980).

The process chamber must be compatible with the growth atmosphere to be used, vapors from the solvent and solute, and the process conditions (heating to the growth temperature, maintaining the system for a prolonged time at the growth temperature, and cooling). The process chamber must also be machinable or formable in the shape required.

For high purity layer growth, the material for the process chamber must be available in high purity form and be easily cleaned. For the growth of III-V semiconductor epilayers, high purity silica is usually used for this purpose, although it reacts at high temperatures with hydrogen which is generally used as an ambient (discussed in Appendix VII). The growth chamber must be carefully cleaned and baked out before epilayer growth (discussed further in Section 2.4.2).

Growth atmosphere

The sealed growth chamber is typically filled with a gas, at varying pressures. This gas helps control the evaporation loss of the solution components because as the gas pressure in the chamber rises, the evaporation process is dominated more by diffusion through the vapor than by the molecular streaming which is dominant at lower pressures (Draper, 1975). High purity flowing gases continuously flushing the process chamber can be used to keep impurity contamination minimal.

For LPE growth of III-V semiconductor epilayers, the gas inside the process chamber is usually hydrogen purified by diffusing it through a Pd-Ag alloy at 300-400 ^{o}C. This gas is of high purity, normally containing << 1 ppm by volume of H_2O and O_2 (Engelhard, 1995). Hydrogen has the advantage of being able to reduce metal oxides which may be present on the surface of the growth solutions and on the substrate surface, and so is the most commonly used gas (Shah, 1975; Astles, 1990).

The effect of small concentrations of O_2 or H_2O in the ambient gas during LPE growth on the purity of epilayers makes the control of these two impurities during growth runs extremely important (Otsubo *et al.*, 1973; Morkoç and Eastman, 1976).

Gas delivery system

For high-purity layer growth, care must also be taken with the gas delivery system. The gas delivery system must be leak tight, and made of materials and components which will not contribute impurities to the flowing gas. Stainless steel was generally used as the material for the gas delivery system used for the research conducted for this thesis. All gas piping, connections and components that will be exposed to the process gas must be carefully cleaned and baked out (discussed in

Section 2.4.1). These connections and components are checked for leaks, and are repaired if leaks greater than 10^{-7} cc/sec are found[34].

Furnace design

One of the critical elements of LPE growth is that the solution and substrate must be kept at a precisely controlled temperature. The most common ways of heating the growth materials use radio frequency (r.f.) or resistive heating because they are the easiest to control and do not impose many constraints on the crystal growing system (Draper, 1975). As a resistively-heated furnace was used for the research conducted for this thesis, r.f. heating will not be discussed.

Astles (1990) has summarized some of the main considerations of a furnace design. The first is thermal mass of the furnace. Low thermal mass furnaces are used when rapid temperature changes are required, for example for step-cooled LPE growth. A commonly used low thermal mass furnace has an outer gold reflector tube composed of a silica tube coated on the inside with a thin, semitransparent film of gold [the gold film reflects 95% of the infrared energy (Shah, 1975)]. By reflecting most of the infrared radiation back into the tube, acceptable temperature stability and good temperature profiles may be obtained. These furnaces have low heat capacity, and consequently fast heat-up and cool-down times (Shah, 1975).

High thermal mass furnaces are usually used when temperature stability is important. High thermal mass can be achieved by installing bulky insulation between the heating element and outer furnace walls or by using a heavy furnace liner such as mullite or alumina tube. The thermal inertia of these furnaces normally limits the rate of cooling that can be achieved, to a maximum of approximately 5 ^{o}C per minute (Greene, 1986).

---

[34]Leak testing performed using a Varian mass spectrometer leak detector, model 959-50T, from Varian Vacuum Products, Lexington, MA

A high thermal mass, resistively heated furnace was used for the research conducted for this thesis. The high thermal mass of the furnace was achieved by using bulky insulation (high temperature ceramic fiber) between the heating element (resistance wire) and the outer furnace walls. The resistance wire is wound on to a ceramic tube and held in place with a refractory cement. To avoid short-circuiting of the turns in the windings at an operating temperature, each turn is placed in a groove in the refractory. Two types of resistance wires were used during the course of experimentation for this thesis, "Nichrome" (80% Ni, 20%Cr; 1100 °C maximum temperature) and "Kanthal A-1" (A-1: 22% Cr, 5.5% Al, 0.5% Co, balance Fe; 1300 °C maximum temperature). Resistance wires that can be used for higher temperature operation are platinum (maximum temperature approximately 1550 °C) and tungsten (maximum temperature 2950 °C) (Shah, 1975). The advantage of resistance furnaces is that a flat temperature profile can be maintained, which is critical for LPE growth.

Although various temperature profiles have been employed for LPE growth, in order to simplify control of the growth conditions most workers use a temperature profile that is as flat as possible (Hsieh, 1980). It is important that the temperature profile have a region that is at least as long as the LPE growth boat where the temperature is constant to within +/- 1 °C, called the 'flat zone'. To achieve a flat profile of adequate length, three-zone furnaces are often used, which require three separate temperature controllers. Such a furnace is being used for the research conducted for this thesis.

Vacuum attachments

Vacuum systems are used with LPE equipment as part of a procedure to evacuate and backfill the process chamber with the ambient gas to be used during the

epilayer growth process. This procedure is used to shorten the time required to purge the growth system with the ambient gas.

Astles (1990) summarized the vacuum system requirements for LPE growth. At their most basic, vacuum systems consist of a small roughing pump (which may be a rotary or sorption pump) used to evacuate the LPE process chamber after loading, followed by backfilling with the gas to be used during epilayer growth. A more sophisticated arrangement, for example for high purity epilayer growth, may consist of a high-vacuum system including a turbo-molecular, cryogenic, ion, diffusion, or titanium sublimation pump for thorough outgassing, possibly incorporating a mass spectrometer to monitor the presence of impurity gases in the growth environment. The vacuum system can also be used for leak testing the process chamber and gas delivery system or for in situ vacuum baking of the growth boat.

Even with careful selection and preparation of system materials, residual impurities are still identified in the layers. This will be discussed for the case of GaAs high purity epilayer growth in Section 3.1.1, and in Appendix VII.

APPENDIX VI: DETERMINATION OF CONVECTION CONDITIONS IN THE SOLUTION

Natural convection in the solution can have a strong influence on the solute concentration profile and thus on growth rate of the epilayer (see Figure 44). Cellular convection patterns in the solution may lead to uneven solute concentration and thus to an uneven growth rate. It is therefore generally of interest to minimize convection in the solution during LPE growth.

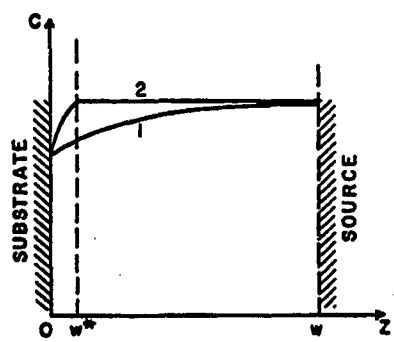

Figure 44. Solute concentration profile determined by diffusion-limited transport (curve 1) and convective transport (curve 2). The boundary layer thickness is at w^* (Long *et al.*, 1974).

In a two-component system such as GaAs, there are two means for driving natural convection, which is caused by density inversion. Density inversion can be created by thermal gradients (bottom hotter than top) or by solute gradients, such that the density at the top of the solution is greater than at the bottom of the solution. There is a critical value of temperature and/or (temperature-induced) solute gradient which must be exceeded before convection will occur.

Rayleigh (1920) originally showed that stability against convection due to thermal gradients is predicted by the following condition:

$$N_{Ra} = \frac{g\beta G_L W^4}{\alpha v} < 1700 \tag{37}$$

where g is the acceleration due to gravity, b is the coefficient of volume expansion, α is the thermal diffusivity, v is the kinematic viscosity, W is the height of the fluid layer, and G_L is the temperature gradient, and N_{Ra} is called the Rayleigh number. For Ga solutions Long *et al.* (1974) plotted the critical value of solution height vs. G_L. This is shown in Figure 45, where it can be seen that heights of less than approximately 1.5 cm should be stable against convection (even with a temperature gradient in the solution of 1.0 °C/cm).

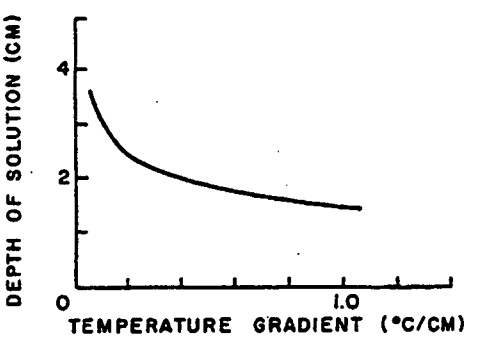

Figure 45. Critical solution height (above which convection will occur) for thermally induced density inversion as a function of temperature gradient (Long *et al.*, 1974).

For stability against convection due to solute gradients, a modified expression is used (Tiller, 1968):

$$N_{Ra} = \frac{g\phi W^3(\Delta C)}{Dv} < 1700 \tag{38}$$

where ϕ is the change of volume of solution with a change of solute concentration, ΔC is the concentration change over the length W (determined by the phase diagram), and D is the diffusion coefficient.

In Figure 46, the critical solution heights as a function of the temperature gradient G_L are plotted. It can be seen that the solute gradient contribution to convection (instability due to density inversion) is several times larger for the same temperature gradient than the thermal density gradient.

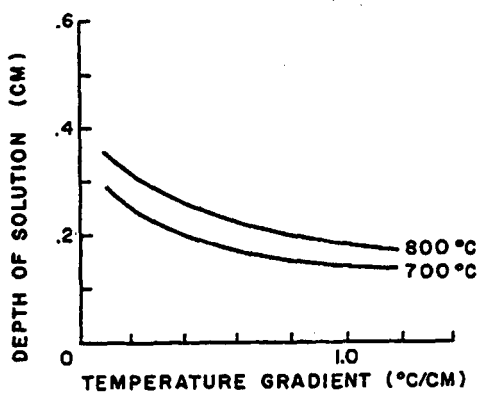

Figure 46. Critical solution height for solute-gradient-induced density inversion as a function of the temperature gradient (Long *et al.*, 1974).

Long *et al.* (1974) also deduced that the solute (As) density must be lower than the solvent (Ga) density, due to the configuration of his experimental set up (epilayer on top of the solution). A lower solute density could occur due to chemical bonding in the solution between Ga-As or As-As to lower the solute density.

Long *et al.* experimented with placing the substrate on top of and underneath the solution, found that tendency toward solutal convection was decreased when placing the substrate below the solution. This is further evidence that the solute density is lower than the solvent density.

APPENDIX VII: MOST COMMON IMPURITIES IN GaAs LPE LAYERS

Table 4 shows the most common impurities detected in high purity GaAs LPE layers, and the sources of these impurities.

Sources of impurities incorporated into high-purity GaAs LPE layers:

Carbon:

(i) The GaAs used for the solution has a maximum of approximately 5×10^{15} cm^{-3} carbon impurities (AXT, 1996). But due to the small amount of GaAs dissolved into the Ga to form the growth solution, this is not a significant contribution to the impurity concentration in LPE layers. For example, carbon was identified as the main residual acceptor in high purity LPE layers which had an approximate net donor concentration of 10^{12} cm^{-3}, and a 77 K electron mobility greater than 200,000 $cm^2/V.s$ (Silier *et al.*, 1992).

(ii) Etching with bromine-methanol mixtures leaves residual carbon contamination (Brozel *et al.*, 1978). Brozel *et al.* report that etching with sulfuric acid-hydrogen peroxide mixtures effectively removes carbon contamination, but leaves residual sulfur. The residual sulfur contamination can be removed with a subsequent HCl etch.

Oxygen:

(i) Hydrogen gas contains oxygen and water vapor contamination unless specially purified (discussed in Appendix V).

(ii) Because the graphite is porous, oxygen, water vapor, and other gaseous impurities are adsorbed onto the graphite when it is exposed to air. To minimize the adsorption of impurities between growth runs, the graphite must be kept in a protective atmosphere such as high-purity argon.

(iii) The gas delivery system must be designed to minimize oxygen/water vapor incorporation. For high-purity gas delivery, vacuum-tight stainless steel gas piping, connections, and components are used (discussed in Appendix V).

Oxygen is a volatile impurity which is removed by baking the growth system and layer materials (Astles, 1990). It has been determined experimentally that the concentration of oxygen donors in LPE layers decreases with increasing growth temperature (Otsubo *et al.*, 1973; Mattes *et al.*, 1975; Houng *et al.*, 1978; Nanishi, 1978).

Silicon:

Silicon contamination is due mainly to reactions between materials in the growth system at the temperatures used for LPE growth (Silier, 1992; Astles, 1990).

Reduction of silica components (such as process chamber) by H_2:

$$H_{2(g)} + SiO_{2(s)} \rightarrow SiO_{(g)} + H_2O_{(g)} \tag{39}$$

Addition of water vapor will reverse this process:

$$SiO_{(g)} + H_2O_{(g)} \rightarrow SiO_{2(s)} + H_{2(g)} \tag{40}$$

Addition of oxygen will also reverse reaction (39), because at the usual LPE growth temperatures the following reaction is to the right:

$$H_{2(g)} + 1/2\ O_{2(g)} \rightarrow H_2O_{(g)} \tag{41}$$

Reaction of evaporated Ga and SiO_2 components:

$$2Ga(\text{at wall}) + SiO_{2(s)} \rightarrow SiO_{(g)} + Ga_2O_{(g)} \tag{42}$$

The following reaction also occurs:

$$2Ga(\text{at wall}) + H_2O_{(g)} \rightarrow Ga_2O_{(g)} + H_{2(g)} \tag{43}$$

It can be seen by reaction (39) that the addition of water vapor or oxygen will decrease the reduction of SiO_2 by the Ga vapor in reaction (42).

Reaction of graphite and silica:

The presence of graphite in contact with the silica leads to silicon contamination in the solution at temperatures greater than 1000 °C (Bauser, 1996):

$$C_{(s)} + SiO_{2(s)} \rightarrow CO_{(g)} + SiO_{(g)} \tag{44}$$

The SiO produced in reactions (39), (42), and (44) draws close to the solution, is then reduced further and dissolves into the solution (Silier, 1992).

As mentioned above, addition of a few ppm of oxygen or water vapor to the H_2 gas has been found to reduce Si contamination in LPE layers by suppressing reactions (39) and (42), and by oxidizing the silicon in the solution through the reaction

$$Si(l) + H_2O(g) \leftrightarrow SiO_2(s) + H_2(g), \tag{45}$$

forming SiO_2 particles in the growth solution (Holmes & Kamath, 1981). However, this addition of oxygen or water vapor must be carefully controlled, because concentrations of water vapor or oxygen in the H_2 gas stream of greater than a few ppm contribute oxygen donors to the epilayer (Astles, 1990).

Sulfur:

The graphite boat and the Ga solvent are sources of sulfur.

To reduce the sulfur contamination in the epilayers, the graphite must be specially purified to remove volatile impurities like sulfur (discussed in Appendix V).

The growth materials are generally baked in the H_2-flushed LPE system at a temperature at or above the growth temperature for at least four hours.

TABLE 4:

IMPURITY	k^*	SOURCES
Carbon (Acceptor)	0.2-0.8 (M)	(i) GaAs material used for the solution. (ii) Chemical preparation of GaAs substrate and GaAs used for the solution.
Oxygen (Donor)	0.3 (M) $3x10^{-4}$ (LPE)	(i) H_2 gas (oxygen and water vapor impurities) (ii) Graphite (oxygen and water vapor adsorbed when graphite is exposed to air). (iii) Air leaks in the gas delivery system
Sulfur (Donor)	0.3 (M)	(i) Graphite (ii) Ga solvent
Silicon (Don. or Acc.)	0.14 (M) $6\text{-}8x10^{-2}$ (LPE)	Reaction of materials in growth system at LPE growth temperatures

k*, segregation coefficient (Appendix II)

Note: Next to the values of k on the chart, there will be either be an "M" which stands for "melt growth" (i.e., bulk crystal growth of GaAs from a GaAs melt), or an "LPE" which stands for LPE growth of GaAs from a dilute solution of As in Ga. Where data is available for both the LPE and melt growth case, k is observed to be much smaller for LPE growth. The values of k (M) are from Kressel and Butler (1977), k (LPE) from Astles (1990).

Incorporation of impurities into the GaAs lattice:

It has been found that atoms of the Group II elements occupy only Ga sites, and atoms of the group VI elements sit only on the As sublattice (Deitch, 1975). The group IV elements are amphoteric dopants in GaAs and theoretically can occupy either the Ga sites to provide donor states or the As sites to provide acceptor states. However, C has only been detected experimentally on the As site, to provide acceptor behavior. The growth of Si-doped GaAs from solution yields either highly compensated n-type or highly compensated p-type epilayers depending on the concentration of Si in the solution, the particular growth rate and temperature range over which the growth occurs, and the crystallographic orientation of the substrate wafer. Figure 47 shows the conductivity-type transition temperature as a function of Si concentration in the growth solution for GaAs LPE layers grown on (111)Ga, (111)As, and (100)GaAs surfaces.

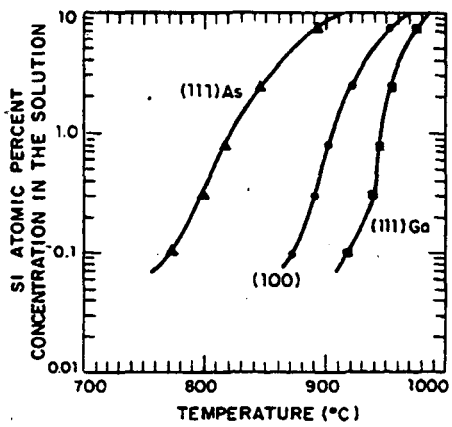

Figure 47. Conductivity-type transition temperature as a function of Si concentration in the growth solution for GaAs LPE layers grown on (111) Ga, (111) As, or (100) GaAs substrates. For a given orientation and Si concentration, epilayers grown at temperatures above the transition temperature are n-type, and those grown at temperatures below the transition temperature are p-type (Ahn *et al.*, 1971).

Germanium acts as an acceptor when it is incorporated at the LPE growth temperatures of 700 - 900 ^{o}C, and acts as a donor when used as the dopant atom in the well-known Ni-Ge-Au alloyed contacts, which are annealed at approximately 450 ^{o}C.

APPENDIX VIII: HALL EFFECT MEASUREMENTS

The Hall effect measurement technique is commonly used for the characterization of semiconductor materials because it provides the net carrier type and the average value of net carrier concentration for a sample. The mobility can be calculated from the Hall factor and the resistivity.

The Hall effect is a consequence of the Lorentz force ($\mathbf{F_L}$) exerted on charge carriers (with charge q) moving with a velocity v in a magnetic induction **B**:

$$\mathbf{F_L} = q\,(\mathbf{v} \times \mathbf{B}) \tag{46}$$

This effect was discovered by the physicist E.H. Hall in 1879 while experimenting with thin metallic foils. He discovered that a magnetic field applied perpendicular to the direction of current flow produced an electric field perpendicular to both the magnetic field and the current.

When the Hall effect is measured in semiconductors, it is usually measured in an extrinsic semiconductor in which one carrier type is dominant, and the other has a negligible density (i.e. n>>p or p>>n). The following derivation is valid only for this case, and is not valid if n is on the order of p. To illustrate the description of the Hall effect for both electrons and holes, however, both carrier types are shown in Figure 48.

The basic theory for the Hall effect can be derived with the aid of Figure 48. A voltage **V** is applied across the sample in so that the right-hand side is negative. There is consequently an electric field $\mathbf{E_x}$ in the positive x-direction, given by

$$\mathbf{E_x} = -\,\partial V/\partial x, \tag{47}$$

and a current density **J** flows in the positive x-direction. This is indicated in Figure 48 by holes flowing to the right or electrons flowing to the left. A constant external magnetic induction **B** is applied in the positive z-direction.

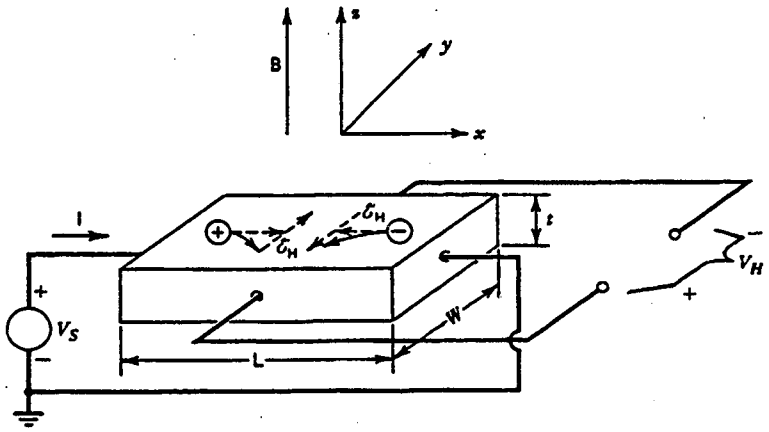

Figure 48. Schematic of the Hall effect. The schematic shows the induced Hall field E_H for electrons and holes due to the applied electric field and magnetic induction.

The Lorentz force on the electrons or holes due to the applied electric field and magnetic induction is

$$\mathbf{F} = q\mathbf{E} + q(\mathbf{v} \times \mathbf{B}), \tag{48}$$

where the vector cross product (x) signifies the product of the vector magnitudes times the sine of the angle between them.

For electrons, in Figure 48 v_x is negative. So $\mathbf{v} \times \mathbf{B} = v_x B_z$, pointing in the y-direction.

Since q for electrons is negative the Lorentz force on the electrons due to the magnetic field is in the -y direction, and the electrons will be deflected in the -y direction. In the sample of Figure 48 there is no closed current path for the carriers in the y-direction, so the electrons will accumulate at the bottom of the sample. An electric

field is generated in the y-direction by this charge distribution, which increases until it exactly counteracts the Lorentz force due to the originally applied magnetic field:

$$\mathbf{E}_y = \mathbf{v}_x\mathbf{B}_z. \tag{49}$$

This induced electric field $\mathbf{E}_y$ is known as the Hall field.

It must be noted that if the balancing of the Hall force by the Lorentz force were achieved for all carriers (i.e., if all carriers had the same drift velocity **v**), then once the Hall field had been established all carriers would move through the sample undeflected by the magnetic field. This would then imply that there would be no change in the sample resistance on applying a magnetic field. But this is not true for semiconductors: there is an associated magnetoresistance, demonstrating that the Lorentz balance condition is not achieved for most of the carriers (Stradling, 1991).

The current density can be written as

$$\mathbf{J}_x = nq\mathbf{v}_x, \text{ yielding } \mathbf{v}_x = \mathbf{J}_x/nq \tag{50}$$

where n is the carrier concentration. The Hall field is then

$$\mathbf{E}_y = \mathbf{J}_x\mathbf{B}_z/nq = R_H\mathbf{J}_x\mathbf{B}_z \tag{51}$$

with

$$R_H = 1/nq \tag{52}$$

R_H is called the Hall coefficient. Since for electrons the charge q = -e, the Hall coefficient for electrons is negative in sign.

The Hall field can be measured by measuring the Hall voltage V_H across the sample as shown in Figure 48. The Hall voltage is:

$$V_H = \int_0^W E_y dy = - E_y W \tag{53}$$

where W is the sample width shown in Figure 48.

The derivation of Hall effect relations for holes follows the same formalism as for electrons. From Figure 48, v_x for holes points in the positive x-direction. The force due to the magnetic induction is again

$$\mathbf{F} = q(\mathbf{v} \times \mathbf{B}); \qquad \mathbf{v} \times \mathbf{B} = - v_x \mathbf{B}_z$$

in the y-direction (= $v_x \mathbf{B}_z$ in the -y direction), and since q for holes is positive, the force on the holes due to the magnetic induction is in the -y direction.

It can be seen from the previous calculations for electrons and holes that the effect of the magnetic induction is to make both electrons and holes tend to drift to the **same** side of the current direction, since both the charge and velocity are of opposite sign for electrons and holes. The induced Hall voltage is therefore of opposite polarity for holes and electrons. The sign of the Hall voltage reveals whether a semiconductor is n- or p-type.

For normal metals V_H is on the order of a few microvolts, but for semiconductors, because of the much lower free carrier concentration, V_H is much higher for the same magnetic induction.

In the previous derivation of the Hall effect equations the ideal case is treated, which assumes that the charge carriers all move with the same (average) drift velocity.

The carrier collision time τ, in general a function of the velocity v, is taken to be a constant so that the equation

$$v_x = \frac{e\tau}{m}\mathbf{E} = \mu\mathbf{E} \tag{54}$$

(where e is the charge of the carrier, m is the mass of the charge carrier, μ is the mobility and E is the electric field) may be applied to the free electrons in the conduction band and free holes in the valence band.

The equation $R_H = 1/nq$ holds exactly only when τ is not a function of the velocity (or energy). A numerical factor, r, is included when the scattering mechanisms are energy dependent:

p = hole carrier concentration = r/qR_H,

n = electron carrier concentration = $-r/qR_H$

where r is the Hall scattering factor, defined by $r = \frac{\langle\tau^2\rangle}{\langle\tau\rangle^2}$, with τ being the mean time between collisions of the carriers. The scattering factor depends on the scattering mechanisms in the semiconductor and generally lies between 1 and 2.

The Hall coefficient R_H is no longer independent of the magnetic induction but changes from r/nq in the limit of low magnetic inductions ($\mu B << 1$) to 1/nq at higher inductions ($\mu B >> 1$). The scattering factor has been measured in n-type GaAs at room temperature as a function of magnetic induction and was found to vary from 1.17 at B = 0.1 kG, as expected from lattice scattering, to 1.006 at B = 83 kG (Rode *et al.*, 1983). Note that r is dependent on the magnetic induction, temperature, and crystal orientation.

Sample geometry, configuration for Hall effect and resistivity measurements

The simplest and most easily evaluated Hall effect sample geometry is the "Hall bar", a parallelepiped shown in Figure 49. However, it is not always straightforward to form a Hall bar with precise dimensions. In an effort to make resistivity and Hall effect measurements less sensitive to geometry, van der Pauw (1958) showed that a continuous sample (no holes) with irregular outer periphery but constant thickness (also called lamellae) can be mathematically transformed into a half plane. The sample periphery maps on the half plane boundary. Four ohmic contacts are applied at the sample boundary. Numbering the contacts as in Figure 50 we define:

$$V_{xy} = V_x - V_y \ (x, y = 1, 2, 3, 4 \text{ and } x \neq y) \tag{55}$$

$$\Delta V_{xy} = (V_x - V_y)_{\text{with B}} - (V_x' - V_y')_{\text{without B}} \tag{56}$$

I_{xy} = current flowing from x to y.

We further define

$$R_{12,34} = V_{34}/I_{12} \tag{57}$$

and

$$R_{14,23} = V_{23}/I_{14}. \tag{58}$$

A set of resistance measurements is performed with current flowing from 1 to 2 and then from 1 to 4. The resistivity ρ is found to be

$$\rho = \frac{\pi t}{\ln 2} \cdot \frac{1}{2}\left[\frac{V_{34}}{I_{12}} + \frac{V_{23}}{I_{14}}\right] \cdot F \tag{59}$$

The correction factor F shown in Figure 51 varies very slowly with the ratio of $R_{12,34}/R_{14,23}$ making such measurements insensitive to the precise geometry.

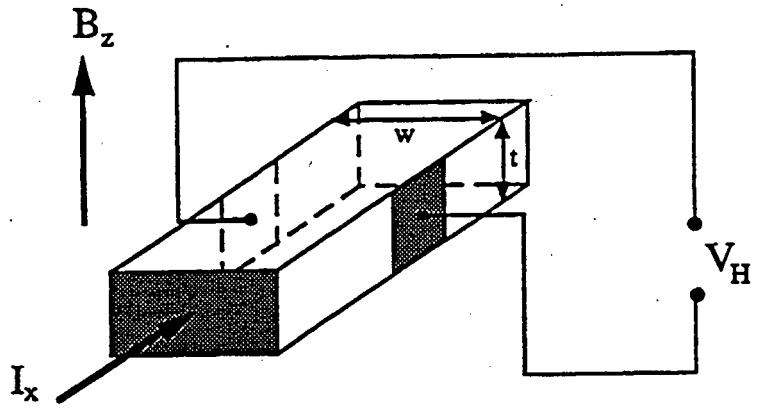

Figure 49. Schematic of "Hall bar". The shaded areas are contacts (Dubon, 1996).

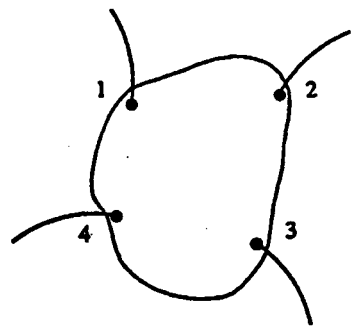

Figure 50. A lamella-type van der Pauw Hall sample (After van der Pauw, 1958).

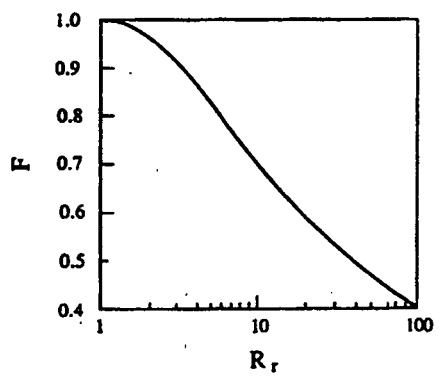

Figure 51. Variation of correction factor F with resistivity ratio (R_r) (After van der Pauw, 1958)

In order to determine the free carrier concentration a Hall effect measurement is performed in the van der Pauw geometry of Figure 50. ΔV_{24} (see Equation 57) is

measured with current flowing from contacts 1 to 3 (and the reverse) with and without magnetic induction, and ΔV_{13} is measured with current flowing from contacts 2 to 4 (and the reverse) with and without magnetic induction. The Hall coefficient R_H is found to be

$$R_H = \frac{t}{2BI} \cdot \frac{1}{4}\left[(\Delta V_{24})_{I_{13}} + (\Delta V_{24})_{I_{31}} + (\Delta V_{13})_{I_{24}} + (\Delta V_{13})_{I_{42}}\right] \tag{60}$$

where t is the thickness of the sample (epilayer), B is the magnetic induction, and I is the magnitude of the current applied (which will be the same for I_{13}, I_{31}, I_{24} and I_{42}). Referring to Equation 52, the free carrier concentration $n = \frac{r}{qR_H}$, where r is the Hall scattering factor.

The mobility, μ, is then determined by the relation

$$\mu = \frac{r}{qn\rho} = \frac{R_H}{\rho} \tag{61}$$

It is important to keep the contacts small and well-separated on the sample so that the current contacts don't short out the Hall field near the Hall contacts and distort the current flow. The influence of the contacts can be reduced by using the clover-shaped "van der Pauw disk" (Figure 52). The shape of Figure 52 is usually fabricated using photolithographic methods. For a detailed discussion of the measurement procedure and for measurement precautions see ASTM standard F76 (1988).

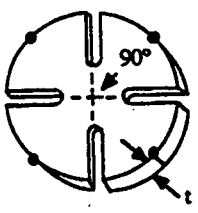

Figure 52. Clover-shaped sample which reduces the effects of the contacts (van der Pauw, 1958)

Several cases of nonideal contacts were treated by van der Pauw (1958a) (Figure 53).

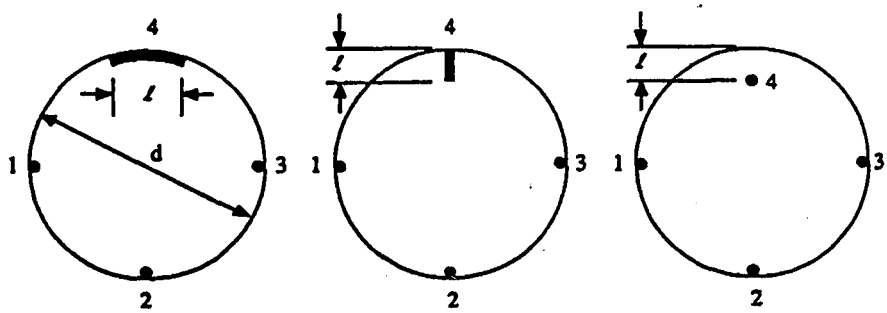

Figure 53. Nonideal contact length or placements evaluated by van der Pauw (1958a).

Errors due to displaced contacts on square samples are discussed in Perloff (1977), and David and Buehler (1977). For square samples with sides of length L having square and triangular contacts of contact length d in the four corners, Chwang *et al.* (1974) reported that less than 10% error was introduced for Hall measurements as long as $d/L < 0.1$.

It is important to note that for epitaxial or implanted thin layers on substrates of opposite conductivity or on semi-insulating substrates, the active film thickness is not necessarily the total film thickness. Depletion effects caused by Fermi level pinned band bending or surface charges and by band bending at the layer-substrate interface must be considered for the correct calculation of the Hall coefficients (Chandra *et al.*, 1979; Ham, 1972).

Preparation of samples For Hall effect and resistivity measurements

- Cleave square samples, generally 3 mm to 5 mm on a side
- Etch samples in hot HCl to ensure that all metallic gallium and surface oxides have been removed

- Rinse in D.D.I. water
- Press small pieces of In-Sn eutectic onto the corners of the sample, anneal at 400 °C for 10 minutes in a nitrogen atmosphere to limit oxidation of sample and contacts

Resistivity measurement -- co-linear four point probe

The use of four probes for resistivity measurement has an important advantage over two probes. Two of the probes will be used to carry current and will have contact and spreading resistance (the resistance encountered by the current when it flows from the small metal probe into the semiconductor) associated with them, and two probes will be used for current-free voltage measurement. It is important to measure the voltage between two probes through which no or very little current is flowing to avoid the effects of contact and spreading resistance on the measurement.

The potential, V, at a distance, r, from the electrode carrying a current, I, in a material of resistivity, ρ, is given by the relationship (Valdes, 1954)

$$V = \frac{\rho I}{2\pi r}; \text{ or } \rho = 2\pi r \frac{V}{I}. \tag{62}$$

For thin samples such as epitaxial layers,

$$\rho = \frac{\pi t}{\ln(2)} \frac{V}{I} = 4.532 t \frac{V}{I} \tag{63}$$

where t is the epilayer thickness.

APPENDIX IX: SECONDARY ION MASS SPECTROSCOPY (SIMS)

SIMS is used to quantitatively measure the depth distributions of impurities or intentional dopants in semiconductor samples. There are two types of SIMS measurements: static and dynamic. Static SIMS probes only the first 1 or 2 monolayers of a sample, and will not be discussed further here. Dynamic SIMS was used as one of the methods of impurity detection in this project, and will be discussed below.

With both types of SIMS, elements and their isotopes from H to U can be identified.

In dynamic SIMS a solid specimen is placed in a vacuum and bombarded with a narrow beam of primary ions that are sufficiently energetic to sputter single and small clusters of atoms from the sample surface. Heavy primary ions (e.g., oxygen, cesium, gallium) are used, having energies between 1 and 20 keV. Some fraction (depending on the energy of the beam and its angle of incidence) of the atoms and atomic clusters are ejected from the sample surface as secondary ions. These secondary ions are accelerated into a mass spectrometer, where they are separated according to their mass-to-charge ratio and counted. A typical SIMS profile is collected as secondary ion counts per second vs. sputtering time and then converted to a plot of concentration vs. depth by measuring the depth of the sputtering crater and comparing the data to standards.

In general, the detection limit of impurities in GaAs lies approximately between 10^{14} cm^{-3} and 10^{17} cm^{-3} (Brundle *et al.*, 1992)). The detection limit of an element is affected by how efficiently it ionizes, known as the ion yield:

$$\text{ion yield} = \frac{\text{\# of A ions}}{\text{total \# of A atoms sputtered from the sample}}$$

The major factor that affects the ion yield of an element or molecule is its ionization potential (in the case of positive ions) or electron affinity (in the case of negative ions).

One of two kinds of primary ion beams commonly used in dynamic SIMS analyses is oxygen (O_2^+ or O^-), or cesium (Cs^+). The use of an oxygen beam can increase the ion yield of of positive ions, while the use of a cesium beam can increase the ion yield of negative ions by as much as four orders of magnitude. The enhanced ion yields of the cesium ion beam can be explained using a work function model (Andersen, 1970), which postulates that because the work function of a cesiated surface is drastically reduced, there are more secondary electrons excited over the surface potential barrier to result in enhanced formation of negative ions. The Cs^+ ion beam was used for the detection of impurities in epilayer #11 grown for this thesis. Results of the SIMS analysis are listed in Table 5. The only element that registered above the detection limits was sulfur.

TABLE 5: Results of SIMS analysis of epilayer 11

Element	Avg. Bulk Concentration (cm^{-3})
C	$\leq 6x10^{15}$
O	$\leq 1x10^{16}$
Si	$\leq 4x10^{14}$
S	$2.3x10^{16}$
Cu	$\leq 5x10^{16}$
Ge	$\leq 3x10^{15}$
Se	$\leq 2x10^{13}$
Te	$\leq 9x10^{12}$

APPENDIX X: PHOTOTHERMAL IONIZATION SPECTROSCOPY (PTIS)

The photothermal ionization effect in semiconductors was first described theoretically by Kogan and Sedunov (1967) and analyzed experimentally by Lifshitz et al. (1968). The PTIS technique was fully developed by Haller (see for example Haller and Hansen 1974, Haller *et al.*, 1974) in the 1970's and 80's in conjunction with ultrapure Ge research. It led to several major discoveries such as electrically active hydrogen containing complexes (Haller 1977, 1978) and hydrogen tunneling (Joós *et al.*, 1980; Falicov and Haller, 1985; Kahn *et al.*, 1986).

The photothermal ionization of a shallow impurity atom requires two steps: absorption of a photon with sufficient energy to excite the bound electron/hole from the ground state of the impurity to one of the bound excited states, followed by absorption of a phonon to promote the carrier in the bound excited state into the conduction/valence band. In the final state the carrier is free and contributes to electrical conduction.

These transitions are represented schematically in Figure 54.

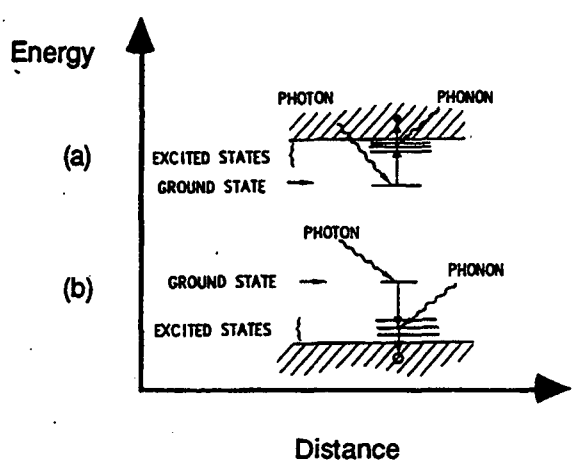

Figure 54. Schematic drawing (energy vs. distance) of photon-excited transition of an electron (a) or hole (b) from the ground state to an excited state, followed by a phonon-stimulated transition to a free state in the conduction or valence band (Bratt, 1977).

To provide a phonon population so that the photothermal ionization effect can take place, the sample temperature must be high enough that there is a significant probability of thermal ionization of the donor electron/acceptor hole from the bound excited state into the conduction/valence band, but not so high that a significant number of the donors/acceptors in the sample are thermally ionized, which would leave too few (neutral) donor electrons/acceptor holes available to absorb the incident far infrared light. For photothermal ionization measurements of n-type GaAs, this limits the temperature to a range between about 1.5 and 6 K. At temperatures higher than about 3 K, nearly every electron which is optically excited into a higher energy state is thermally ionized before it can fall back to the ground state (Stillman *et al.*, 1977).

The method used to study shallow impurities via the photothermal ionization mechanism is called photothermal ionization spectroscopy (PTIS). Usually a PTI spectrum is taken at an appropriate fixed temperature with an incident photon flux (infrared in the case of GaAs) from a broad band light source modified by a Michelson interferometer. The schematic diagram of the essential components of a Michelson interferometer is shown in Figure 55. Referring to Figure 55, the two photon beams reflected by the moving and fixed mirrors impinge on the sample. Moving one of the mirrors continuously changes the wavelength composition of the photon beam impinging on the sample. The two photon beams impinging on the sample interfere constructively or destructively, producing an interferogram. When the beam from the interferometer contains photons with energy matching some ground-to-excited state transition energy for a shallow impurity present in the sample (e.g., the 1s to $2p_{-1}$ transition of a shallow Si donor in GaAs), then an increase in the photoconductivity signal (i.e., the photoinduced change in the current in the sample) will be observed. The photoconductivity interferogram can be changed by mathematical Fourier transformation into a wavelength or more often a wavenumber spectrum. A PTI

spectrum then consists of a plot of the photoconductive signal as a function of far-infrared photon energy. The peaks in such a spectrum are directly related to ground to bound excited states of specific dopants. This allows for an unambiguous identification of the majority type dopants in a semiconductor sample.

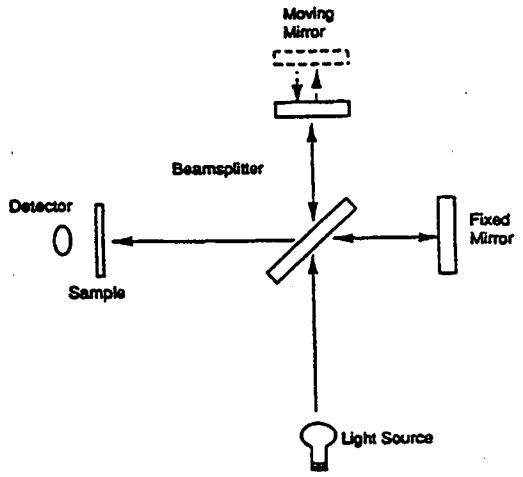

Figure 55. Diagram of essential components of a Michelson interferometer (Hsu, 1994).

For these photoconductivity measurements, ohmic electrical contacts are formed on opposite edges of the epilayer. The epilayers grown for this thesis were all n-type. Contacts were made either using alloyed In-Sn pieces, or by a Au-Ni-Ge film deposited by electron beam evaporation and subsequent alloying. Since four ohmic contacts are required for the van der Pauw Hall effect measurements we can also perform PTIS on the same samples.

Because PTIS is based on a change in photoconductivity in semiconductor samples which have extremely low conductivity because their dopants are frozen out by cooling to liquid He temperatures, this method has an excellent sensitivity for the presence of small concentrations of impurities in a semiconductor sample. Indeed, the purer the sample the sharper are the impurity transition lines due to the absence of

impurity interactions. In ultrapure Ge linewidths as small as a few μeV have been recorded (Haller, 1985).

A major application of PTIS so far has been in the study of impurity excited state transitions, for the detection and identification of residual impurities in high-purity semiconductors (Haller, 1985).

A considerable amount of work has been done by researchers to identify the chemical donor species associated with the peaks in the PTI spectrum of GaAs (For example: Ozeki et al. 1977; Wolfe et al. 1977; Cooke et al 1978; Low et al. 1982a,b).

In a typical semiconductor sample the impurity transitions are inhomogeneously broadened through a variety of processes. In pure structurally perfect GaAs this broadening is believed to be caused by the electric fields and field gradients due to the random distribution of charged impurities in the vicinity of each neutral impurity atom, and the resulting shifts of the donor state energies (linear and quadratic Stark effect) (Larsen 1973, 1976). As the sample purity decreases, the impurity transitions become broader and the peaks in the photoconductivity spectrum broaden as well.

Shallow impurity ionization energies can be estimated by using the following hydrogenic model based on the effective mass theory (Luttinger and Kohn, 1955; Mitchell and Kittel, 1954). With respect to donors, a donor atom has one extra valence electron and one extra positive charge on its ion core than the host crystal atom it replaces. A neutral donor in a semiconductor is an excellent analogy to a hydrogen atom in a vacuum (Ramdas and Rodriguez, 1981). A model Hamiltonian for the donor electron can be written in the same form as the Hamiltonian of the hydrogen atom, replacing the free electron mass m by the electron effective mass in the semiconductor, m^*, and replacing the permittivity of free space e_0 by the static dielectric constant of the semiconductor, ε_s:

$$H = \frac{p^2}{2m^*} - \frac{e^2}{4\pi\varepsilon_s r} \quad , \tag{64}$$

The energy E and Bohr radius a of the *n*th state are

$$E_n = \frac{m^* e^4}{8h^2 \varepsilon_s^2 n^2} = \frac{(m^*/m)}{(\varepsilon_s/\varepsilon_0)^2 n^2} \times 13.61\text{eV}, \tag{65}$$

and

$$a_n = \frac{e^2}{2(4\pi\varepsilon_s)E_n} = \frac{(\varepsilon_s/\varepsilon_0)n^2}{(m^*/m)} \times 0.5292\text{Å}, \tag{66}$$

where m*/m is the effective mass ratio and $\varepsilon_s/\varepsilon_0$ is the relative static dielectric constant of the semiconductor.

From the above equations it can be seen that the energy levels of the shallow donor are much smaller and the Bohr radius of the electron is much larger than that of the hydrogen atom.

For direct-gap semiconductors such as GaAs, having nearly isotropic and parabolic conduction band minima, large dielectric constants, and small effective mass ratios, the donor ionization energies predicted by the hydrogenic model are very small compared with the bandgap (e.g., 5.7 meV vs. a bandgap of 1.42 eV at 300 K in GaAs), and the Bohr radius is large compared with a lattice constant (e.g., a Bohr radius of ~100 Å vs. a lattice constant of $a_l \simeq 5.6$ Å for GaAs). It is observed experimentally that for GaAs, the hydrogenic model predicts the observed donor transition energies very well.

The same derivation of ionization energy and Bohr radius can be performed for shallow acceptor impurities and the equations will be the same as those derived for a shallow donor except that the hole effective mass has to be used.

For a given semiconductor, the hydrogenic model predicts identical ionization energies for different chemical donor species, and identical ionization energies for different chemical acceptor species. However, when the electron/hole resides within a few lattice constants of the impurity ion core, the potential felt by the electron/hole is no longer the simple coulombic potential but depends on the details of the electronic structure of the impurity ion core and the local distortion of the lattice around it. The dependence of the potential on the chemical species of the ion core results in small differences between the ground-state energies of different donors and acceptors. The difference between the ground-state energy of a given donor or acceptor species and the hydrogenic value given by equation (64) is called the central cell correction or chemical shift. (Stillman *et al.*, 1977).

In III-V compounds with direct band-gaps, the donor energies are small and the central cell shifts of the ground states for different donor species differ by no more than a few tenths of a meV. At a residual impurity concentration in the 10^{14} cm^{-3} range, the resultant linewidths are such that the different donor impurity energies can barely be differentiated in photothermal ionization spectra at zero magnetic field (Armistead *et al.*, 1984). Using the Zeeman effect these donor energies can be resolved. See Figure 56 for a schematic of this effect.

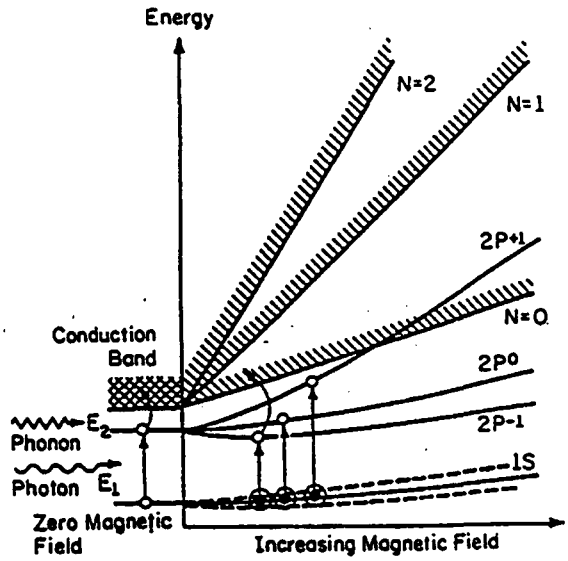

Figure 56. Schematic picture of the magnetic-field dependence of the hydrogenic 1s and 2p state energies. The three different curves for the 1s state represent three different donor species with three different central cell shifts (exaggerated in the figure). Three of the Landau levels are also shown labeled by their N values (Stillman *et al.*, 1977).

Zeeman effect (with respect to donor impurities)

In a magnetic field the (1s-2p) transition peak splits into three distinct components corresponding to the transitions from the 1s to the (2p, m = +/- 1, 0) states. Figure 57 shows the variations of the experimental energies of the (1s → 2p) and (1s → 3p) with magnetic field for GaAs. The normal Zeeman splitting of the m = +/- 1 states of a hydrogenic donor is given by

$$\Delta E_{+1,-1} = E(2p_+) - E(2p_-) = \frac{e\hbar H}{m_0^* c}, \tag{67}$$

where m_0^* is the electron effective mass at the bottom of the conduction band.

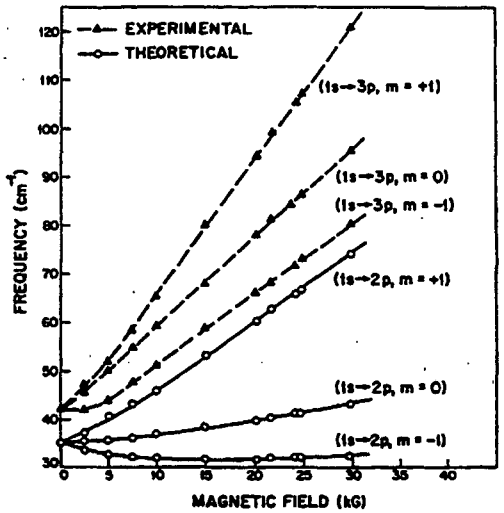

Figure 57. Energies of the (1s → 2p) and higher donor transitions as a function of magnetic field. The solid curves are from the variational calculations of Larsen (1968). (Stillman *et al.*, 1977)

The separation between the different peaks (splitting) in a given transition group (such as 1s → 2p, m = +/- 1 or 1s → 2p, m = 0) increases with increasing magnetic field. It was confirmed that the splitting observed in the (1s → 2p) transition was due to central cell corrections and that the increase in the splitting with increasing magnetic field was due to the shrinking of the wave function of the bound electron into the central cell by the magnetic field (Stillman *et al.*, 1977).

The 1s → $2p_{-1}$ transitions are of particular interest for analytical donor spectroscopy since they have the largest amplitude and the narrowest peak widths of all of the hydrogenic transitions. A substantial narrowing of the 1s → $2p_{-1}$ photothermal ionization peaks is observed as the magnetic field is increased up to 5 T and higher (Korn and Larsen, 1973). (In zero magnetic field the $2p_{+/-1}$ wave functions are pancake-shaped; with increasing magnetic field the $2p_{+/-1}$ wave functions are elongated and at high magnetic fields have a cigar shape.) This peak narrowing, together with the fact that central cell shifts of the ground state of different donor species increase with increasing magnetic field due to the compression of the 1s wavefunction into the central

cell (Fetterman *et al.*, 1971) has the effect of allowing the closely spaced $1s \rightarrow 2p_{-1}$ photothermal ionization peaks due to individual donor species to be more easily resolved at high magnetic fields. For this reason photothermal ionization spectra are often recorded at high magnetic fields (B = 3-12 T).

APPENDIX XI: PHOTOLUMINESCENCE (PL) MEASUREMENTS

Note that only the aspects of PL related to impurity identification in semiconductors (particularly in GaAs) will be discussed here.

Photoluminescence refers to any emission of light that results from optical stimulation. The light involved in PL excitation and emission measurement usually falls in the range 0.6-6 eV (200-2000 nm), because this energy range covers the majority of semiconductor materials.

A more detailed description with respect to semiconductors is that PL is the spontaneous emission of radiation from a semiconductor when it is optically excited by radiation with photons of energies greater than the bandgap of the semiconductor. With this kind of optical excitation, photons are strongly absorbed near the surface with the creation of free holes and electrons. At low temperatures (e.g., liquid helium temperatures) in insulators and semiconductors, these free electrons and holes can form bound states (excitons) due to the Coulomb attraction between them.

The excitons created reach thermal equilibrium through the emission of phonons (Stillman *et al.*, 1994). Excitons can move freely throught the crystal or can be bound to impurities or defects in the crystal. After a characteristic lifetime, the excitons will recombine. In luminescent materials some or all of the energy emitted during this recombination is in the form of light. Figure 58 is a schematic illustration of this process.

We distinguish between free and bound excitons. Upon recombination free excitons create the highest energy photons while bound excitons lose a small amount of binding energy which is very characteristic for the defect or impurity to which the exciton was bound. This energy dependence leads to multiple PL peaks and lines which

offer precise information on the impurities and defects in the semiconductor sample.

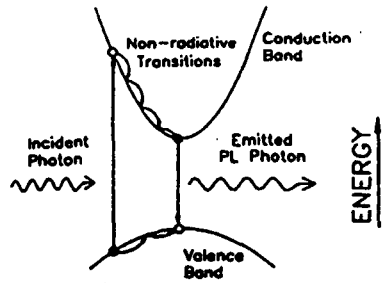

Figure 58. Schematic of PL for a crystalline system (Brundle *et al.*, 1992).

Typically, light is directed onto the sample for excitation, and the emitted luminescence is collected by a lens and passed through an optical spectrometer onto a photodetector. The spectral distribution and time dependence of the emission from the sample are evaluated. The main uses of PL measurements for semiconductors are for the determination of band gaps, carrier lifetimes, shallow and deep impurity or defect detection, sample quality and structure (Stillman *et al.*, 1994). Photoluminescence is generally most useful in semiconductors with direct bandgaps, in which transitions are momentum-allowed. However, especially at low temperatures, localized bound states and phonon assistance allow certain photoluminescent transitions to appear even in materials with an indirect band gap.

The typical depth and width probed in PL measurements are a few micrometers. The sample to be measured must be a liquid or solid having optical transitions. The sample may be in air, vacuum, or in any transparent, nonfluorescing medium. The experimental conditions have been discussed in more detail by Skromme (1984).

The energy quantification capability of PL is excellent. Sensitivity is a further strength of the PL technique, allowing very small quantities (nanograms) or low

concentrations (ppt) of material to be analyzed. Examples of identifiable impurities in GaAs, down to around 10^{13} cm^{-3} and lower, are C, Si, Be, Mn, and Zn (Brundle *et al.*, 1992). Unfortunately, an accurate determination of impurity concentration in a sample is difficult unless conditions can be carefully controlled.

Radiative recombination processes

Under optical excitation at low temperature, the types of radiative recombination processes which may occur in GaAs are shown schematically in Figure 59.

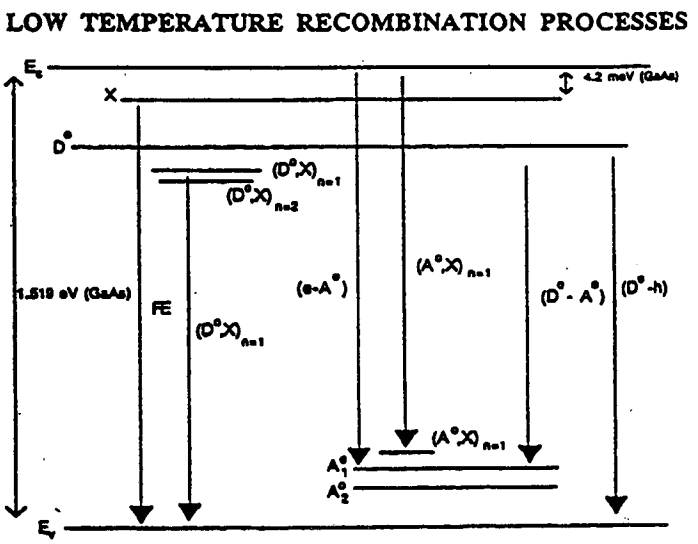

Figure 59. Diagram showing low-temperature radiative recombination mechanisms for GaAs (Stillman *et al.*, 1994).

As mentioned previously, the transitions which involve impurities and free electrons and holes (bound excitons) can be used for the identification of impurity species. For example, the transition which involves the recombination of an electron from the conduction band with a hole on a neutral acceptor (e-A^0) or an electron of a neutral donor with a hole on a neutral acceptor (D^0-A^0) can be used to identify

acceptors. Since the differences in binding energies of different acceptor species are large compared to the linewidths of these transitions (at low temperature), and since the differences in binding energy for different donor species are very small, the (D^0-A^0) transitions are especially useful for the identification of acceptor impurity species in GaAs. The donor binding energy differences in GaAs are too small (< 0.1 meV) to be of use for the identification of donor species. Figure 60 shows the energy diagrams for the (D^0-A^0) and (e-A^0) transitions.

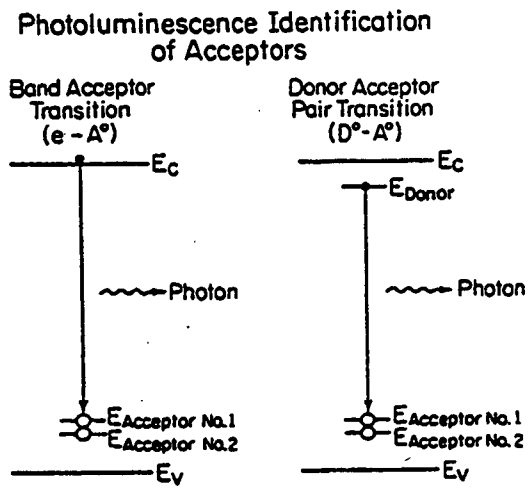

Figure 60. Donor/conduction-band-to-acceptor transitions for the identification of acceptors (Stillman *et al.*, 1994).

The energy of a photon emitted in a (D^0-A^0) transition is given by

$$h\nu = E_g - (E_A + E_D) + \frac{q^2}{\varepsilon_s \varepsilon_0 r}, \tag{68}$$

where E_g (= E_c - E_v) is the bandgap, E_A the acceptor binding energy, E_D the donor binding energy, and $\frac{q^2}{\varepsilon_s \varepsilon_0 r}$ is the coulomb energy term [r is the separation between (ionized) donor and (ionized) acceptor impurities, ε_s is the relative dielectric constant, and ε_0 is the permittivity of vacuum].

The emitted photon energy (peak position) of the (e-A^0) transition is given by

$$h\nu = E_g - E_A + (1/2)kT \qquad (k = \text{Boltzman's constant}). \tag{69}$$

An important feature of low-temperature photoluminescence is that it can be used to identify acceptor impurities in both n- and p-type GaAs.

The measurement temperature is an important factor in photoluminescence measurements. Optical transitions that are used to identify acceptors in GaAs require that measurements be performed at liquid helium temperatures so that electrons or holes are frozen out on donors or acceptors at those temperatures. At low temperatures, PL emission is often stronger because there are fewer phonon modes which can be excited. Photoluminescence measurements must be performed over the temperature range $T \leq 20$ K for the reliable identification of acceptors in GaAs. As the temperature is increased, (e-A^0) peaks shift to higher energy because the average kinetic energy of electrons increases as the temperature is increased. The (D^0-A^0) peaks also shift to higher energy with higher temperature, because there are more ionized impurities -- the distance (r) between the ionized impurities decreases, so the coulombic energy term in equation (67) increases. As the temperature is increased from that of liquid helium, the (e-A^0) peaks grow stronger relative to the (D^0-A^0) peaks [the (D^0-A^0) peaks also decrease in intensity as temperature increases due to the ionization of impurities]. The (e-A^0) peaks also broaden due to the greater distribution of electron kinetic energies with higher temperature; the (D^0-A^0) peaks do not broaden as temperature increases. At a high

enough temperature, only the (e-A^0) peaks are present. At room temperature PL emission is thermally broadened due to the possibility of energy transfer to or from phonon modes.

The excitation level is another important parameter in PL measurements. For transitions involving donor/acceptor impurities and free electrons and holes, peaks are well-resolved at low excitation levels. Under weak excitation and at liquid helium temperature, (D^0-A^0) transitions are strong in GaAs PL spectra and the (e-A^0) transitions are weak or not observed. The low excitation level also makes it possible to avoid heating effects which will cause thermal broadening of the peaks. Higher excitation levels tend to broaden/and or shift peak positions of donor-to-acceptor (D^0-A^0) transitions. Under high excitation, free carriers are present in the bands, and their concentration depends on the excitation. Therefore at high excitation, (e-A^0) transitions grow relative to (D^0-A^0) transitions. At high excitation, (D^0-A^0) transitions saturate, while (e-A^0) transitions grow with excitation. These transitions have been discussed by Bebb and Williams (1972), Ozeki *et al.*, (1974), and Ashen *et al.*, (1975).

It is sometimes necessary to identify (D^0-A^0) and (e-A^0) transitions by their unique excitation and temperature dependencies in cases where there is overlap of (D^0-A^0) and (e-A^0) transitions for different acceptors. For example, in GaAs the C(D^0-A^0) peak overlaps the Zn(e-A^0) peak and the Zn(D^0-A^0) peak overlaps the Si(e-A^0) peak. Variable-temperature PL measurements with weak optical excitation in most cases permit the descrimination between these two types of transitions.

The effect of higher impurity concentrations is that the (D^0-A^0) peak shifts to higher energy at higher impurity concentrations. This occurs because the distance between (ionized) donors and acceptors decreases and the coulomb energy term increases.

The PL spectra of $(D^0\text{-}A^0)/(e\text{-}A^0)$ transitions can be used in conjunction with Hall-effect measurements to obtain the concentration of individual acceptor species in high-purity GaAs (Stillman *et al.*, 1994).

APPENDIX XII: X-RAY ROCKING CURVE ANALYSIS

The basic principles of an X-ray diffraction (XRD) experiment will first be described. This description follows that of Brundle *et al.* (1992). For more details, see for example Cullity (1978); Warren (1969); and Schwartz and Cohen (1987).

Figure 61 illustrates the basic features of an XRD experiment, where 2θ is the angle between the incident and diffracted X-rays. In a typical experiment, the diffracted intensity is measured as a function of 2θ and the orientation of the specimen, which yields the diffraction pattern.

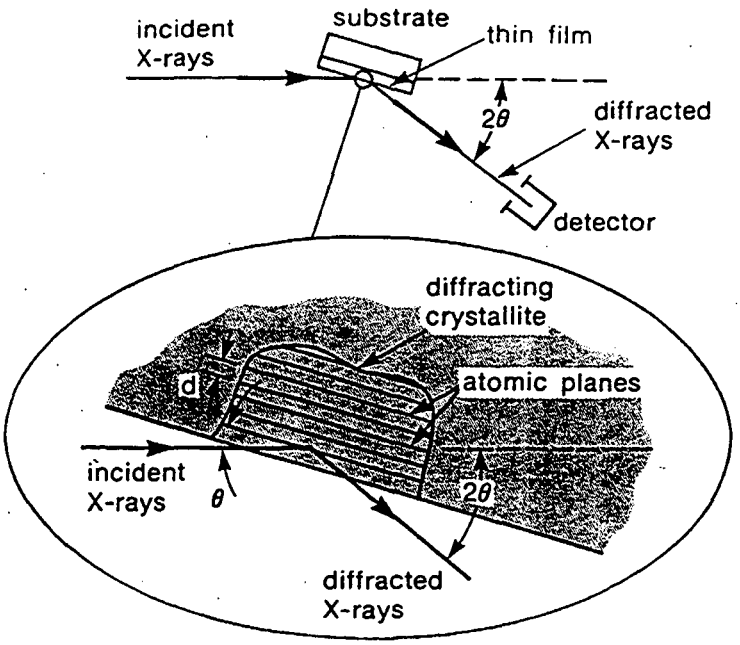

Figure 61. Basic features of a typical X-ray diffraction experiment (Brundle *et al.*, 1992).

The d-spacing between (hkl) planes, d_{hkl}, for cubic crystals is

$$d_{hkl} = \frac{a_0}{\sqrt{h^2 + k^2 + l^2}}, \tag{70}$$

where a_0 is the lattice constant of the crystal.

The condition for constructive interference from planes with spacing d_{hkl} is given by Bragg's law:

$$\lambda = 2d_{hkl} \sin\theta \tag{71}$$

where θ is the angle between the atomic planes and the incident (and diffracted) X-ray beam (Figure 61). For diffraction to be observed, the detector must be positioned so that the diffraction angle is 2θ, and the crystal must be oriented so that the normal to the diffracting plane is coplanar with the incident and diffracted X-rays and so that the angle between the the diffracting plane and the incident X-rays is equal to the Bragg angle θ. For a single crystal or epitaxial film, there is only one specimen orientation for each (hkl) plane where these diffraction conditions are satisfied.

In near-perfect crystals the incident X-rays undergo multiple reflections from atomic planes and the dynamical theory describes the interference between these reflections. The attenuation in the crystal is not by absorption, but is determined by the way in which the multiple reflections interfere. When the diffraction conditions are satisfied, the diffracted intensity from near-perfect crystals is essentially the same as the incident intensity. The diffraction peak widths depend on 2θ and a parameter known as the structure factor F_{hkl}, and are extremely small (less than ~0.001-0.005°).

The fact that atoms are arranged in a periodic fashion in space means that the diffracted X-ray directions are limited, and are referred to as a set of diffracted beams. The resultant wave diffracted (scattered) by all the atoms of the unit cell is called the structure factor, because it describes how the atom arrangement affects the diffracted

beam. The structure factor, designated by F, is obtained by adding together all the waves diffracted (scattered) by the individual atoms (Cullity, 1978).

Coherent scattering by an atom is due only to the electrons contained in that atom (the nucleus is much heavier and does not oscillate due to the impinging X-ray beam to any appreciable extent). Partial interference occurs between the waves scattered by electrons A and B; f, the atomic scattering factor, is used to describe the "efficiency of scattering of a given atom in a given direction."

$$f = \frac{\text{amplitude of the wave scattered by an atom}}{\text{amplitude of the wave scattered by one electron}}$$

where f = Z for any atom scattering in the forward direction. The atomic scattering factor is sometimes called the form factor because it depends on the way that the electrons are distributed around the nucleus.

The structure factor F expresses both the amplitude and phase of the resultant wave, and is proportional to f. The absolute value |F| gives the amplitude of the resultant wave in terms of the amplitude of the wave scattered by a single electron.

$$|F| = \frac{\text{amplitude of the wave scattered by all the atoms of a unit cell}}{\text{amplitude of the wave scattered by one electron}} .$$

The intensity of the beam diffracted by all the atoms of the unit cell in a direction predicted by the Bragg law is proportional to $|F|^2$, the square of the amplitude of the resultant beam.

So, the calculation of the intensity of any *hkl* reflection can be calculated from a knowledge of the atomic positions.

Due destructive interference of diffracted beams from different atoms of the unit cell, some *hkl* reflections will be absent (intensities will be zero). The conditions for a non-zero structure factor for GaAs (the form factors for Ga and As are very similar) are that all *hkl* are odd or all *hkl* are even, and $h + k + l = 4n$. for GaAs, the first {100}-type reflection with a non-zero structure factor is {400}. This reflection was used for the X-ray diffraction study of a representative LPE layer grown for this thesis.

A type of X-ray diffraction used to characterize the quality of single crystal bulk materials or thin films uses a Double-Crystal Diffractometer (DCD) (Brundle et al., 1992). As illustrated schematically in Figure 62, the incident beam of $K\alpha$ radiation is first diffracted from a single crystal which is as nearly perfect as possible [(a) in Figure 62], and then from the crystal to be measured [(b) in Figure 62]. Diffraction first from a single crystal ensures that the X-ray beam reaching the crystal to be measured is monochromatic and well-collimated. This permits high-resolution measurements to be made of the diffraction peak detected from the sample. Typically, the detector is fixed near 2θ, the (Bragg) diffraction angle for the (hkl) plane of interest, and the detector receiving slits are open to accept a large range in 2θ. The crystal to be measured is then rotated ("rocked") through 2θ, and the resulting curve of intensity vs. θ is called a "rocking curve". Since the diffraction peak widths in DCD measurements are narrow, this method enables accurate determination of very small deviations of 2θ due to changes in d-spacings due to inhomogeneous strain or variations in orientation.

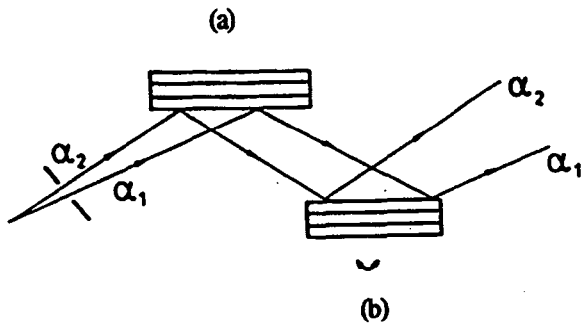

Figure 62. The double crystal arrangement for high resolution X-ray diffraction (Tanner, 1996)

The width of a rocking curve is a direct measure of the range of orientations present in the irradiated area of the crystal, because each subgrain of a polycrystalline sample will successively come into reflecting position as the crystal is rotated. Note that in DCD, nonuniform lattice strain is revealed, but uniform strain is not. Strain alters *d* spacings, which alter 2θ values; but the receiving slit of the detector is wide enough to admit this variation in 2θ and with a uniform strain the 2θ value will be altered but the spread in 2θ values will still be small as in the perfect crystal case.

The DCD was used quite a bit in the early days of X-ray diffraction to compare the width and height of the rocking curve for a real crystal with the values predicted by theory for a perfect crystal (Warren, 1969). This theory predicted a width on the order of 10 arc sec. (0.003°) for typical experimental conditions, and some crystals were found with rocking-curve widths approaching this value. However, most crystals exhibit widths 10 to 100 times greater (Cullity, 1978).

REFERENCES

T. **Abe**, *J. Cryst. Growth* **24/25**, p. 463 (1974)

B. H. **Ahn**, R. R. Shurtz, C. W. Trussel, *J. Appl. Phys.* **42**, 4512 (1971)

D. **Alexiev**, K. S. A. Butcher, *Nucl. Instr. and Meth. in Phys. Res.* **A317**, p. 111 (1992)

A. M. **Alper**, *Phase Diagrams: Materials Science and Technology*, Academic Press, N. Y. (1970)

T. **Amano**, S. Kondo, H. Nagai, S. Maruyama, *Japan. J. Appl. Phys.* **32**, p. 3692 (1993)

American Xtal Technology, private communication (1996)

E. **Andre**, J.-M. Le Duc, *U.S. Patent 3,632,431* (1972)

C. J. **Armistead**, P. Knowles, S. P. Najda, R. A. Stradling, *J. Phys. C: Solid State Phys.* **17**, 6415 (1984)

J. R. **Arthur** *et al.*, *J. Phys. Chem. Solids* **28**, 2257 (1967)

D. J. **Ashen**, P. J. Dean, D. T. J. Hurley, J. B. Mullin, A. M. White, P. D. Greene, *J. Phys. and Chem. Solids* **36**, p. 1041 (1975)

M. G. **Astles**, *Liquid Phase Epitaxial Growth of III-V Semiconductor Materials and Their Device Applications*, IOP Publishing Ltd. (1990)

M. G. **Astles**, J. C. H. Birbeck, C. J. Laversuch, M. C. Rowland, *J. Cryst. Growth* **34**, 24 (1976)

ASTM Standard F6, *1988 Annual Book of ASTM Standards*, Am. Soc. Test. Mat., Philadelphia (1988)

C. R. **Barrett**, W. D. Nix, A. S. Tetelman, *The Principles of Engineering Materials*, Prentice-Hall Inc, N. J. (1973)

E. **Bauser** (1996): private communication

E. **Bauser**, M. Frick, K. S. Loechsner, L. Schmidt, R. Ulrich, *J. Cryst. Growth* **27**, p. 148 (1974)

E. **Bauser**, B. Fischer, P.A. Sullivan in *Semiconductor Characterization Techniques*, P. A. Barnes, G. A. Rozgonyi, eds., Electronic Div. of Electrochem. Soc., Princeton (1978)

E. **Bauser**, G. A. Rozgonyi, *Appl. Phys. Lett.* **37**, p. 1001 (1980)

E. **Bauser**, K. S. Loechsner, *J. Cryst. Growth* **55**, p. 475 (1981)

E. **Bauser** in *Crystal Growth of Electronic Materials*, E. Kaldis, ed., No.-Holland Physics Publ., Amsterdam, Ch. 4 (1985)

E. **Bauser** *et al.*, Inst. Phys. Conf. Ser. No. 136, p. 355 (1994)

H. B. **Bebb**, E. W. Williams in *Semiconductors and Semimetals*, Vol. 8, eds. R. K. Willardson, A. C. Beer, Academic Press, N. Y., p. 182 (1972)

H. **Beneking**, W. Vits, *Proc. of the Second Int.Symp.on GaAs: Inst. Phys. Phys. Soc. Conf. Ser. No. 7*, 96 (1968)

P. **Bennema**, G. H. Gilmer in *Crystal Growth, an Introduction*, P. Hartman, ed., No.-Holland, Amsterdam (1973)

K. W. **Benz**, E. Bauser in *Crystals -- Growth, Properties and Applications*, Vol. 3, H. C. Freyhardt, ed., Springer-Verlag, Berlin-Heidelberg, p. 1 (1980)

P. R. **Bratt** in *Semiconductors and Semimetals*, R. K. Willardson and A. C. Beer, eds., Vol. 12, Ch. 2, Academic Press Inc. (1977)

R. F. **Brebrick**, *J. Appl. Phys.* **33** (1), p. 422 (1962)

M. R. **Brozel**, R. C. Newman, J. B. Clegg, *J. Phys. D* **11** (9), p. 1331 (1978)

C. R. **Brundle**, C. A. Evans, Jr., S. Wilson, *Encyclopedia of Materials Characterization*, Reed Publishing Inc, Mass. (1992)

H. E. **Buckley**, *Crystal Growth*, John Wiley and Sons Inc., N.Y., N.Y., Ch. 10 (1951)

J. A. **Burton**, R. C. Prim, W. P. Slichter, *J. Chem. Phys.* **21**, 1987 (1953)

W. K. **Burton**, N. Cabrera, F. C. Frank, Phil. Trans. Royal Soc. London **A243**, p. 299 (1951)

H. C. **Casey**, Jr., M. B. Panish, K. B. Wolfstirn, *J. Phys. Chem. Solids* **32**, 571 (1971)

H. C. **Casey**, Jr., M. B. Panish, *J. Cryst. Growth* **13/14**, 818 (1972)

A. **Chandra**, C. E. C. Wood, D. W. Woodward, L. F. Eastman, *Solid-State Electron.* **22**, 645 (1979)

C. Y. **Chang**, Y. K. Su, M. K. Lee, L. G. Chen, M. P. Houng, *J. Cryst. Growth* **55** (1), 24 (1981)

C. **Chang-Hasnain**, *Class notes for EECS290P*, Dept. of Electrical Engineering and Computer Science, U.C. Berkeley, 1996

A. A. **Chernov**, *Surface Morphology and Growth Kinetics*, in ISSCG2, *Second Int. Spring School of Crystal Growth, Japan* (1974)

A. A. **Chernov**, Modern Crystallography III, B. K. Vainshtein, ed., Springer, Berlin (1983)

R. **Chwang**, B. J. Smith, C. R. Crowell, *Solid-State Electron.* **17**, 1217 (1974)

R. A. **Cooke**, R. A. Hoult, R. K. Kirkman, R. A. Stradling, *J. Phys. D* **11**, p. 945 (1978)

I. **Crossley**, M. B. Small, *J. Cryst. Growth* **11**, p. 157 (1971)

I. **Crossley**, M. B. Small, *J. Cryst. Growth* **15**, p. 275 (1972)

I. **Crossley**, M. B. Small, *J. Cryst. Growth* **15**, p. 268 (1972b)

I. **Crossley**, M. B. Small, *J. Cryst. Growth* **19**, 160 (1973)

B. D. **Cullity**, *Elements of X-ray Diffraction*, Addison-Wesley Publishing Co. (1978)

J. M. **David**, M. G. Buehler, *Solid-State Electron.* **20**, 539 (1977)

L. R. **Dawson** in *Progress in Solid State Chemistry*, Vol. 7, H. Reiss, J. O. McCaldin, eds., Pergamon Press, Ch. 4 (1972)

R. H. **Deitch**, *Crystal Growth*, B. Pamplin, ed., Vol. 6, Pergamon Press, Ch. 11 (1975)

A. **Doi**, T. Asano, M. Migitaka, *J. Appl. Phys.* **47** (4), p. 1589 (1976)

A. **Dorrity**, J. D. Grange, D. K. Wickenden in *Gallium Arsenide -- Materials, Devices and Circuits*, M. J. Howes and D. V. Morgan, eds., John Wiley and Sons Ltd, Ch. 3 (1985)

R. C. **Draper** in *Crystal Growth*, B. Pamplin, ed., Vol. 6, Pergamon Press, Ch. 12 (1975)

T. J. **Drummond**, H. Morkoç, A. Y. Cho, *J. Appl. Phys.* **52** (3), p. 1380 (1981)

O. **Dubon**, *Ph. D. Thesis*, U. C. Berkeley Dept. of Materials Science and Mineral Eng. (1996)

J. E. **Eberhardt**, R. D. Ryan, A. J. Tavendale, *Appl. Phys. Lett.* **17**, p. 427 (1970)

D. **Elwell** in *Crystal Growth*, B. R. Pamplin, ed., Pergamon Press, Ch. 12 (1980)

Engelhard Industries, private communication (1995)

Epitaxial Products International, private communication (1997)

H. R. **Fetterman**, D. M. Larsen, G. E. Stillman, P. E. Tannenwald, J. Waldman, *Phys. Rev. Lett.* **26**, p. 975 (1971)

B. **Fischer**, *Appl. Phys. Lett.* **33**, p. 78 (1978)

F. C. **Frank**, *Disc. Faraday Soc.* **5**, p. 48 (1949)

M. L. **Frankenheim**, *Ann. Phys.* **37**, p. 576 (1836)

P. E. **Gibbons**, J. H. Howes, *IEEE Trans. Nucl. Sci.* **NS-19**, p. 353 (1972)

R. **Ghez**, *J. Cryst. Growth* **19** (3), p. 153 (1973)

R. **Ghez**, E. A. Giess in *Epitaxial Growth, Part A*, J. W. Matthews, ed., Academic Press, Ch. 2.6 (1975)

A. R. **Goodwin**, C. D. Dobson, J. Franks, *Symp.on GaAs, Dallas: Inst. Phys. Phys. Soc.*, p. 36 (1969)

S. M. **Grant,** T. J. Sumner, J. P. Warren, D. Alexiev, K. S. A. Butcher, submitted to *Proc. SPIE* **2006** (1993)

P. D. **Greene,** *Advanced Crystal Growth*, P. M. Dryburgh, B. Cockayne, K. G. Barraclough, eds., Prentice-Hall, p. 221 (1986)

R. **Haase,** *Physical Chemistry*, Vol. 1, W. Jost, ed., Academic Press, N. Y., p. 84 (1971)

R. N. **Hall,** *Proc. IRE* **40** (11), p. 1512 (1952)

R. N. **Hall,** *J. Phys. Chem.* **57**, p. 836 (1953)

E. E. **Haller**, F. S. Goulding in *Handbook on Semiconductors*, Vol. 4, C. Hilsum, ed., Elsevier No.-Halland Inc., N. Y., p. 937 (1993)

W. E. **Ham,** *Appl. Phys. Lett.* **21**, p. 440 (1972)

F. **Hasegawa** in *Properties of GaAs*, Publ. by INSPEC, The Institution of Electrical Engineers, London and N. Y., p. 609 (1990)

Hewlett-Packard Optoelectronics Division, private communication (1997)

H. G. B. **Hicks,** P. D. Greene, *Proc. of the Third Int. Symp. on GaAs and Related Compounds: Inst. Phys. Conf. Ser. No. 9*, p. 92 (1970)

D. E. **Holmes**, G. S. Kamath, *J. Crystal Growth* **54**, p. 51 (1981)

Y. M. **Houng**, G. L. Pearson, B. L. Mattes, *J. Electrochem. Soc.* **125**, p. 2058 (1978)

J. J. **Hsieh,** *J. Cryst. Growth* **27**, p. 49 (1974a)

J. J. **Hsieh,** *Solid State Res. Report 1974:3, MIT Lincoln Laboratory*, p. 25 (1974b)

J. J. **Hsieh,** *Appl. Phys. Lett.* **28**, p. 283 (1976a)

J. J. **Hsieh** in *Handbook on Semiconductors*, Vol. 3, S. P. Keller, ed., Elsevier No.-Holland, Ch. 6 (1980)

J. J. **Hsieh**, unpublished work (1975b) in *Handbook on Semiconductors*, Vol. 3, S. P. Keller, ed., Elsevier No.-Holland, Ch. 6 (1980)

L. **Hsu**, *Professor Haller Group Seminar*, U.C. Berkeley Dept. of Materials Science and Mineral Eng. (Nov. 1994)

D. T. J. **Hurle**, *J. Phys. Chem. Solids* **40**, p. 613, 627, 639, 647 (1979)

H. **Jacob**, G. Müller in *Landolt-Börnstein New Series*, Group III, Vol. 17d, O. Madelung, M. Schulz, H. Weiss, eds., Springer-Verlag (1984)

C. S. **Kang**, P. E. Greene, *Proc. of the Second Int. Symp. on GaAs: Inst. Phys. Phys. Soc. Conf. Ser. No. 7*, 18 (1968)

T. **Kajimura**, K. Aiki, J. Umeda, *Appl. Phys. Lett.* **30**, 526 (1977)

L. **Kaufman**, in *Alloy Phase Diagrams*, L. H. Bennet, T. B. Massalski, B. C. Giessen, eds., No.-Holland, N.Y., p. 105 (1983)

S. E. **King**, W. J. Moore, R. L. Henry, P. E. R. Nordquist, *IEEE Trans. Nucl. Sci.* **43** (3), p. 1376 (1996)

Sh. M. **Kogan**, B. I. Sedunov, *Sov. Phys. Solid State* **8**, 1898 (1967)

K. **Konuma**, E. Czech, I. Silier, E. Bauser, *Appl. Phys. Lett.* **63** (2) (1993)

D. M. **Korn**, D. M. Larsen, Solid State Commun. **13**, p. 807 (1973)

H. **Kressel**, J. K. Butler, *Semiconductor Lasers and Heterojunction LEDs*, Academic Press (1977)

F. A. **Kröger**, *The Chemistry of Imperfect Crystals*, Vol. 1, No.-Holland, Amsterdam (1973)

K. **Kumar**, M. Takagi, *Japan. J. Appl. Phys.* **16**, p. 957 (1977)

D. M. **Larsen**, *Phys. Rev. B* **8**, p. 535 (1973)

D. M. **Larsen**, *Phys. Rev. B* **13**, p. 1681 (1976)

J. **Lauter**, *et al.*, *Nucl. Phys. B (Proc. Suppl.)* **44**, p. 381 (1995)

S. Y. **Lien**, J. L. Bestel, *Electrochem. Soc. Meeting, Houston*, Abs **50**, 143 (1972)

T. M. **Lifshitz**, N. P. Likhtman, V. T. Sidorov, *Sov. Phys. Semicond.* **2**, 652 (1968)

R. **Linnebach**, E. Bauser, *J. Cryst. Growth* **57**, 43 (1982)

Y. Z. **Liu**, *Proc. of the Seventh Int. Symp. on GaAs and Related Compounds: Inst. of Phys. Conf. Series No. 45*, 103 (1978)

S. I. **Long**, J. M. Ballantyne, L. F. Eastman, *J. Cryst. Growth* **26**, 13 (1974)

R. L. **Longini**, R. F. Greene, *Phys. Rev.* **102**, 992 (1956)

T. S. **Low**, G. E. Stillman, C. M. Wolfe in *Proc. Conf. on GaAs and Related Compounds, Inst. Phys. Conf. Ser. 63*, p. 143 (1982a)

T. S. **Low**, G. E. Stillman, T. Nakanisi, T. Udagawa, C. M. Wolfe, *Appl. Phys. Lett.* **41**, p. 183 (1982b)

C. H. **Lupis**, *Chemical Thermodynamics of Materials*, Prentice-Hall Inc., N. J. (1983)

J. M. **Luttinger**, W. Kohn, Phys. Rev. **98** (4), p. 915 (1955)

M/A Com, private communication (1995)

A. Ju. **Malinin**, O. B. Nevsky, *J. Electron. Mater.* **7** (6), p. 757 (1978)

A. Ju. **Malinin**, *et al.*, *J. Electron. Mater.* **7** (6), p. 775 (1978)

H. M. **Manasevit**, W. I. Simpson, *J. Electrochem. Soc.* **116**, p. 1725 (1969)

B. L. **Mattes**, Y. M. Houng, G. L. Pearson, *J. Vac. Sci. Technol.* **12**, p. 869 (1975)

D. S. **McGregor**, R. A. Rojeski, G. F. Knoll, F. L. Terry, Jr., J. East, Y. Eisen, *Nucl. Instr. and Meth. in Phys.* **A343**, p. 527 (1994)

H. T. **Minden**, *J. Cryst. Growth* **6**, 228 (1970)

A. H. **Mitchell**, C. Kittel, *Phys. Rev.* **96** (6), p. 1488 (1954)

T. **Mitsuhata**, *Japan. J. Appl. Phys.* **9**, 90 (1970)

R. L. **Moon**, *J. Cryst. Growth* **27**, p. 62 (1974)

R. L. **Moon**, S. I. Long, *J. Cryst. Growth* **32**, p. 68 (1976)

R. L. **Moon** in *Crystal Growth*, B. R. Pamplin, ed., Pergamon Press Ltd, Ch. 11 (1980)

W. J. **Moore**, R. L. Henry, P. E. R. Nordquist, *Nucl Instr. Meth. in Phys. Res.* **380** (1-2), p. 102 (1996)

H. **Morkoç**, L. F. Eastman, *J. Cryst. Growth* **36**, 109(1976)

A. **Mühlbauer**, E. Sirtl, *Phys. Stat. Sol.* **(a)23**, p. 555 (1974)

Y. **Nanishi**, Japan. *J. Appl. Phys.* **17**, p. 1177 (1978)

Y. **Nannichi**, G. L. Pearson, *Solid-State Electron.* **12**, p. 341 (1969)

H. **Nelson**, *RCA Rev.* **24**, p. 603 (1963)

H. **Nelson**, *U.S. Patent 3,565,702* (1971)

T. **Nishinaga**, T. Kazuno, T. Tanbo, J. Koide, K. Pak, T. Nakamura, Y. Yasuda, *J. Cryst. Growth* **65**, p.607 (1983)

D. **Nohavica**, *Int. Conf. Heterojunctions and Layer Structures*, Part III, Publ. by Adler, Chicago, p. 209 (1970)

K. **Oe**, K. Sugiyama, *Appl. Phys. Lett.* **33**, p. 449 (1978)

G. H **Olsen**, T. J. Zamerowski, Prog. Cryst. Growth and Charact. **2**, p. 309 (1979)

M. **Otsubo**, K. Segawa, H. Miki, *Japan. J. of Appl. Phys.* **12**, 797 (1973)

M. **Ozeki**, K. Nakai, K. Dazai, O. Ryuzan, *Japan. J. Appl. Phys.* **13**, p. 1121 (1974)

M. **Ozeki**, K. Kitahara, A. Nakai, A. Shibatomi, K. Dazai, S. Ohkawa, O. Ryuzan, *Japan J. Appl. Phys.* **16**, p. 1617 (1977)

M. B. **Panish**, *J. Chem. Thermodyn.* **2**, p. 319 (1970)

M. B. **Panish**, I. Hayashi, S. Sumski, *IEEE J. Quantum Electron.* **5**, 210 (1969)

M. B. **Panish**, I. Hayashi, S. Sumski, *Appl. Phys. Lett.* **16**, 326 (1970)

W. G. **Pfann**, *Trans. A.I.M.E.* **194**, 747 (1952)

C. **Pupp**, J. J. Murray, R. F. Pottie, *J. Chem. Thermodyn.* **6**, 123 (1974)

A. K. **Ramdas**, S. Rodriguez, *Reports on Progress in Physics* **44**, 1297 (1981)

A. P. **Ratner**, *J. Chem. Phys.* **1**, 789 (1933)

Lord **Rayleigh**, *Scientific Papers*, Vol. 6, Cambridge University Press, 432 (1920)

A. **Reisman**, *Phase Equilibria*, Academic Press, N .Y. (1970)

H. **Reiss**, C. S. Fuller, *J. Metals* **8**, 276 (1956)

D. L. **Rode**, *J. Cryst. Growth* **20**, 13 (1973)

D. L. **Rode**, *Phys. Stat. Sol.* **(a)32**, p. 425 (1975)

D. L. **Rode**, C. M. Wolfe, G. E. Stillman, in *GaAs and Related Compounds: Inst. Phys. Conf. Ser. No. 65*, 569 (1983)

F. **Rosenberger**, *Fundamentals of Crystal Growth I -- Macroscopic Equilibrium and Transport Concepts*, Springer Series in Solid State Sciences Vol. 5, M. Cardona, P. Fulde, H.-J. Queisser, eds., Springer-Verlag Berlin-Heidelberg (1979)

C. **Rossington**, private communication (1996, 1997)

F. E. **Rosztoczy**, *Abstr. of Electrochem. Soc. Montreal Meeting No. 526*, 516 (1968)

L. **Royer**, *Bull. Soc. Fr. Miner.* **51**, 7 (1928)

H. **Rupprecht**, *Proc. of the First Int. Symp. on GaAs and Related Compounds: Inst. Phys. Phys. Soc. Conf. Ser. No. 3*, 57 (1966)

H. **Rupprecht**, J. M. Woodall, G. D. Pettit, Appl. Phys. Lett. **11**, 81 (1967)

R. H. **Saul**, *J. Electrochem Soc.* **118**, p. 793 (1971)

R. H. **Saul**, W. H. Hackett, Jr., (1970) *J. Electrochem. Soc.* **117**, 921 (1970)

R. H. **Saul**, D. D. Roccasecca, *J. Electrochem. Soc.* **20**, p. 1128 (1973a)

R. H. **Saul**, D. D. Roccasecca, *J. Appl. Phys.* **44**, p. 1983 (1973b)

H. J. **Scheil**, *J. Cryst. Growth* **42**, p. 301 (1977)

L. H. **Schwartz**, J. B. Cohen, *Diffraction From Materials*, Springer-Verlag (1987)

J. S. **Shah** in *Crystal Growth*, B. Pamplin, ed., Vol. 6, Pergamon Press, Ch. 4 (1975a)

J. S. **Shah** in *Crystal Growth*, B. Pamplin, ed., Vol. 6, Pergamon Press, Ch. 9 (1975b)

J. R. **Shealy**, J. M. Woodall, *Appl. Phys. Lett.* **41**, p. 88 (1982)

M. **Shur**, *GaAs Devices and Circuits*, Plenum Press (1987)

I. **Silier**, S. Subramanian, E. Diebel, H.-J. Queisser, E. Bauser (submitted to *Appl. Phys. Lett.*, 1992)

B. J. **Skromme**, T. S. Low, G. E. Stillman, *Proc. of the Tenth Int. Symp. on GaAs and Related Compounds: Inst. Phys. Conf. Ser. No. 65*, p. 485 (1982)

B. J. **Skromme**, *Ph.D. Thesis*, Dept. of Electrical Engineering, Univ. of Illinois, Urbana-Champaign, IL (1984)

M. B. **Small**, J. F. Barnes, *J. Cryst. Growth* **5**, p.9 (1969)

R. **Soloman**, *Proc. of Second Int. Symp. on GaAs and Related Compounds: Inst. Phys. Conf. Ser. No. 7*, p. 11 (1968)

R. A. **Stradling** in *Growth and Characterization of Semiconductors*, R. A. Stradling, P. C. Klipstein, eds., IOP Publishing Ltd, 165 (1991)

G. E. **Stillman**, C. M. Wolfe, J. O. Dimmock in *Semiconductors and Semimetals*, Vol. 12, R. K. Willardson, A. C. Beer, eds., Academic Press Inc., p. 169 (1977)

G. E. **Stillman**, S. S. Bose, M. H. Kim, B. Lee, T. S. Low in *Handbook on Semiconductors*, Vol. 3A, T. S. Moss, ed., Elsevier Science, Ch. 10 (1994)

R. F. **Strickland-Constable**, *Kinetics and Mechanisms of Crystallization*, Academic Press, London (1968)

G. B **Stringfellow**, P. D. Greene, *J. Electrochem. Soc.* **118**, p. 805 (1971)

Sumitomo Electric Co., private communication (1995)

T. J. **Sumner**, S. M. Grant, A. Bewick, J. P. Li, K. Smith, S. P. Beaumont, *Nucl. Instr. and Meth. in Phys.* **A322**, p. 514 (1992)

T. J. **Sumner**, S. M. Grant, D. Alexiev, K. S. A. Butcher, *Nucl. Instr. and Meth. in Phys.* **A348**, p. 518 (1994)

S. M. **Sze**, *Physics of Semiconductor Devices*, John Wiley and Sons Inc., N.Y., N.Y., (1981)

B. K. **Tanner** in *Semiconductor Characterization -- Present Status and Future Needs*, W. M. Bullis, D. J. Seiler, A. C. Diebold, eds., AIP Press, N. Y., 263 (1996)

C. D. **Thurmond**, *J. Phys. Chem. Solids* **26**, p. 785 (1965)

W. A. **Tiller**, *J. Cryst. Growth* **2**, 69 (1968)

W. A. **Tiller**, C. Kang, *J. Cryst. Growth* **2**, p. 345 (1968)

L. B. **Valdes**, *Proc. IRE* **42**, 420 (1954)

L. J. **van der Pauw**, *Philips Res. Repts* **13**, 1 (1958a)

L.J. **van der Pauw**, *Philips Tech Rev.* **20**, p. 220 (1958b)

F. **Vaslow**, G. E. Boyd, *J. Am. Chem. Soc.* **74**, p. 4691 (1952)

H. W. **Verleur**, P. R. Moest, *A.I.M.E. Meeting*, Las Vegas, Nev (1973)

W. **Walukielwicz**, J. Lagowski, H. C. Gatos, *J. Appl. Phys.* **53** (1), p. 769 (1982)

B. E. **Warren**, *X-ray Diffraction*, Addison-Wesley (1969)

M. **Weinstein**, H. E. LaBelle, Jr., A. I. Mlavsky, *J. Appl. Phys.* **37**, p. 2913 (1966)

G. H. **Westphal**, R. Rosenberger, *J. Cryst. Growth* **43**, p. 687 (1978)

C. **Weyrich**, ( ) Plihal in *Landolt-Börnstein New Series*, Group III, Vol. 17d, O. Madelung, M. Schulz, H. Weiss, eds., Springer-Verlag (1984)

E. A. D. **White**, J. D. C. Wood, *J. Cryst. Growth* **17**, p. 315 (1972)

W. R. **Wilcox**, *J. Cryst. Growth* **12**, p. 93 (1972)

A. F. **Witt**, H. C. Gatos, *J. Electrochem. Soc.* **113**, p. 808 (1966)

C. M. **Wolfe**, G. E. Stillman, *Proc. Third Int. Symp. on GaAs: Inst. Phys. Phys. Soc. Conf. Ser. No. 9*, 3 (1970)

C. M. **Wolfe**, G. E. Stillman, D. M. Korn, *Proc. Conf. on GaAs and Related Compounds, Inst. Phys. Conf. Ser. No. 33b*, p. 120 (1977)

J. M. **Woodall**, *J. Vac. Sci. Technol.* **20** (3), p. 730 (1982)

J. **Zernike**, *Chemical Phase Theory*, N. V. Uitgevers-Maatschapp, Deventer (1955)

K.-H. **Zschauer** and A. Vogel, *Proc. of the Third Int. Symp. on GaAs: Inst. Phys. Phys. Soc. Conf. Ser. No. 9*, 100 (1970)

Ernest Orlando Lawrence Berkeley National Laboratory
One Cyclotron Road | Berkeley, California 94720

Prepared for the U.S. Department of Energy under Contract No. DE-AC03-76SF00098